UNIVERSIDADE FEDERAL DO PARANÁ

LUCAS SEIFFERT

UM ALGORITMO COM PREDITOR MONOLÍTICO PARA PROBLEMAS DO TIPO INTERAÇÃO FLUIDO-ESTRUTURA

CURITIBA
2020

LUCAS SEIFFERT

UM ALGORITMO COM PREDITOR MONOLÍTICO PARA PROBLEMAS DO TIPO INTERAÇÃO FLUIDO-ESTRUTURA

Dissertação apresentada ao curso de Pós-Graduação em Matemática, Departamento de Matemática, Setor de Ciências Exatas, Universidade Federal do Paraná, como requisito parcial à obtenção do título de Mestre em Matemática.

Orientador: Prof. Dr. Yuan Jin Yun

CURITIBA
2020

Catalogação na Fonte: Sistema de Bibliotecas, UFPR
Biblioteca de Ciência e Tecnologia

S459a Seiffert, Lucas
Um algoritmo com preditor monolítico para problemas do tipo interação fluido-estrutura [recurso eletrônico] Lucas Seiffert. – Curitiba, 2020.

Dissertação - Universidade Federal do Paraná, Setor de Ciências Exatas, Programa de Pós-Graduação em Matemática, 2020.

Orientador: Yuan Jin Yun.

1. Método dos elementos finitos. 2. Algoritmos. 3. Equações diferenciais parciais. I. Universidade Federal do Paraná. II. Jin Yun, Yuan. III. Título.

CDD: 510

Bibliotecária: Vanusa Maciel CRB- 9/1928

MINISTÉRIO DA EDUCAÇÃO
SETOR DE CIENCIAS EXATAS
UNIVERSIDADE FEDERAL DO PARANÁ
PRÓ-REITORIA DE PESQUISA E PÓS-GRADUAÇÃO
PROGRAMA DE PÓS-GRADUAÇÃO MATEMÁTICA - 40001016041P1

TERMO DE APROVAÇÃO

Os membros da Banca Examinadora designada pelo Colegiado do Programa de Pós-Graduação em MATEMÁTICA da Universidade Federal do Paraná foram convocados para realizar a arguição da Dissertação de Mestrado de **LUCAS SEIFFERT** intitulada: **Um algoritmo com preditor monolitico para problemas do tipo interacao fluido-estrutura**, sob orientação do Prof. Dr. YUAN JIN YUN, que após terem inquirido o aluno e realizada a avaliação do trabalho, são de parecer pela sua APROVAÇÃO no rito de defesa.

A outorga do título de mestre está sujeita à homologação pelo colegiado, ao atendimento de todas as indicações e correções solicitadas pela banca e ao pleno atendimento das demandas regimentais do Programa de Pós-Graduação.

CURITIBA, 05 de Fevereiro de 2020.

YUAN JIN YUN
Presidente da Banca Examinadora (UNIVERSIDADE FEDERAL DO PARANÁ)

ELÍAS ALFREDO GUDIÑO ROJAS
Avaliador Interno (UNIVERSIDADE FEDERAL DO PARANÁ)

CASSIO MACHIAVELI OISHI
Avaliador Externo (UNIVERSIDADE EST.PAULISTA JÚLIO DE MESQUITA FILHO/PR.PRUDENT)

AGRADECIMENTOS

À minha família, pela paciência até que eu encontrasse meu caminho; pelo apoio logístico e financeiro; pela compreensão durante maus-humores, estresse e ansiedade.

Ao meu orientador, prof. Yuan, pela confiança depositada em mim durante a graduação e pós-graduação; pela liberdade dada a mim para seguir meus interesses e abordar os projetos da forma que eu achasse melhor, mesmo que significasse que tomei um caminho mais longo do que o necessário para, enfim, entender o que ele quis dizer. E, mais importante, agradeço pela sua insistência para que eu fosse mais ambicioso e saísse da minha zona de conforto.

Ao prof. Elías, por sua generosa ajuda, desde meu trabalho de graduação; por ter assistido a meus (sofríveis) seminários, sempre partilhando o que sabia; pelo aceite para fazer parte da minha banca de defesa de mestrado.

Ao prof. Cassio, pelas dicas para este trabalho e por também ter aceito fazer parte da minha banca de defesa.

Aos professores do DMAT da UFPR, pelo apoio desde a graduação; pelo interesse no meu trabalho, presença em seminários, e respostas a perguntas confusas e a pedidos de referências bibliográficas.

Aos amigos e colegas, pela companhia, conversas, dicas, trocas de lamentações e reclamações, que tornaram meu dia-a-dia mais leve.

Finalmente, e não menos importante, à Capes, pelo suporte financeiro.[1]

[1] O presente trabalho foi realizado com apoio da Coordenação de Aperfeiçoamento de Pessoal de Nível Superior - Brasil (CAPES) - Código de Financiamento 001

RESUMO

O objetivo deste trabalho é desenvolver um novo algoritmo para a solução de equações diferenciais parciais que modelam problemas do tipo Interação Fluido-Estrutura. Apresentamos, inicialmente, como essas equações são obtidas, a partir da versão das equações de Navier-Stokes em sua formulação Lagrangeana-Euleriana Arbitrária, acoplada a uma estrutura hiperelástica genérica. Revisamos, como motivação para nosso método, alguns métodos de Elementos Finitos da literatura desenvolvidos para estes sistemas de equações, enfatizando sua classificação em métodos particionados e monolíticos. Nosso método é então apresentado como um meio-termo entre essas duas classes. Descrevemos duas versões para ele, dependendo das condições de contorno que consideramos no preditor monolítico: condições de Dirichlet constantes ou dependentes do tempo. Por fim, reportamos alguns resultados numéricos, de modo a comparar nosso método com condições constantes de Dirichlet com um método monolítico e um método particionado.

Palavras-chave: Interação fluido-estrutura. Formulação Lagrangeana-Euleriana Arbitrária. Método de Elementos Finitos. Preditor monolítico.

ABSTRACT

In this work, we develop a new algorithm for the solution of the systems of partial differential equations that model Fluid-Structure Interaction problems. We first present how these equations are obtained, through an Arbitrary Lagrangian-Eulerian version of the Navier-Stokes equations, coupled with a generic hyperelastic structure. We then review some Finite Element methods already available to solve such system of equations, emphasizing the rough classification between monolithic and partitioned methods. This motivates the presentation of our method, which stands somewhat in between those alternatives. Two flavors of our algorithm are described, which depend on the Dirichlet conditions imposed on the monolithic predictor: one uses constant conditions and the other uses time-dependent ones. Lastly, we report numerical results that compare our method with constant Dirichlet conditions with a monolithic and a partitioned method.

Keywords: Fluid-Structure Interaction. Arbitrary Lagrangian-Eulerian formulation. Finite Element Method. Monolithic predictor.

CONTENTS

1 INTRODUCTION

Fluid-structure interaction (FSI) is the generic name for problems which, as suggested by its name, consist mainly of a structure and a fluid that depend on each other's behaviour. For example, such problems appear in mechanical engineering, such as in aerodynamics of airplane wings, parachutes and wind turbines (BAZILEVS; TAKIZAWA; TEZDUYAR, 2013). No less relevant are problems in biomedicine, through the modelling and simulation of haemodynamics, that is, blood flow (FORMAGGIA; QUARTERONI; VENEZIANI, 2009).

FSI problems and their corresponding systems of partial differential equations possess no analytical solution up to now, except for in very simplified models. Thus, they usually require numerical methods, and it was the advance in computer's processing capability that propelled the research for this topic. Indeed, while there are foundational articles dating from the 1970's, such as Peskin (1972), it is from the end of the 00's that a number of academic books were published on the subject, such as Formaggia, Quarteroni, and Veneziani (2009), Bazilevs, Takizawa, and Tezduyar (2013) and Richter (2017).

The mathematical difficulties start with the fact that we are coupling two active and challenging areas: the modelling and simulation of solids or structures, and the modelling and simulation of fluids. What is more, since one phenomenon influences the other, we are usually faced with the problem of tracking their domains. This already requires one to take a modelling decision that will influence the numerical methods. For instance, two different modern tracks of research are that of Immersed Boundary methods, such as in recent articles from Kadapa, Dettmer, and Perić (2018) and Kim, Lee, and Choi (2018), and the Arbitrary Eulerian-Lagrangian (ALE) type of methods (RICHTER, 2017). In this work, we have chosen to work with the latter, for we consider it to be simpler in approach.

As will be developed in **Chapter 3**, the ideal method in FSI would be the one which would allow the use of the finely-tuned methods for structure simulation and fluid simulation as black boxes, and hopefully use them only once for each time step. This has been shown, both experimentally and analytically, using simplified models, not to always be feasible. What we have, then, is the choice to either build a new method, and somewhat lose all the optimization done in the specialized fluid and structure methods, or to use these specialized methods many times for each time step, in an iterative procedure.

The goal of this dissertation is to propose a new method, perhaps an intermediate solution between these two options, to both reduce computational time and use the specialized methods. We would still need a monolithic method, but run in a smaller domain around the interface, to predict more accurately the values of the variables on the interface, and then use the specific fluid and structure solutions only once at a time step.

To achieve such objective, we begin in **Chapter 2** with some theory and mathematical modelling topics, such as function spaces and concepts of continuum mechanics, to then present Newtonian fluids and elastic structures. We then present the ALE formulation for fluids, so that we can couple both fluid and structure to give the full FSI problem.

In **Chapter 3**, we summarize, as hinted above, some developments in monolithic and partitioned methods for FSI problems. We also include concepts that have been developed to analyze these methods, such as the *added-mass effect* and the *Geometric Conservation Law*.

Our method is then introduced in **Chapter 4**. After a brief presentation, we use a simple parabolic problem to analyse some of its properties. Two flavours of the method are given, one using time-dependent and non-constant Dirichlet boundary conditions, and another with constant Dirichlet conditions.

Finally, we show in **Chapter 5** our results from numerical tests in the FSI problem of an elastic tube filled with a fluid, presented with a constant pressure on one of its openings, and closed on the other. We have performed tests with the constant Dirichlet conditions version of our method, using two different domain sizes for our predictor. Additional tests have checked what happens when we double the pressure condition, and whether refining the problem's mesh improves the performance of our predictor.

2 MODELLING STRATEGY

In this chapter, we gather ideas related to the modelling of a Fluid-Structure Interaction problem and fix some notations for the following chapters. Nothing here is new, and our main reference was Formaggia, Quarteroni, and Veneziani (2009, Chap. 3).

2.1 SOME FUNCTION SPACES

Let us quickly define the function spaces we need for the weak formulations of our equations. This section is just a summary of the detailed presentations from Adams and Fournier (2003) and Quarteroni and Valli (1994).

Let $\Omega \subset \mathbb{R}^d$ be an open, bounded set. We assume also that $\partial\Omega$ is Lipschitz continuous, that is, it can be locally represented as the graph of a Lipschitz continuous function. These assumptions allow us to apply Green and Stokes theorems for integrals in Ω.

It is convenient to introduce the notation of a multi-index,

$$\boldsymbol{\alpha} = (\alpha_1, \alpha_2, \ldots, \alpha_d),\ \alpha_i \in \mathbb{N} \quad \text{and} \quad |\boldsymbol{\alpha}| \doteq \sum_{i=1}^{d} \alpha_i. \tag{2.1}$$

This multi-index used to abbreviate the notation of derivatives of functions and distributions, by

$$D^{\boldsymbol{\alpha}}\varphi \doteq \frac{\partial^{|\boldsymbol{\alpha}|}\varphi}{\partial x^{\alpha_1}\partial x^{\alpha_2}\cdots\partial x^{\alpha_d}}. \tag{2.2}$$

The set $L^2(\Omega)$ is defined to be the space of Lebesgue-measurable functions $u\colon \Omega \to \mathbb{R}$ such that $\int_\Omega u^2 d\lambda < \infty$, where λ is the usual Lebesgue measure. It can be shown that $L^2(\Omega)$ is a Hilbert space, with inner product

$$(u, v) \doteq \int_\Omega uv\, d\lambda,\ \forall u, v \in L^2(\Omega). \tag{2.3}$$

Let also $\mathcal{D}(\overline{\Omega})$ be the space of infinitely differentiable functions with compact support in Ω. By support of a function u we mean

$$\operatorname{supp}(u) \doteq \overline{\{x \in \Omega |\, u(x) \neq 0\}}. \tag{2.4}$$

Its topology is defined in such a way that the convergence of a sequence has the meaning that $\{\phi_j\}_j$, $\phi_j \in \mathcal{D}(\overline{\Omega})$ converges to $\phi \in \mathcal{D}(\overline{\Omega})$ when

(i) there exists an open set K, such that $\overline{K} \subset \Omega$, $\overline{K}$ compact in $\mathbb{R}^d$ with $\operatorname{supp}(\phi_j - \phi) \subset K$, $\forall j$, and

(ii) $\lim_{j\mapsto\infty} D^{\boldsymbol{\alpha}}\phi_j(\mathbf{x}) = D^{\boldsymbol{\alpha}}\phi(\mathbf{x})$ uniformly on K above $\forall\boldsymbol{\alpha}$,

and that a linear functional T is continuous if, and only if, $T(\varphi_j) \to T(\varphi)$ when the convergence as above happens. Its topological dual $\mathcal{D}'(\Omega)$ is called the *space of distributions*, and the convergence $T_j \to T$ means $T_j(\phi) \to T(\phi)$ in $\mathbb{R}$ for all $\phi \in \mathcal{D}(\overline{\Omega})$ (weak-* topology).

Let $L \in \mathcal{D}'(\Omega)$ be a distribution and $\boldsymbol{\alpha}$, a multi-index. The derivative $D^{\boldsymbol{\alpha}} L \in \mathcal{D}'(\Omega)$, in the sense of distributions, is defined as

$$\langle D^{\boldsymbol{\alpha}} L, v\rangle \doteq (-1)^{|\boldsymbol{\alpha}|}\langle L, D^{\boldsymbol{\alpha}} v\rangle, \quad \forall v \in \mathcal{D}(\Omega) \tag{2.5}$$

The family of Sobolev spaces we shall use are the

$$H^k(\Omega) \doteq \{v \in L^2(\Omega) | D^{\boldsymbol{\alpha}} v \in L^2(\Omega) \quad \forall \boldsymbol{\alpha}, |\boldsymbol{\alpha}| \leq k\}, \tag{2.6}$$

with norms and seminorms

$$||v||_{k,\Omega} \doteq \left(\sum_{|\boldsymbol{\alpha}|\leq k} ||D^{\boldsymbol{\alpha}} v||^2_{L^2(\Omega)}\right), \quad |v|_{k,\Omega} \doteq \left(\sum_{|\alpha|=k} ||D^{\alpha} v||^2_{L^2(\Omega)}\right). \tag{2.7}$$

They are Hilbert spaces with inner product

$$(w, v)_{k,\Omega} \doteq \sum_{|\boldsymbol{\alpha}|\leq k} (D^{\boldsymbol{\alpha}} w, D^{\boldsymbol{\alpha}} v)_{L^2(\Omega)}. \tag{2.8}$$

When a function depends on space and time, for instance $v(t, \mathbf{x})$, with $(t, \mathbf{x}) \in Q_T \doteq (0, T) \times \Omega$, we might consider the spaces

$$L^p(0, T; H^k(\Omega)) \doteq \left\{v\colon (0, T) \to H^k(\Omega) |\, v \text{ is measurable and } \int_0^T ||v(t)||^p_{k,\Omega} dt < \infty\right\} \tag{2.9}$$

with norm

$$||v||_{L^p(0,T;H^k(\Omega))} \doteq \left(\int_0^T ||v(t)||^p_{k,\Omega} dt\right)^{1/p}. \tag{2.10}$$

When dealing with partial differential equations, it is important to be able to define suitable boundary conditions. However, $\partial\Omega$ has Lebesgue-measure zero in Ω, which means that imposing that a function u in $L^2(\Omega)$ or $H^k(\Omega)$ is equal to another on the boundary might not make sense unless u is continuous. In the general case, the following theorem is very important to allow for these boundary conditions. It uses $H^s(\Omega)$ spaces, with $s \in \mathbb{R}$, which generalise the ones we just defined, through a definition using Fourier transforms. We shall not define them here, and refer to the references from the beginning of this section.

Theorem 2.1 (Trace theorem). Let Ω be a bounded open set of $\mathbb{R}^d$ with Lipschitz continuous boundary $\partial\Omega$ and let $s > 1/2$.

1. There exists a unique linear continuous map $\gamma_0\colon H^s(\Omega) \to H^{s-1/2}(\partial\Omega)$ such that $\gamma_0 v = v|_{\partial\Omega}$ for each $v \in H^s(\Omega) \cap C^0(\overline{\Omega})$.

2. There exists a linear continuous map $\mathcal{R}_0 \colon H^{s-1/2}(\partial\Omega) \to H^s(\Omega)$ such that $\gamma_0 \mathcal{R}_0 \varphi = \varphi$ for each $\varphi \in H^{s-1/2}(\partial\Omega)$.

The same is true for the trace γ_Σ over a Lipschitz continuous subset Σ of the boundary $\partial\Omega$.

The important observation from this theorem is that the functions restricted to $\partial\Omega$ or parts of it have less regularity.

Lastly, we recall a useful theorem.

Theorem 2.2 (Gronwall Lemma). (QUARTERONI, 2016) Let $A \in L^1(t_0, T)$ be a non-negative function, φ a continuous non-negative function in $[t_0, T]$, and g a non-negative constant, such that

$$\varphi^2(t) \leq g + \int_{t_0}^{t} A(\tau)\varphi(\tau)d\tau, \quad \forall t \in [t_0, T]. \tag{2.11}$$

Then,

$$\varphi(t) \leq \sqrt{(g)} + \frac{1}{2}\int_{t_0}^{t} A(\tau)d\tau, \quad \forall t \in [t_0, T]. \tag{2.12}$$

2.2 THE FRAMEWORK OF CONTINUUM MECHANICS

This section is mostly based on Formaggia, Quarteroni, and Veneziani (2009) and Gurtin (1981), which contain these fundamental theorems and their proofs.

The approach of continuum mechanics is similar to that of thermodynamics, in the sense that we study macroscopic phenomena on a body $\mathcal{B}$ of a certain material. We thus assume that the functions of study, such as velocity, pressure and traction, are defined on a continuum. Such assumption is usually called the *continuum hypothesis*. In this way, every point in space is treated as a volume element, containing enough molecules for the study of its macroscopic properties.

The macroscopic setting also allows us to divide the forces acting on the material as

1. body/long range forces f_v: like gravity, they act on all elements of the material;

2. contact/short-range forces f_s: like traction on boundaries, that act on a surface of the material.

Its reasoning from physics can be seen at Batchelor (2000) and Landau and Lifshitz (1970).

Lastly, we postulate that contact forces can be described in a unified manner as a tensor field $\mathbf{S} \colon \mathcal{B} \times \mathbb{R}^{3\times3} \to \mathbb{R}^{3\times3}$, that provides us with the traction $\mathbf{T} \in \mathbb{R}^3$ on a point $\mathbf{x}$ of a (fictitious) surface inside $\mathcal{B}$, with normal vector $\mathbf{n}$: $\mathbf{T}(\mathbf{x}) = \mathbf{S}(\mathbf{x}, \mathbf{n})$. This is also known as the *Cauchy's hypothesis*.

We shall now quickly present the basics of continuum mechanics, starting with kinematics, i. e., the description of movement, and later dynamics, i. e., the study of what causes this movement.

2.2.1 Kinematics

To begin the description of movement, we choose a time t, usually denoted as t_0, and use the position of elements $\hat{\mathbf{x}} \in \mathbb{R}^3$ of the body $\mathcal{B}$ at t_0 as a reference. The set of elements $\widehat{\Omega} \subset \mathbb{R}^3$ is called the reference configuration. Thus,

$$\widehat{\Omega} = \{\hat{\mathbf{x}} \in \mathbb{R}^3;\ \hat{\mathbf{x}} \text{ is the position in space of a material element of } \mathcal{B} \text{ at time } t_0\}.$$

We can then define a time-dependent function, from time t_0 until a time $\widetilde{t}$, called the *motion function*, $\varphi\colon \widehat{\Omega}\times[t_0,\widetilde{t}] \to \mathbb{R}^d$, that describes the movement of the material elements in time, from the reference $\widehat{\Omega}$. Hence, for fixed t, we may denote as $\varphi_t(\hat{\mathbf{x}}) \doteq \varphi(\hat{\mathbf{x}}, t)$ the *deformation function at time t* that indicates where the material element $\hat{\mathbf{x}}$ was moved to in time t. Both physics and analysis impose different requirements for φ. For instance, the simplest requirement is that $\det\nabla_{\hat{\mathbf{x}}}\varphi_t > 0$ for all t, since $\det\nabla_{\hat{\mathbf{x}}}\varphi_t = 0$ would mean that the material would locally vanish and $\det\nabla_{\hat{\mathbf{x}}}\varphi_t < 0$ implies a change in orientation of the body.

Once we have defined the deformation function, we can define the *displacement* vector field $\widehat{\boldsymbol{\eta}}\colon \widehat{\Omega} \times [t_0,\widetilde{t}] \to \mathbb{R}^d$,

$$\widehat{\boldsymbol{\eta}}(\hat{\mathbf{x}}, t) \doteq \varphi(\hat{\mathbf{x}}, t) - \hat{\mathbf{x}}. \tag{2.13}$$

Remark. While it is more logical to define first the deformation function and then the displacement vector using φ, it is the opposite that happens in numerical methods. We calculate $\widehat{\boldsymbol{\eta}}$ and use it to calculate φ when necessary.

The velocity of a material element $\hat{\mathbf{x}}$ in time is straightforward,

$$\widehat{\mathbf{v}} \doteq \frac{\partial \widehat{\mathbf{u}}}{\partial t}. \tag{2.14}$$

The description of change in lengths, areas and volumes is given by the *deformation gradient* at a time t,

$$\widehat{\mathbf{F}}(\hat{\mathbf{x}}, t) \doteq \nabla_{\hat{\mathbf{x}}}\varphi_t. \tag{2.15}$$

It is also convenient to denote it as $\widehat{\mathbf{F}}_t$, when we fix a time t. We also consider its Jacobian,

$$\widehat{J}_t = \det(\widehat{\mathbf{F}}_t), \tag{2.16}$$

which can also be denoted as $\widehat{J}(\hat{\mathbf{x}}, t) \doteq \widehat{J}_t$.

Calculations, detailed in the references we gave in the beginning of the chapter, lead to the relationship between differentials,

$$||d\mathbf{x}|| = \sqrt{d\hat{\mathbf{x}}^T \widehat{\mathbf{F}}_t^T \widehat{\mathbf{F}}_t d\hat{\mathbf{x}}}. \tag{2.17}$$

Therefore, it might be interesting to define a tensor field

$$\mathbf{C}_t \doteq \widehat{\mathbf{F}}_t^T \widehat{\mathbf{F}}_t, \tag{2.18}$$

called the *right Cauchy-Green* tensor of the deformation.

As expected, $\widehat{J}_t$ is crucial for changes of variables in integrals, as for any $V \subset \widehat{\Omega}$ and fixed t,

$$\text{vol}(V) = \int_V d\mathbf{x} = \int_{\widehat{V}} \widehat{J}_t(\hat{\mathbf{x}}) d\hat{\mathbf{x}}. \tag{2.19}$$

Also, by the chain rule, we can push-forward any (regular enough) $\hat{f}\colon \widehat{\Omega} \to \mathbb{R}$ into $f\colon \Omega_t \to \mathbb{R}$, by $f(x) = \hat{f} \circ \varphi_t^{-1}(\mathbf{x})$ and $\nabla \hat{f} = \nabla \varphi_t \nabla f$.

Another important tensor field is the *strain rate tensor*

$$\mathbf{D}(\mathbf{u})_{ij} \doteq \frac{1}{2}\left(\frac{\partial u_i}{\partial x_j} + \frac{\partial u_j}{\partial x_i}\right), \tag{2.20}$$

or, written in compact form,

$$\mathbf{D}(\mathbf{u}) = \frac{1}{2}(\nabla \mathbf{u} + (\nabla \mathbf{u})^T). \tag{2.21}$$

Lastly, we define the *Green-Lagrange Strain tensor*,

$$\widehat{\mathbf{E}} \doteq \frac{1}{2}\left(\widehat{\mathbf{F}}^T \widehat{\mathbf{F}} - \mathbf{I}\right) = \frac{1}{2}(\nabla_{\hat{\mathbf{x}}} \widehat{\boldsymbol{\eta}} + (\nabla_{\hat{\mathbf{x}}} \widehat{\boldsymbol{\eta}})^T) + \frac{1}{2}(\nabla_{\hat{\mathbf{x}}} \widehat{\boldsymbol{\eta}})^T \nabla_{\hat{\mathbf{x}}} \widehat{\boldsymbol{\eta}}. \tag{2.22}$$

The transformation below makes it easier to "transfer" tensors from the reference to the Ω_t configuration.

Definition 2.3. Let $\boldsymbol{\sigma}\colon \Omega_t \to \mathbb{R}^{3\times 3}$ be a smooth tensor field on Ω_t. Its first Piola transform is the tensor field $\widehat{\boldsymbol{\Pi}}\colon \widehat{\Omega} \to \mathbb{R}^{3\times 3}$ defined as

$$\widehat{\boldsymbol{\Pi}}(\hat{\mathbf{x}}) \doteq \widehat{J}_t(\hat{\mathbf{x}}) \boldsymbol{\sigma}(\varphi(\hat{\mathbf{x}})) \widehat{\mathbf{F}}_t^{-T}(\hat{\mathbf{x}}). \tag{2.23}$$

We may recover $\boldsymbol{\sigma}$ from $\widehat{\boldsymbol{\Pi}}$ by the formula

$$\boldsymbol{\sigma}(\mathbf{x}) = \hat{J}_t^{-1}(\varphi^{-1}(\mathbf{x})) \widehat{\boldsymbol{\Pi}}(\varphi^{-1}(\mathbf{x})) \mathbf{F}_t^T(\varphi^{-1}(\mathbf{x})). \tag{2.24}$$

Its advantage is the

Proposition 2.4. (FORMAGGIA; QUARTERONI; VENEZIANI, 2009) Under sufficient regularity of $\boldsymbol{\sigma}$,

$$\text{div}\, \widehat{\boldsymbol{\Pi}} = \widehat{J}\, \text{div}\, \boldsymbol{\sigma}. \tag{2.25}$$

Corollary 2.5.(FORMAGGIA; QUARTERONI; VENEZIANI, 2009) For $V \subset \Omega_t$ sufficiently regular,

$$\int_{\partial \widehat{V}} \hat{\mathbf{\Pi}} \hat{\mathbf{n}} \, d\hat{\boldsymbol{\gamma}} = \int_{\partial V} \boldsymbol{\sigma} \mathbf{n} \, d\boldsymbol{\gamma}. \tag{2.26}$$

This comes in handy when we want to describe the behaviour of the material. Instead of observing what one material element does in time, we observe which elements pass through a point in space. Those points of view are called Lagrangian and Eulerian, respectively.

Another convenient definition is the *material time derivative,*

Definition 2.6. Let $q\colon \Omega(t) \to \mathbb{R}$ be a scalar field. Its material time derivative is defined as

$$\frac{Dq}{Dt}(\cdot, t) = \frac{\partial \widehat{q}}{\partial t}(\cdot, t) \circ \varphi_t^{-1}. \tag{2.27}$$

We now recall some useful properties in tensor analysis.

Proposition 2.7. (GURTIN, 1981, p. 30) Let ψ, $\mathbf{v}$, $\mathbf{w}$ and $\mathbf{S}$ be smooth fields with ψ scalar valued, $\mathbf{v}$ and $\mathbf{w}$ vector valued, and $\mathbf{S}$ tensor valued. Then

1. $\nabla(\psi \mathbf{v}) = \psi \nabla \mathbf{v} + \mathbf{v} \otimes \nabla \psi$;
2. $\operatorname{div}(\psi \mathbf{v}) = \psi \operatorname{div} \mathbf{v} + \mathbf{v} \cdot \nabla \psi$;
3. $\nabla(\mathbf{v} \cdot \mathbf{w}) = (\nabla \mathbf{w})^T \mathbf{v} + (\nabla \mathbf{v})^T \mathbf{w}$;
4. $\operatorname{div}(\psi \mathbf{S}) = \psi \operatorname{div} \mathbf{S} + \mathbf{S} \nabla \psi$.

Proposition 2.8 (Reynolds transport theorem). (GURTIN, 1981, p. 78) Let $V(t) \subset \Omega_t$ be a material domain, that is, an open subset with a boundary with enough regularity, and $f\colon \Omega_t \to \mathbb{R}$ a continuously differentiable field. Then

$$\frac{d}{dt} \int_{V(t)} f \, d\mathbf{x} = \int_{V(t)} \left(\frac{Df}{Dt} + f \operatorname{div} \mathbf{u} \right) d\mathbf{x} = \int_{V(t)} \left(\frac{\partial f}{\partial t} + \operatorname{div}(f \mathbf{u}) \right) d\mathbf{x}. \tag{2.28}$$

2.2.2 Dynamics

We now come to the study of dynamics. The basic tool we need is that of a conservation law, taken from Newtonian mechanics. In particular, we use explicitly two: (RICHTER, 2017, p. 24)

1. *Conservation of mass.* The mass of a part of the body is independent of deformation in time.

2. *Conservation of linear momentum.* It is the second Newton's Law: the linear momentum on a part of the body equals the sum of forces acting on it.

The conservation of angular momentum is used in constitutive theories, and the conservation of energy is considered when we need an extra equation. This happens, for instance, when a fluid is compressible.

Proposition 2.9. Assuming conservation of mass, we have that

$$\frac{\partial \rho}{\partial t} + \nabla \cdot (\rho \mathbf{u}) = 0 \text{ in } \Omega_t, \quad \text{and} \quad \frac{\partial}{\partial t}(\widehat{J}\widehat{\rho}) = 0, \text{ in } \widehat{\Omega}. \tag{2.29}$$

Proof. The conservation of mass states that, during the movement, for any subset of materials $V \subset \hat{\Omega}$, its mass must be constant in time. Thus, $\text{mass}(V_t) = \text{cte}$, $\forall t$. Using the Reynolds transport theorem,

$$0 = \frac{d}{dt}\int_{V_t} \rho d\mathbf{x} = \int_{V_t} \left(\frac{\partial \rho}{\partial t} + \nabla \cdot (\rho \mathbf{u}) \right) d\mathbf{x}. \tag{2.30}$$

Hence,

$$\int_{V_t} \left(\frac{\partial \rho}{\partial t} + \nabla \cdot (\rho \mathbf{u}) \right) d\mathbf{x} = 0. \tag{2.31}$$

Using a localization argument, we find that

$$\frac{\partial \rho}{\partial t} + \nabla \cdot (\rho \mathbf{u}) = 0, \text{ in } \Omega_t. \tag{2.32}$$

We may also write this equation in the reference domain, using $\widehat{J}$. We get

$$0 = \frac{d}{dt}\int_{V(t)} \rho \, d\mathbf{x} = \frac{d}{dt}\int_{\widehat{V}} \widehat{J}\widehat{\rho} \, d\hat{\mathbf{x}} = \int_{\widehat{V}} \frac{\partial(\widehat{J}\widehat{\rho})}{\partial t} d\hat{\mathbf{x}}. \tag{2.33}$$

Therefore,

$$\frac{\partial}{\partial t}(\widehat{J}\widehat{\rho}) = 0. \quad //// \tag{2.34}$$

Proposition 2.10. Assuming conservation of linear momentum, we have that

$$\rho \frac{\partial \mathbf{u}}{\partial t} + \rho(\mathbf{u} \cdot \nabla)\mathbf{u} - \text{div}\boldsymbol{\sigma} = \rho \mathbf{f}, \text{ on } \Omega_t, \tag{2.35}$$

or

$$\widehat{J}\widehat{\rho}\frac{\partial^2 \widehat{\boldsymbol{\eta}}}{\partial t^2} - \widehat{J}\widehat{\text{div}\boldsymbol{\sigma}} = \widehat{J}\widehat{\rho}\widehat{\mathbf{f}}, \text{ on } \widehat{\Omega}. \tag{2.36}$$

Proof. By writing the Second Newton's Law,

$$\int_{V(t)} \rho \frac{D\mathbf{u}}{Dt} dV = \int_{V(t)} \rho F_v dV_t + \int_{\partial V(t)} \boldsymbol{\sigma} \cdot \mathbf{n}\, dS \tag{2.37}$$

$$= \int_{V(t)} \rho F_v dV_t + \int_{V(t)} \operatorname{div} \boldsymbol{\sigma}\, dV \tag{2.38}$$

From it, we get the two possible forms for the continuity of linear momentum. The conservative one reads

$$\frac{\partial(\rho \mathbf{u})}{\partial t} + \operatorname{div}(\rho \mathbf{u} \otimes \mathbf{u} - \boldsymbol{\sigma}) = \rho \mathbf{f}, \tag{2.39}$$

and the other is

$$\rho \frac{\partial \mathbf{u}}{\partial t} + \rho(\mathbf{u} \cdot \nabla)\mathbf{u} - \operatorname{div} \boldsymbol{\sigma} = \rho \mathbf{f}. \tag{2.40}$$

We can also find this equation in the reference domain, using change of variables in the integrals,

$$\frac{d}{dt} \int_{\widehat{V}} \widehat{J}\widehat{\rho} \frac{\partial \widehat{\boldsymbol{\eta}}}{\partial t} d\hat{\mathbf{x}} - \int_{\widehat{V}} \widehat{J} \widehat{\operatorname{div} \boldsymbol{\sigma}}\, d\hat{\mathbf{x}} = \int_{\widehat{V}} \widehat{J}\widehat{\rho}\widehat{\mathbf{f}}\, d\hat{\mathbf{x}}. \tag{2.41}$$

Thus,

$$\widehat{J}\widehat{\rho} \frac{\partial^2 \widehat{\boldsymbol{\eta}}}{\partial t^2} - \widehat{J} \widehat{\operatorname{div} \boldsymbol{\sigma}} = \widehat{J}\widehat{\rho}\widehat{\mathbf{f}}. \quad //// \tag{2.42}$$

However, $\widehat{\operatorname{div} \boldsymbol{\sigma}}$ is unsatisfactory, so it is replaced by $\operatorname{div}_{\hat{\mathbf{x}}} \widehat{\boldsymbol{\Pi}}$, where $\widehat{\boldsymbol{\Pi}}$ is the Piola transform of $\boldsymbol{\sigma}$. This last tensor is called *first Piola-Kirchhoff tensor* (FORMAGGIA; QUARTERONI; VENEZIANI, 2009). Since it is not symmetric, we define a *second Piola-Kirchhoff tensor*, by $\widehat{\boldsymbol{\Sigma}} \doteq \widehat{\mathbf{F}}^{-1} \widehat{\boldsymbol{\Pi}}$, which is symmetric and thus more suitable for discussions on constitutive rules.

Finally, we still need the internal description of dynamics, given by constitutive relations. They are what indicates how $\boldsymbol{\sigma}$ is connected to $\boldsymbol{\eta}$ or $\mathbf{u}$.

2.3 INCOMPRESSIBLE NEWTONIAN FLUIDS

We'll describe only incompressible Newtonian fluids. Therefore, we do not need energy-related equations and the system is somewhat simplified. We take the general system from the previous section and add the following equations. The first is its constitutive relation (BATCHELOR, 2000)

$$\boldsymbol{\sigma} \doteq -P\mathbf{I} + 2\mu(\mathbf{D}(\mathbf{u})), \text{ in } \Omega_t, \tag{2.43}$$

with viscosity coefficient μ, and the second is the incompressibility condition

$$\frac{\partial \rho}{\partial t} = 0, \text{ in } \Omega_t. \tag{2.44}$$

The system of equation for the fluid can be written as

$$\begin{cases} \rho\dfrac{\partial \mathbf{u}}{\partial t} + \rho(\mathbf{u}\cdot\nabla)\mathbf{u} + \nabla P - 2\,\mathrm{div}(\mu\mathbf{D}(\mathbf{u})) = \rho\mathbf{f} \\ \nabla\cdot\mathbf{u} = 0 \end{cases} \quad \text{in } \Omega_t. \tag{2.45}$$

We must then prescribe conditions to guarantee the existence and uniqueness of a solution. We require an initial condition for the velocity, $\mathbf{u}(\mathbf{x}, t_0) = \mathbf{u}_0(\mathbf{x}), \quad \forall \mathbf{x} \in \Omega$. Moreover, we may divide the boundary of Ω_t into $\partial\Omega_t = \Gamma_N \cup \Gamma_D \cup \Gamma_R$, to apply some boundary conditions. They can be the Neumann condition (applied stresses),

$$\boldsymbol{\sigma}\cdot\mathbf{n} = \mathbf{h} \text{ on } \Gamma_N, \tag{2.46}$$

the Dirichlet condition (prescribed velocity)

$$\mathbf{u} = \mathbf{g} \text{ on } \Gamma_D, \tag{2.47}$$

or the Robin condition

$$\alpha\mathbf{u} + \gamma\sigma\mathbf{n} = \mathbf{0} \text{ on } \Gamma_R, \tag{2.48}$$

where α and γ are chosen coeficients.

Since our example will have a Neumann condition, we do not need to worry about additional conditions for the uniqueness of the solution, such as requiring that the average pressure is equal to zero (QUARTERONI; VALLI, 1994).

The weak formulation for the fluid problem will be discussed ahead.

2.4 ISOTROPIC STRUCTURES

The class of structures in this work are restricted to isotropic elastic or hyperelastic materials. They can be defined by constraints to their constitutive relations, as below.

Definition 2.11. An isotropic structure is one in which its response to deformation $\boldsymbol{\eta}$ is independent of the direction of stress $\boldsymbol{\sigma}$. It is called *homogeneous* if the response is independent of $\mathbf{x}$.

Definition 2.12. An elastic material is one in which the stress $\boldsymbol{\sigma}$ depends on the deformation, but not on time.

Definition 2.13. A hyperelastic material is one in which the *second Piola-Kirchhoff tensor* $\widehat{\boldsymbol{\Sigma}}$ is written as the derivative of another function $W\colon \mathbb{R}^{3\times3} \to \mathbb{R}^{+}$, called the density of elastic energy.

$$\widehat{\boldsymbol{\Sigma}}(\widehat{\mathbf{E}}) = \frac{\partial W}{\partial \widehat{\mathbf{E}}}(\widehat{\mathbf{E}}), \quad \widehat{\Sigma}_{ij} = \frac{\partial W}{\partial \widehat{E}_{ij}} \tag{2.49}$$

In this case, the modelling of the structure is given by W. For instance, a classical material is the Saint-Venant-Kirchhoff model,

$$W(\widehat{\mathbf{E}}) = \frac{L_1}{2}(\operatorname{tr}\widehat{\mathbf{E}})^2 + L_2 \operatorname{tr}\widehat{\mathbf{E}}^2, \tag{2.50}$$

in which L_1 and L_2 have an experimental meaning (LANDAU; LIFSHITZ, 1970).

Deciding adequate models for constitutive relations is a research field in itself. Many times, we can simplify the equations by assuming that the displacement is small and around an equilibrium (unstressed) configuration. In this way, it is possible to talk about a linear elasticity problem.

2.4.1 Weak formulation

We first define the space of test functions we are working with,

$$\mathcal{V} = [H^1_{\Gamma_D}(\widehat{\Omega}_s)]^3 = \{\widehat{\mathbf{v}} \in [H^1(\widehat{\Omega})]^3 : \widehat{\mathbf{v}} = \mathbf{0} \text{ on } \widehat{\Gamma}_D\}. \tag{2.51}$$

The Dirichlet condition is treated through a lifting technique. We consider the lifting of $g_{s,D} \in H^{1/2}(\widehat{\Omega}_s)$ to $G \in H^1(\widehat{\Omega}_s)$. Then, a weak formulation for our problem can be: we want to find, for each $t > 0$, $\widehat{\boldsymbol{\eta}}(t) = \breve{\boldsymbol{\eta}}(t) + G(t)$, with $\breve{\boldsymbol{\eta}}(t) \in \mathcal{V}$ such that, for all $\widehat{\mathbf{v}} \in \mathcal{V}$,

$$\int_{\widehat{\Omega}} \widehat{\rho}_{s,0} \frac{\partial^2 \breve{\boldsymbol{\eta}}}{\partial t^2} \cdot \widehat{\mathbf{v}} + a(\breve{\boldsymbol{\eta}}, \widehat{\mathbf{v}}) = F(\widehat{\mathbf{v}}), \tag{2.52}$$

$$a(\breve{\boldsymbol{\eta}}, \widehat{\mathbf{v}}) = \int_{\widehat{\Omega}} \widehat{\boldsymbol{\Pi}} : \widehat{\mathbf{v}}\, d\Omega, \quad F(\widehat{\mathbf{v}}) = \int_{\widehat{\Omega}} \widehat{\mathbf{f}} \cdot \widehat{\mathbf{v}}\, d\Omega + \int_{\widehat{\Gamma}_N} \hat{\mathbf{h}} \cdot \widehat{\mathbf{v}}\, d\widehat{\gamma}, \tag{2.53}$$

where $\widehat{\rho}_{s,0} \doteq \widehat{J}\widehat{\rho}$ and $\mathbf{T} : \mathbf{S}$ is the inner product in the tensor field space.

The regularity of the solid problem is of major importance for the FSI problem, to guarantee the well-posedness of the coupling conditions. Such conditions require the existence of trace spaces on the boundary for the velocity of the structure. Since $\widehat{\boldsymbol{\eta}} \in H^1(\widehat{\Omega}_s)$, its derivative is well-defined, but it may not be regular enough — $H^1(\widehat{\Omega})$, for instance — for its trace to exist on the interface $\widehat{\Gamma}$ (RICHTER, 2017).

2.5 ALE COUPLING

We describe here one approach towards the coupling of the equations. The main difficulty is how to describe the movement of the domains, with the coupling conditions. For example, the time discretization might not make sense when one describes function spaces that are different in time. How would one interpret $u(t+h) - u(t)$ if they are in different spaces (RICHTER, 2017)? One way to do this is by the *Arbitrary Lagrangian-Eulerian* (ALE) approach, which we now describe.

2.5.1 ALE mapping

The ALE approach is conceptually simple, and was first presented in Hirt, Amsden, and Cook (1974). We define a new time-dependent domain ω_t, with reference to a domain ω_0. Usually, $\omega_0 = \widehat{\Omega}_f$. In this work, we consider this to be the case. Such new domain is described by a new variable in our system of PDEs, called the fluid domain's velocity $\mathbf{w}\colon \Omega_t \to \mathbb{R}^3$.

The coupling between the solid and fluid on an interface $\Gamma_t = \Omega_t^f \cap \Omega_t^s$ gives us the value of $\mathbf{w}$ on Γ_t, that is,

$$\mathbf{w} = \mathbf{u}^s, \quad \text{on } \Gamma_t. \tag{2.54}$$

From there, we must choose how to extend this value for the entire domain ω_t. What is crucial here is $\mathbf{w}$'s regularity. Indeed, as summarised in (RICHTER, 2017), the lack of appropriate regularity for $\mathbf{w}$ will mean that our FSI equations with ALE will not be equivalent to the original problem. Corners in the domain are also very problematic when it comes to such regularity.

That being said, there are two popular ways to extend the interface value to the entire domain. The first is to use a harmonic extension, and the second is a fictitious elasticity problem. A third, safer but rather unfeasible computationally, is the biharmonic problem. Further comparisons are done in Richter (2017).

One of the disadvantages of the ALE approach is when the change in domain results in topological changes as well. When that happens, the ALE mapping will no longer be continuous. For instance, when an immersed ball in a water tank, treated on the fluid domain as a hole, touches the tank's wall, we no longer have a hole in the domain, and its fundamental group changes.

The other disadvantage of the ALE approach is the insertion of another convective term, $\rho(\mathbf{w} \cdot \nabla)\mathbf{u}$, in the fluid equation. This adds, then, added another nonlinearity to the problem.

The notation for functions defined on the ALE domain is the tilde. Thus, $\widetilde{\boldsymbol{\eta}}(\hat{\mathbf{x}}, t)$ is the displacement for the domain point $\hat{\mathbf{x}} \in \widehat{\Omega}$, at time t. It is given by a new motion function $\widetilde{\mathcal{A}}\colon \widehat{\Omega} \times \mathbb{R}^+ \to \mathbb{R}^d$. The velocity of this motion is calculated by

$$\widetilde{w}(\hat{\mathbf{x}}, t) = \frac{\partial \widetilde{\mathcal{A}}}{\partial t}(\hat{\mathbf{x}}, t). \tag{2.55}$$

Analogous to the material derivative is the definition of an ALE derivative.

Definition 2.14. Let $q\colon \omega_t \to \mathbb{R}$. Its ALE time-derivative is defined as

$$\frac{\partial q}{\partial t|_{\widetilde{\mathcal{A}}}} \doteq \frac{d}{dt} q(\widetilde{\mathcal{A}}(\hat{\mathbf{x}}, t), t). \tag{2.56}$$

It also leads to a transport formula (FORMAGGIA; QUARTERONI; VENEZIANI, 2009).

Proposition 2.15 (ALE transport formula).

$$\frac{d}{dt}\int_{\omega_0(t)} f\,d\mathbf{x} = \int_{\omega_0(t)} \left(\frac{\partial}{\partial t}|_{\widetilde{\mathcal{A}}} f + f\,\mathrm{div}\,\mathbf{w}\right) d\mathbf{x} = \int_{\omega_0(t)} \left(\frac{\partial f}{\partial t} + \mathrm{div}(f\mathbf{w})\right) d\mathbf{x} \tag{2.57}$$

Using this theorem, the Navier-Stokes system becomes

$$\begin{cases} \rho\dfrac{\partial \mathbf{u}}{\partial t}|_{\widetilde{\mathcal{A}}} + \rho[(\mathbf{u}-\mathbf{w})\cdot\nabla]\mathbf{u} + \nabla P - 2\,\mathrm{div}(\mu\mathbf{D}(\mathbf{u})) = \rho\mathbf{f}, \\ \mathrm{div}\,\mathbf{u} = 0. \end{cases} \tag{2.58}$$

As previously noted, the point of using the ALE technique is to be able to enforce that the fluid domain, now coinciding with ω_t, has the same velocity in its interface as the velocity of the solid. This is usually called a *geometric coupling condition*, and it means that

$$\widetilde{\mathcal{A}}(\hat{\mathbf{x}}) = \widehat{\varphi}_s(\hat{\mathbf{x}}, 0),\ \text{on}\ \widehat{\Gamma} \quad \text{or} \quad \widetilde{\boldsymbol{\eta}}(\hat{\mathbf{x}}) = \widehat{\boldsymbol{\eta}}(\hat{\mathbf{x}}),\ \text{on}\ \widehat{\Gamma}. \tag{2.59}$$

The physical coupling conditions are the continuity of velocity on the interface,

$$\mathbf{u}_f(\mathbf{x}) = \mathbf{w}(\mathbf{x}) \quad \text{on}\ \Gamma(t), \tag{2.60}$$

and the continuity of stress,

$$\boldsymbol{\sigma}_f \cdot \mathbf{n} = \boldsymbol{\sigma}_s \cdot \mathbf{n}\ \text{on}\ \Gamma(t). \tag{2.61}$$

Considering the initial values as zero, that is, that the system is initially at rest, and considering the following tube domain, with an axial cut, with the gray region as the solid, and the white interior region as the fluid.

FIGURE 1 - Domain for the FSI problem, axial cut

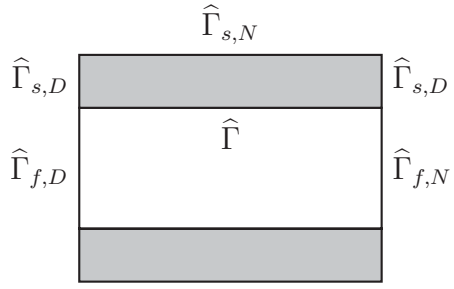

SOURCE: The author (2020).

The full system, with $\widehat{\Gamma}_{s,N} = 0$ and $\widehat{\Gamma}_{s,D} = 0$, becomes

$$\begin{cases} \rho_f \dfrac{\partial \mathbf{u}_f}{\partial t}|_{\widetilde{\mathcal{A}}} + \rho_f(\mathbf{u}_f - \mathbf{w})\cdot\nabla\mathbf{u}_f - \mathrm{div}\boldsymbol{\sigma}_f(\mathbf{u}_f, P) = \mathbf{0} & \text{in} \quad \Omega_f(t) \\ \mathrm{div}\,\mathbf{u}_f = 0 & \text{in} \quad \Omega_f(t) \\ \boldsymbol{\sigma}_f(\mathbf{u}_f, P) = \mathbf{g}_{f,N} & \text{on} \quad \Gamma_{f,N} \\ \mathbf{u} = \mathbf{h}_{f,D} & \text{on} \quad \Gamma_{f,D} \end{cases} \tag{2.62}$$

$$\begin{cases} \widehat{\rho}_{s,0}\dfrac{\partial^2\widehat{\boldsymbol{\eta}}_s}{\partial t^2} - \operatorname{div}_{\hat{\mathbf{x}}}(\widehat{\mathbf{F}}_s\widehat{\boldsymbol{\Sigma}}) = \mathbf{0} \quad \text{in} \quad \widehat{\Omega}_s \\ \widehat{\boldsymbol{\eta}}_s = \mathbf{0} \quad \text{on} \quad \Gamma_{s,D} \\ \widehat{\mathbf{F}}_s\widehat{\boldsymbol{\Sigma}}\hat{\mathbf{n}}_s = \mathbf{0} \quad \text{on} \quad \widehat{\Gamma}_{s,N} \end{cases} \tag{2.63}$$

$$\begin{cases} \widetilde{\boldsymbol{\eta}}_f = \operatorname{Ext}(\widehat{\boldsymbol{\eta}}_s|_{\widehat{\Gamma}}), \quad \Omega_f(t) = \widetilde{\mathcal{A}}(\widetilde{\Omega}_f, t), \quad \widetilde{\mathbf{w}} = \dfrac{\partial\widetilde{\boldsymbol{\eta}}_f}{\partial t} \quad \text{in} \quad \widetilde{\Omega}_f \\ \mathbf{u}_f = \mathbf{w} \quad \text{on} \quad \Gamma(t) \\ \boldsymbol{\sigma}_f \cdot \mathbf{n} = \boldsymbol{\sigma}_s \cdot \mathbf{n} \quad \text{on} \quad \Gamma(t) \end{cases} \tag{2.64}$$

The coupling approach and above and its system of equations were taken from Formaggia, Quarteroni, and Veneziani (2009). Another possible approach is given in Tallec and Mouro (2001), in which the equations of fluid and structure are deduced as two main conservation equations in ALE form and the constitutive equations separate the domain into fluid and structure. The trial spaces are treated differently, and the end result is a Dirichlet-Neumann approach.

2.5.2 Weak formulation

We may now summarise the procedure to find a weak formulation of the coupled problem, from Formaggia, Quarteroni, and Veneziani (2009). To avoid the extra notation needed for the lifting of Dirichlet conditions, they are assumed to be zero.

As test functions for the fluid, we use time-independent functions defined on the reference configurations, $\widehat{\mathbf{v}}_f \colon \widehat{\Omega}_f \to \mathbb{R}^3$ that vanishes on $\Gamma_{f,D}$ and $\widehat{q} \colon \widehat{\Omega}_f \to \mathbb{R}$, for the first and second equations, respectively.

We also use their Eulerian counterparts, $\mathbf{v}_f(\mathbf{x}, t) \doteq \widehat{\mathbf{v}}_f(\widetilde{\mathcal{A}}_t^{-1}(\mathbf{x}))$ and $q(\mathbf{x}, t) \doteq \widehat{q}(\widetilde{\mathcal{A}}_t^{-1}(\mathbf{x}))$. We use the many properties from tensor analysis.

$$\begin{aligned} &\int_{\Omega_f(t)} \rho_f \frac{\partial \mathbf{u}_f}{\partial t}|_{\widetilde{\mathcal{A}}} \cdot \mathbf{v}_f \, d\mathbf{x} + \int_{\Omega_f(t)} \rho_f(\mathbf{u}_f - \mathbf{w}) \cdot \nabla \mathbf{u}_f \cdot \mathbf{v}_f \, d\mathbf{x} \\ &\qquad + \int_{\Omega_f(t)} \boldsymbol{\sigma}(\mathbf{u}_f, P) : \nabla \mathbf{v}_f \, d\mathbf{x} - \int_{\Gamma_{f,N}(t)} \mathbf{g}_{f,N} \cdot \mathbf{v}_f \, d\gamma \\ &\qquad - \int_{\Gamma(t)} \boldsymbol{\sigma}_f(\mathbf{u}_f, P)\mathbf{n}_f \cdot \mathbf{v}_f \, d\gamma + \int_{\Omega_f(t)} q \operatorname{div} \mathbf{u}_f \, d\mathbf{x} = 0 \end{aligned} \tag{2.65}$$

For the solid, we use $\widehat{\mathbf{v}}_s \colon \widehat{\Omega}_s \to \mathbb{R}^3$ that vanishes on $\widehat{\Gamma}_{s,D}$.

$$\int_{\widehat{\Omega}_s} \widehat{\rho}_{s,0} \frac{\partial^2 \widehat{\boldsymbol{\eta}}_s}{\partial t^2} \cdot \widehat{\mathbf{v}}_s \, d\hat{\mathbf{x}} + \int_{\widehat{\Omega}_s} \widehat{\mathbf{F}}_s\widehat{\boldsymbol{\Sigma}} : \nabla_{\hat{\mathbf{x}}}\widehat{\mathbf{v}}_s \, d\hat{\mathbf{x}} - \int_{\widehat{\Gamma}} \widehat{\mathbf{F}}_s\widehat{\boldsymbol{\Sigma}}\hat{\mathbf{n}}_s \cdot \widehat{\mathbf{v}}_s \, d\hat{\gamma} = 0 \tag{2.66}$$

There are only two steps left to be done: we commute the derivative with the integral in the first equation,

$$\int_{\Omega_f(t)} \rho_f \frac{\partial \mathbf{u}_f}{\partial t}|_{\widetilde{\mathcal{A}}} \cdot \mathbf{v}_f d\mathbf{x} = \int_{\widehat{\Omega}_f} \rho_f \widetilde{J}_{\widetilde{\mathcal{A}}} \frac{\partial \widehat{\mathbf{u}}_f}{\partial t} \cdot \widehat{\mathbf{v}}_f \, d\hat{\mathbf{x}} \tag{2.67}$$

$$= \frac{d}{dt} \int_{\widehat{\Omega}_f} \widetilde{J}_{\widetilde{\mathcal{A}}} \rho_f \widehat{\mathbf{u}}_f \cdot \widehat{\mathbf{v}}_f \, d\hat{\mathbf{x}} - \int_{\widehat{\Omega}_f} \widetilde{J}_{\widetilde{\mathcal{A}}} \rho_f \widehat{\mathrm{div}\, \mathbf{w}} \widehat{\mathbf{u}}_f \cdot \widehat{\mathbf{v}}_f \, d\hat{\mathbf{x}} \tag{2.68}$$

$$= \frac{d}{dt} \int_{\Omega_f(t)} \rho_f \mathbf{u}_f \cdot \mathbf{v}_f \, d\mathbf{x} - \int_{\Omega_f(t)} \rho_f \mathrm{div}\, \mathbf{w} \mathbf{u}_f \cdot \mathbf{v}_f \, d\mathbf{x} \tag{2.69}$$

The second step is to change the integral from $\Gamma(t)$ to $\widehat{\Gamma}$, which requires a special property called *Nanson's formula*, described in the reference. We skip such step and report its result,

$$\int_{\Gamma(t)} \boldsymbol{\sigma}_f(\mathbf{u}_f, P)\mathbf{n}_f \cdot \mathbf{v}_f \, d\gamma = \int_{\widehat{\Gamma}} \widetilde{J}_{\widetilde{\mathcal{A}}} \widetilde{\boldsymbol{\sigma}(\mathbf{u}_f, P)} \widetilde{\mathbf{F}}^{-T}_{\widetilde{\mathcal{A}}} \hat{\mathbf{n}}_f \cdot \widehat{\mathbf{v}}_f \, d\hat{\gamma}. \tag{2.70}$$

Finally, the whole weak formulation reads: find $\widehat{\mathbf{u}}_f \colon \widehat{\Omega}_f \times \mathbb{R}^+ \to \mathbb{R}^3$, $\widehat{P} \colon \widehat{\Omega}_f \times \mathbb{R}^+ \to \mathbb{R}$, $\widetilde{\boldsymbol{\eta}}_f \colon \widehat{\Omega}_f \times \mathbb{R}^+ \to \mathbb{R}^3$ and $\widehat{\boldsymbol{\eta}} \colon \widehat{\Omega}_s \times \mathbb{R}^+ \to \mathbb{R}^3$ such that, for all $(\widehat{\mathbf{v}}_f, \widehat{q}) \in [H^1_{\widehat{\Gamma}_{f,D}}(\widehat{\Omega}_f)]^3 \times L^2(\widehat{\Omega}_f)$ and $\widehat{\mathbf{v}}_s \in [H^1_{\widehat{\Gamma}_{s,D}}(\widehat{\Omega}_s)]^3$ with $\widehat{\mathbf{v}}_f = \mathbf{v}_s$ on $\widehat{\Gamma}$,

$$\begin{aligned}
&\frac{d}{dt} \int_{\Omega_f(t)} \rho_f \mathbf{u}_f \cdot \mathbf{v}_f \, d\mathbf{x} + \int_{\Omega_f(t)} \rho_f (\mathbf{u}_f - \mathbf{w}) \cdot \nabla \mathbf{u}_f \cdot \mathbf{v}_f \, d\mathbf{x} \\
&\qquad - \int_{\Omega_f(t)} \rho_f \mathrm{div}\, \mathbf{w}\, \mathbf{u}_f \cdot \mathbf{v}_f \, d\mathbf{x} + \int_{\Omega_f(t)} \boldsymbol{\sigma}(\mathbf{u}_f, P) : \nabla \mathbf{v}_f \, d\mathbf{x} - \int_{\Gamma_{f,N}(t)} \mathbf{g}_{f,N} \cdot \mathbf{v}_f \, d\gamma \\
&\qquad - \int_{\Gamma_{f,N}(t)} \mathbf{g}_{f,N} \cdot \mathbf{v}_f \, d\gamma + \int_{\Omega_f(t)} q \, \mathrm{div}\, \mathbf{u}_f \, d\mathbf{x} \\
&\qquad + \int_{\widehat{\Omega}_s} \widehat{\rho}_{s,0} \frac{\partial^2 \widehat{\boldsymbol{\eta}}_s}{\partial t^2} \cdot \widehat{\mathbf{v}}_s \, d\hat{\mathbf{x}} + \int_{\widehat{\Omega}_s} \widehat{\mathbf{F}}_s \widehat{\boldsymbol{\Sigma}} : \nabla_{\hat{\mathbf{x}}} \widehat{\mathbf{v}}_s \, d\hat{\mathbf{x}} = 0
\end{aligned} \tag{2.71}$$

3 A REVIEW OF SOME NUMERICAL METHODS FOR FSI

3.1 A SKETCH OF THE FINITE ELEMENT APPROACH

The methods we discuss in this work are all based on the approximation of partial differential equations using Finite Element Methods (FEM). We shall introduce its main ideas very briefly, and refer to the references Quarteroni and Valli (1994) and Ciarlet (2002) for details and this topics' many nuances.

The starting point of the FEM approach is usually the weak formulation of a problem, as developed in the first chapter. For illustration purposes, we denote a generic weak formulation for a stationary PDE on a domain Ω by

$$\text{find } \mathbf{v} \in \mathcal{V} \text{ such that } a(\mathbf{v}, \mathbf{w}) = f(\mathbf{w}),\ \forall \mathbf{w} \in \mathcal{W}.$$

When the PDE is linear, then $a\colon \mathcal{V} \times \mathcal{W} \to \mathbb{R}$ is a bilinear form and $f\colon \mathcal{W} \to \mathbb{R}$ is also linear. This is not the case if the PDE is non-linear, as in more realistic models for fluids and structures.

A *Galerkin approximation* is applied on the equation above: we choose two families $\{V_h\}_h$ and $\{W_h\}_h$ of finite dimensional spaces that are usually required to satisfy $V_h \subset \mathcal{V}$, $W_h \subset \mathcal{W}$, and $\dim V_h = \dim W_h$, $\forall h$. The idea is that, as $h \to 0$, the finite-dimensional space V_h gets also closer to $\mathcal{V}$. The rigorous version of this statement can be found in Quarteroni and Valli (1994).

Once we have these finite dimensional spaces, we choose convenient bases for both, $\{\psi_k\}_{k=1}^m$ for V_h and $\{\varphi_j\}_{j=1}^m$ for W_h. Then, we write $\mathbf{v}_h \in V_h$ as

$$\mathbf{v}_h(\mathbf{x}) = \sum_{i=1}^{m} v_i \varphi_i(\mathbf{x}),\ \forall \mathbf{x} \in \Omega \tag{3.1}$$

or, if the problem is time dependent,

$$\mathbf{v}_h(\mathbf{x}, t) = \sum_{i=1}^{m} v_i(t) \varphi_i(\mathbf{x}),\ \forall \mathbf{x} \in \Omega. \tag{3.2}$$

We replace $\mathbf{v}_h$ written in the basis, as above, on the weak formulation, along with the basis of W_h, to obtain a finite-dimensional system

$$\sum_{i=1}^{m} v_i\, a(\varphi_i, \psi_j) = f(\psi_j), \text{ for } j \in \{1, 2, \ldots, m\}, \tag{3.3}$$

if no time is involved. If the problem is time dependent, the result is a system of ODEs. This process is then called semi-discretisation of the system, and the derivatives act on the coefficients $v_i(t)$. It is then necessary to choose a time discretisation procedure.

Finally, linear PDEs result in linear systems. Nonlinear problems will lead to nonlinear systems that can be solved either by using Newton methods or other optimisation-like procedures.

The finite element method provides a framework to construct the families V_h, W_h and its bases. The first thing to do is to find a *triangulation* $\mathcal{T}_h$ for the domain Ω. For example, when Ω is a polygonal domain,

$$\Omega = \bigcup_{K \in \mathcal{T}_h} K, \tag{3.4}$$

where $K \in \mathcal{T}_h$ have disjoint interiors, and their intersection must be coincide either with one of their nodes or edge. Although it is called a triangulation, K can be all triangular (and similar polyhedrons in higher dimension) or all parallelepipeds (CIARLET, 2002). The parameter h can be chosen in many ways. It can either be the largest diameter of the circle inscribed or circumscribed around the polygons K, or a simple maximum of K's edge sizes. We shall enumerate the nodes in $\mathcal{T}_h$ and denote them by $\mathbf{d}_j$.

On the triangular case, a simple and usual family of spaces defined using $\mathcal{T}_h$ is

$$V_h^k \doteq \{v_h \in C^0(\overline{\Omega}) |\, v_h|K \in \mathbb{P}_k, \forall K \in \mathcal{T}_h\}, \tag{3.5}$$

with $\mathbb{P}_k$ the space of polynomials of degree less than or equal to k. A convenient basis for V_h^k is the *Lagrangian basis* $\{\varphi_j\}_j$, defined as

$$\varphi_i(\mathbf{d}_j) = \delta_{ij}, \quad \forall i, j \in \{1, 2, \ldots, m\}. \tag{3.6}$$

Another important topic is how to deal with the Dirichlet boundary conditions, say $\mathbf{v} = \mathbf{g}$ on $\partial\Omega_D$. We might "interpolate" $\mathbf{g}$ on the triangulated version of $\partial\Omega_D$, by enforcing that $v_i = \mathbf{g}(\mathbf{d}_i)$ on these nodes. Another approach is the Nitzche's approach, which enforces the Dirichlet condition as a penalisation of constant μ on the weak formulation. This amounts to rewriting the equation on the weak formulation as

$$a(\mathbf{v}, \mathbf{w}) + \mu \int_{\partial\Omega_D} (\mathbf{v} - \mathbf{g}) dS = f(\mathbf{w}). \tag{3.7}$$

3.2 OVERVIEW OF THE METHODS

General books about numerical methods for FSI problems include the already mentioned Formaggia, Quarteroni, and Veneziani (2009) and Richter (2017), although the latter focuses on monolithic methods. A survey of partitioned methods is Hou, Wang, and Layton (2012), which also includes immersed-boudary versions.

The classification of numerical methods for FSI problems using the ALE formulation, is still not standard. What may be called a *monolithic method* by one author might not be called as such by another author. Still, there are two popular ways of classifying these methods:

1. Partitioned versus monolithic

2. Loosely coupled versus strongly coupled

Partitioned methods are usually the ones in which there is an explicit separation between the fluid solver and the structure solver, and both might be used as *black boxes* in a staggered fashion, that is, one after the other in an attempt to find the solution to the problem. On the other hand, custom-made algorithms that attempt to solve the FSI problem in unity as a single, big system are called monolithic methods.

TABLE 1 - Partitioned methods

Advantages	Problems
Can use the preexisting methods	Satisfying the coupling
Less use of computer memory	Avoiding the Added-mass effect

SOURCE: The author (2020).

TABLE 2 - Monolithic methods

Advantages	Problems
Easy to enforce strong coupling	Big system of nonlinear equations
Less stability issues	Needs new, expensive methods

SOURCE: The author (2020).

The classification using the coupling condition indicates how precisely that condition is enforced at each time step. Loosely coupled algorithms usually solve the solid and fluid problems only once, using some prediction as well. Strongly coupled methods usually involve iterative methods which solve the subproblems many times to guarantee a better approximation of the coupling condition at a time step and are, thus, more computationally expensive. However, strongly coupled partitioned methods are known to be susceptible to a phenomenon called *added-mass effect* (check *Section 3.5.1*), which may render the method unconditionally unstable even if one reduces the time step.

The possibility to use loosely coupled algorithms depends on the properties of the FSI problem we want to solve. Haemodynamic problems have shown to have issues with stability, and thus loosely-coupled methods are avoided there (FORMAGGIA; QUARTERONI; VENEZIANI, 2009). It is believed, as we shall discuss in the last section of this chapter, that the issue has to do with the closeness of density of the fluid and solid for this type of problem.

We also indicate the possibility to classify methods by how each field is discretised in time, that is, whether they are done implicitly or explicitly. For instance, Fernández and Mullaert (2015) explore the possibility of using extrapolations to linearise parts of the algorithms, and so does Crosetto (2011), which explores the extrapolation on the convective terms of the fluid on the method he called *geometry-convective explicit*.

It is useful to create a special notation for the fluid and structure solvers used as *black-boxes*, and there are at least three popular descriptions for them.

1. *The three-field formulation*

This approach, popular to describe some monolithic methods (CROSETTO, 2011), separates the entire weak formulation from the previous chapter into F, S and G, with the equations as below.

a. Fluid field Using the solid displacement $\widehat{\boldsymbol{\eta}}_s$ and ALE domain displacement $\widetilde{\boldsymbol{\eta}}$, we find $\mathbf{u}_f$ and P for the fluid,

$$F(\mathbf{u}_f, P, \widehat{\boldsymbol{\eta}}_s, \widetilde{\boldsymbol{\eta}}_f) = 0. \tag{3.8}$$

b. Solid field Using the fluid velocity $\mathbf{u}_f$, find the solid displacement $\widehat{\boldsymbol{\eta}}_s$,

$$S(\widehat{\boldsymbol{\eta}}_s, \mathbf{u}_f) = 0. \tag{3.9}$$

c. ALE field Using $\widehat{\boldsymbol{\eta}}_s$, find $\widetilde{\boldsymbol{\eta}}_f$,

$$G(\widetilde{\boldsymbol{\eta}}_f, \widehat{\boldsymbol{\eta}}_s) = 0. \tag{3.10}$$

If needed (for instance, in nonconforming grids), the balance of traction on the interface might be included into one of the equations above.

2. *The Lagrange multiplier approach.*

This approach is also used in monolithic methods, as will be explained in *Section 3.4*. We add another variable $\boldsymbol{\lambda}$ to our problem, either the displacement or interface on the border.

a. $\mathcal{I}(\mathbf{u}_f, P, \widetilde{\boldsymbol{\eta}}_f, \widehat{\boldsymbol{\eta}}_s) = 0$ corresponds to the term on the weak formulation that enforces the interface traction balance, if $\boldsymbol{\lambda}$ is the displacement, or the continuity of velocity, if $\boldsymbol{\lambda}$ represents the traction.

b . $\mathcal{F}(\mathbf{u}_f, P, \widetilde{\boldsymbol{\eta}}_f, \boldsymbol{\lambda}) = 0$ corresponds to the fluid and ALE extension terms.

c. $\mathcal{S}(\widehat{\boldsymbol{\eta}}_s, \boldsymbol{\lambda}) = 0$ corresponds to the solid terms.

3. *The Domain Decomposition approach*

The operators we shall define are called *Dirichlet-to-Neumann* operators, that have a special meaning in the theory of domain decomposition methods. The idea behind these operators is that a solver (fluid or solid) receives a boundary displacement $\boldsymbol{\lambda}$, then it is run to get a solution and finally returns the interface traction from that solution.

S_f is defined as a numerical extension operator that solves the fluid problem and calculation of its ALE domain with the given Dirichlet condition on Γ and returns its traction on that interface,

$$\begin{aligned} S_f \colon \boldsymbol{\lambda} \mapsto \text{find } (\mathbf{u}, p, \widetilde{\mathcal{A}}_t) \text{ for the fluid-ALE problem with } \mathbf{u}|_{\Gamma_t} = \frac{\boldsymbol{\lambda} - \widehat{\boldsymbol{\eta}}^n|_{\widehat{\Gamma}}}{\delta t} \\ \mapsto (\boldsymbol{\sigma}_f(\mathbf{u}, p) \cdot \mathbf{n})|_{\Gamma_t} \end{aligned}$$

Its "inverse" S_f^{-1} is the Neumann-Dirichlet operator, that takes the traction $\boldsymbol{\sigma}$ on the interface to solve the fluid+ALE problem and returns the displacement of the solution on the interface.

We define the same for the solid,

S_s: $\boldsymbol{\lambda} \mapsto$ find $\widehat{\boldsymbol{\eta}}$ for the structure problem with $\widehat{\boldsymbol{\eta}}|_{\widehat{\Gamma}} = \boldsymbol{\lambda} \mapsto \boldsymbol{\sigma}_s(\boldsymbol{\eta}) \cdot \mathbf{n}$,

and its Neumann-Dirichlet operator S_s^{-1}.

3.3 PARTITIONED METHODS

In Tallec and Mouro (2001), foundations are laid to the framework that is now used in partitioned methods. Firstly, the problem is modelled in full as in the previous chapter and divided, as a weak formulation, into the *three fields formulation*. The main issue is to distribute the coupling conditions for these problems. The approach of choice was the Dirichlet-Neumann method, in which the continuity of the velocity is enforced on the fluid subproblem as a Dirichlet condition and the traction problem on the solid as a Neumann condition. A similar method is described in Dettmer and Perić (2005).

3.3.1 Strongly coupled

Deparis, Discacciati, and Quarteroni (2006) summarised the Dirichlet-Neumann strategies using the Domain Decomposition notation.

1. *Fixed point methods*
This is the most popular approach. It can be abstractly written as to find $\boldsymbol{\lambda}$ such that

$$S_s^{-1}(-S_f(\lambda)) = \lambda. \tag{3.11}$$

In practice, a typical loop, at iteration k, is done as

(i) $\boldsymbol{\sigma}^k = S_f(\boldsymbol{\lambda}^k)$: we use the fluid solver with the Dirichlet condition $\boldsymbol{\lambda}^k$ on the interface

(ii) $\overline{\boldsymbol{\lambda}}^k = S_s^{-1}(-\boldsymbol{\sigma}^k)$: we feed that result into the structure solver with Neumann condition on the interface

(iii) $\boldsymbol{\lambda}^{k+1} = \boldsymbol{\lambda}^k + \omega^k(\overline{\boldsymbol{\lambda}}^k - \boldsymbol{\lambda}^k)$: relaxation step

(iv) Check for convergence

One can use Aitken-like choices for ω^k (FORMAGGIA; QUARTERONI; VENEZIANI, 2009)

2. *Newton methods*
First, we write the problem as to find λ such that $\Phi(\lambda) = 0$, where

$$\Phi(\lambda) = S_s^{-1}(-S_f(\lambda)) - \lambda \tag{3.12}$$

Then, we use $D(\lambda)$ = Jacobian matrix of $(S_s^{-1}(-S_f(\lambda)))$. The first two steps of a typical iteration k are the same as in the previous method

(i) $\boldsymbol{\sigma}^k = S_f(\boldsymbol{\lambda}^k)$

(ii) $\overline{\boldsymbol{\lambda}}^k = S_s^{-1}(-\boldsymbol{\sigma}^k)$

(iii) $(D(\boldsymbol{\lambda}^k) - \mathbf{I})\boldsymbol{\mu}^k = -(\overline{\boldsymbol{\lambda}}^k - \boldsymbol{\lambda}^k)$: we must build $D(\boldsymbol{\lambda}^k)$ and solve the linear system

(iv) $\boldsymbol{\lambda}^{k+1} = \boldsymbol{\lambda}^k + \omega^k \boldsymbol{\mu}^k$

(v) Check for convergence

The tricky and expensive part is indeed the calculation of the Jacobian matrix. While it is possible to find the exact formulas for it when we build the fluid and structure algorithms, the point of partitioned methods is also the use of *black-box* solvers. When that is the case, we may have no access to the solvers' internals or the methods are too sophisticated. The calculation of the Jacobian is then likely to be done by finite difference approximations (KÜTTLER; WALL, 2008).

3. *Steklov-Poincaré methods*

We rewrite $S_s^{-1}(-S_f(\boldsymbol{\lambda})) = \boldsymbol{\lambda}$ as

$$S_s(\boldsymbol{\lambda}) + S_f(\boldsymbol{\lambda}) = 0. \tag{3.13}$$

The typical iteration k is

(i) $\boldsymbol{\sigma}_f^k = S_f(\boldsymbol{\lambda}^k)$

(ii) $\boldsymbol{\sigma}_s^k = S_s(\boldsymbol{\lambda}^k)$

(iii) $\boldsymbol{\mu}_k = -P^{-1}(\boldsymbol{\sigma}_f^k + \boldsymbol{\sigma}_s^k)$

(iv) $\boldsymbol{\lambda}^{k+1} = \boldsymbol{\lambda}^k + \omega^k \boldsymbol{\mu}^k$

The operator P is seen as a preconditioner in the theory of domain decomposition methods. One possible family of preconditioners is, for iterations k, coefficients α_f^k and α_s^k and linearisations $S_f'(\cdot)$ and $S_s'(\cdot)$ for the operators $S_f(\cdot)$ and $S_s(\cdot)$,

$$P_k^{-1} = \alpha_f^k S_f'(\boldsymbol{\lambda}^k)^{-1} + \alpha_s^k S_s'(\boldsymbol{\lambda}^k)^{-1}. \tag{3.14}$$

The study of preconditioners can be seen in Deparis, Discacciati, and Quarteroni (2006).

Other possibilities beyond the Dirichlet-Neumann approach have also been tested for partitioned schemes. Later studies summarise some of these possibilities into the Robin-Robin methods (FERNÁNDEZ; MULLAERT, 2015; BADIA; NOBILE; VERGARA,

2008). For example, Badia, Nobile, and Vergara (2008) develop a method in which the ALE part is extrapolated, with predicted interface at time t^n denoted as Γ^*. Two parameters control the Robin conditions, α_f and α_s, in which $\alpha_f \neq -\alpha_s$ and $\alpha_f, \alpha_s \geq 0$. A typical iteration $k+1$ would be

(i) solve the fluid problem with Robin condition on Γ^* as

$$\alpha_f \mathbf{u}_f^{k+1} + \boldsymbol{\sigma}_f^{k+1} \cdot \mathbf{n}_f = \alpha_f \frac{\boldsymbol{\eta}_s^k - \boldsymbol{\eta}_s^{k-1}}{\Delta t} - \boldsymbol{\sigma}_s^k \cdot \mathbf{n}_s, \tag{3.15}$$

(ii) use the u_f^{k+1} and σ_f^{k+1} found above to solve the structure problem with Robin condition on Γ^* as

$$\frac{\alpha_s}{\Delta t}\boldsymbol{\eta}_s^{k+1} + \boldsymbol{\sigma}_s^{k+1} \cdot \mathbf{n}_s = \frac{\alpha_s}{\Delta t}\boldsymbol{\eta}_s^k + \alpha_s \mathbf{u}_f^{k+1} - \boldsymbol{\sigma}_f^{k+1} \cdot \mathbf{n}_f \tag{3.16}$$

(iii) Check for convergence

Depending on α_s and α_f, many methods can be recovered. For example, for a very large α_f and with $\alpha_s = 0$, we recover a Dirichlet-Neumann method. The studies in Badia, Nobile, and Vergara (2008) are done using a structure as a surface (or thin wall) and using a linearised fluid. Then, those authors were able to show that the structure can, in a way, be "embedded" into the fluid using the Robin condition, so that the interface values would converge in one iteration. Similarly, with the added-mass operator (check *Section 3.5.1*), they were able to describe the fluid problem inside the Robin condition of the solid to obtain the same one-iteration convergence. More interestingly, they have shown that their Robin-Neumann method has better convergence properties and less susceptibility to the *added-mass effect* (check *Section 3.5.1*) than a Dirichlet-Neumann algorithm. Lastly, numerical experiments were performed in the simplified model to show the faster convergence.

Fernández and Mullaert (2015) have also studied the Robin-Neumann method. Once again, stability and convergence is proved for a simplified model, a Stokes-linearised viscoelastic solid system. It extends the work done for Robin-Robin methods from thin walls to full-dimensional structures.

Other studies in strongly coupled methods include Degroote et al. (2008), in which a 1D model is used to study convergence/stability of the fixed-point method, using Fourier error analysis. Nobile, Pozzoli, and Vergara (2014) analysed if some nonlinear terms can be approximated through extrapolations, in the context of haemodynamics. There, the Newton's method has been used along with the BDF time discretisations.

3.3.2 Loosely coupled

Loosely coupled methods usually solve, at each time t^n, only one fluid and structure solver, or a fixed and small number of iterations of both. They usually employ some prediction

step as well. All of the strongly coupled methods we mentioned can, in principle, be used as loosely coupled methods if we apply only one iteration for each time step. For instance, in Tallec and Mouro (2001), we have a strong coupling method, but its iteration structure is the basis for simple loosely coupled methods.

At a time step t^n,

(i) use an explicit predictor for the interface displacement,

$$\widetilde{\boldsymbol{\eta}}^*|_\Gamma = (\widehat{\boldsymbol{\eta}}^s|_{\widehat{\Gamma}})^n + \frac{3\Delta t}{2}(\widehat{\mathbf{u}}^s|_{\widehat{\Gamma}})^n - \frac{\Delta t}{2}(\widehat{\mathbf{u}}^s|_{\widehat{\Gamma}})^{n-1} \tag{3.17}$$

(ii) deduce a prediction of the interface velocity

$$\widetilde{\mathbf{w}}^*|_{\widehat{\Gamma}} = \frac{\widetilde{\boldsymbol{\eta}}^* - (\widetilde{\boldsymbol{\eta}}|_{\widehat{\Gamma}})^n}{\Delta t} \tag{3.18}$$

(iii) update the mesh on the fluid part using the predicted interface $\widetilde{\boldsymbol{\eta}}^*|_{\widehat{\Gamma}}$

(iv) solve the fluid problem with Dirichlet condition $\widehat{\mathbf{u}}^f|_{\widehat{\Gamma}} = \widetilde{\mathbf{w}}^*|_{\widehat{\Gamma}}$ and compute the traction $\boldsymbol{\sigma}$ on the interface.

(v) solve the structure problem with Neumann boundary condition using the traction $\boldsymbol{\sigma}$.

Many predictors for the interface displacement have been studied and tested, and we refer to the survey Hou, Wang, and Layton (2012). In Dettmer and Perić (2013), the prediction is done on the fluid traction, that is used to solve the solid problem first. Then, the fluid is solved through a Dirichlet condition on the interface, with the displacement just calculated from the solid. The average from the actual traction from the fluid and the predicted one is used to calculate the predictions from further steps. The convergence analysis is done on a 1D model.

The the other topic of research for this type of methods has been on how to best distribute the traction among the fluid and structure subproblems. We mention a recent contribution called *Lie splitting scheme*, from Bukac and Muha (2016). It comes from the idea of dividing the fluid traction using a coefficient $\beta \in [0, 1]$,

$$\boldsymbol{\sigma}_f\mathbf{n} = (\boldsymbol{\sigma}_f\mathbf{n} - \beta\boldsymbol{\sigma}_f\mathbf{n}) + \beta\boldsymbol{\sigma}_f\mathbf{n}. \tag{3.19}$$

At a time t^{n+1}, the structure solver uses the fluid traction $\beta\boldsymbol{\sigma}_f\mathbf{n}$ from the previous time step. The fluid is then solved using a Robin condition,

$$\rho_s\frac{\mathbf{u}_f^{n+1} - \mathbf{u}_s^{n+1}}{\Delta t} + \boldsymbol{\sigma}_f(\mathbf{u}_f^{n+1}, p^{n+1})\mathbf{n} = \beta\boldsymbol{\sigma}_f(\mathbf{u}_f^{n+1}, p^{n+1}). \tag{3.20}$$

The method has been named *kinematically coupled* or *β-scheme*. Convergence and unconditional stability is proved through simplifying assumptions on a FSI model with linear membrane as a structure, and the optimum β should be close to 1. On thick structures, it has been shown that stability is conditional and the convergence is slower than in membranes.

3.4 MONOLITHIC METHODS

We shall describe monolithic methods from decision steps to design them.

1. *How is the domain discretized?*

As in partitioned methods, the fluid and structure domains can be discretised so that they have nodes coinciding on the interface (*conforming grids*) or not (*non-conforming grids*). This will dictate the need of mortar methods, for instance, to deal with the interface (MAYR et al., 2015; FORMAGGIA; QUARTERONI; VENEZIANI, 2009).

The method we construct, in the next chapter, assumes that the grid is conforming in this sense, since it allows for simpler methods. However, as pointed out in Mayr et al. (2015), the simulation of fluids usually requires meshes that are finer close to boundaries, which would require the non-conforming treatment.

2. *How are coupling conditions enforced?*

There are at least three options for the coupling, and they may depend on the choice of the step 1. above.

a. if the domains are conforming, then the continuity of velocity can be enforced on the basis functions (i. e., the basis functions are continuous functions on $\Omega^s \cup \Omega^f$), as in the partitioned method from Tallec and Mouro (2001) as explained before. That means that the test functions automatically satisfy $\mathbf{v}^s = \mathbf{v}^f$ on the interface Γ. Thus, as developed in the last chapter, the traction balance is also satisfied in the weak form. Then, what is left of the coupling conditions is the construction of the fluid domain with the ALE velocity.

b. in nonconforming grids, the continuity of velocity may be enforced on the weak formulation as

$$\int_\Gamma (\boldsymbol{\eta}^{ALE} - \boldsymbol{\eta}^s) \cdot \xi d\gamma, \tag{3.21}$$

as in Mayr et al. (2015). The space of the new test function ξ may come from the application of a mortar method.

c. a more flexible approach is through a Lagrange multiplier (FORMAGGIA; QUARTERONI; VENEZIANI, 2009). The idea is, from the condition of balance of traction

$$\boldsymbol{\sigma}^f \cdot \mathbf{n} + \boldsymbol{\sigma}^s \cdot \mathbf{n} = 0, \quad \text{on } \Gamma, \tag{3.22}$$

to use a new variable $\boldsymbol{\lambda}$ to divide this condition into two equations on Γ,

$$\begin{cases} \boldsymbol{\sigma}^f \cdot \mathbf{n} = \boldsymbol{\lambda} \\ \boldsymbol{\sigma}^s \cdot \mathbf{n} + \boldsymbol{\lambda} = 0 \end{cases} \tag{3.23}$$

and treat the continuity condition on the interface as another equation to be satisfied on the system. Another idea is to use the extra variable as the displacement on

the interface and treat the traction balance as the additional equation (FORMAGGIA; QUARTERONI; VENEZIANI, 2009). In Crosetto (2011), $\boldsymbol{\lambda}$ is inserted instead when the equations have already been discretised in space and it is written in terms of the block operators.

3. *How is time discretised?*

There are two main choices in this step. Firstly, one must decide what will be treated implicitly or explicitly. By this we mean which terms will be calculated directly from the previous iterations (*explicit*) and which ones will be found through a nonlinear equation (*implicit*).

From the experience on partitioned methods above, the choice of explicit treatment is usually avoided. However, for some terms, like the convective ones, successful attempts have been made to treat them explicitly, i.e., as if they were predicted to be

$$\nabla \cdot \mathbf{w}^{n+1} \simeq \nabla \cdot \mathbf{w}^{n}. \tag{3.24}$$

The idea to treat them explicitly and everything else implicitly has been denoted in the literature as a *semi-implicit* or *geometry-convective-explicit* approach (CROSETTO et al., 2011; CROSETTO, 2011; FERNÁNDEZ; MOUBACHIR, 2005). This allows the problem to be rid of at least one nonlinearity.

The second choice is of the time discretisation for the fluid and solid parts. This has been studied, for instance, in Hay et al. (2015), which uses a model of incompressible ALE- Navier-Stokes coupled with a rigid body to verify the stability of BDF methods. One complication that may arise is in methods that require a mid-step, for example, in $t^{n+1/2}$ for only the solid or fluid. Ways to overcome this issue have been studied in Mayr et al. (2015), with an incompressible ALE-Navier-stokes fluid. They have proposed a time discretisation scheme that allows for more freedom of choice in the fluid and solid parts.

4. *How is the nonlinear system solved?*

The usual choice to solve the nonlinear system of implicit monolithic methods at each time-step is the Newton method or a variation of it. The difficulties are the size of the system and the calculation of its Jacobian matrix.

We describe the sketch of a Newton method with Lagrange multiplier as in Formaggia, Quarteroni, and Veneziani (2009), chap. 9., with a similar description in Mayr et al. (2015).

On a time-step t^n, we use the notations $\mathbf{x} = (\widehat{\mathbf{u}}_f^n, \widetilde{P}^n, \widetilde{\boldsymbol{\eta}}_f)$ and $\mathbf{y} = \widehat{\boldsymbol{\eta}}_s$. Then, the method can be sketched as

1. Initialise $\mathbf{x}_0, \mathbf{y}_0, \boldsymbol{\lambda}_0$. It could be the previous iteration or the previous iteration corrected by a predictor as in Mayr et al. (2015).

2. For each iteration $k \geq 0$, until convergence, do:

a) Evaluate the residual

$$\mathcal{R}_k = \begin{bmatrix} \mathcal{F}(\mathbf{x}_k, \boldsymbol{\lambda}_k) \\ \mathcal{S}(\mathbf{y}_k, \boldsymbol{\lambda}_k) \\ \mathcal{I}(\mathbf{x}_k, \mathbf{y}_k) \end{bmatrix}; \tag{3.25}$$

b) Solve the tangent problem, with Jacobian matrix $\mathcal{J}_k$,

$$\mathcal{J}_k \begin{bmatrix} \delta\mathbf{x} \\ \delta\mathbf{y} \\ \delta\boldsymbol{\lambda} \end{bmatrix} = -\mathcal{R}_k; \tag{3.26}$$

c) Update the variables

$$\begin{bmatrix} \mathbf{x}_{k+1} \\ \mathbf{y}_{k+1} \\ \boldsymbol{\lambda}_{k+1} \end{bmatrix} = \begin{bmatrix} \mathbf{x}_k \\ \mathbf{y}_k \\ \boldsymbol{\lambda}_k \end{bmatrix} + \begin{bmatrix} \delta\mathbf{x} \\ \delta\mathbf{y} \\ \delta\boldsymbol{\lambda} \end{bmatrix}. \tag{3.27}$$

The Jacobian $\mathcal{J}_k$ takes the form

$$\mathcal{J}_k = \begin{bmatrix} D_{\mathbf{x}}\mathcal{F}(\mathbf{x}_k, \boldsymbol{\lambda}_k) & \mathbf{0} & D_{\boldsymbol{\lambda}}\mathcal{F}(\mathbf{x}_k, \boldsymbol{\lambda}) \\ \mathbf{0} & D_{\mathbf{y}}\mathcal{S}(\mathbf{y}_k, \boldsymbol{\lambda}) & D_{\boldsymbol{\lambda}}\mathcal{S}(\mathbf{y}_k, \boldsymbol{\lambda}) \\ D_{\mathbf{x}}\mathcal{I}(\mathbf{x}_k, \mathbf{y}_k) & D_{\mathbf{y}}(\mathbf{x}_k, \mathbf{y}_k) & \mathbf{0} \end{bmatrix}, \tag{3.28}$$

and the description and full calculation of the blocks is found in Fernández and Moubachir (2005), Crosetto (2011) or Richter (2017, chap. 5). Attempts have been made to use a less expensive Jacobian matrix, ignoring for instance the derivatives involving the movement of domain (also called *shape derivatives*) or using, as in partitioned methods, some finite difference estimates. Still, it is argued in the papers cited above that this may influence negatively the convergence of the method and the full Jacobian might be needed.

Mayr et al. (2015) study the possibility of using extrapolation predictors at each time step to improve the Newton method, considering an incompressible ALE-Navier-Stokes fluid. In Fernández and Moubachir (2005), a monolithic method is proposed and all the shape derivatives calculated to build the full/exact Jacobian for the Newton method.

How to make the Newton method scalable?

Since some applications may require monolithic methods, because of a stronger *added-mass effect*, research has been done to make the methods faster. When it comes to scalability and parallelisation of these methods, much of the work is focused on domain decomposition methods and preconditioners, as in Barker and Cai (2010), Cai and Keyes (2002) and Crosetto (2011). Most of these ideas are about interpreting the partitioned methods from the previous section as preconditioners for the nonlinear system.

3.5 CONCEPTS IN STABILITY OF METHODS FOR FSI

In this section, we briefly describe two popular concepts in the study of stability of methods for fluid-structure interaction. Both were created as attempts to explain why some algorithms do not work well for this type of problem.

3.5.1 Added-mass effect

Numerical experiments with partitioned methods in haemodynamics have shown that the convergence rate of strongly coupled methods, with relaxation parameters, would worsen if the density of the fluid got close to that of the structure, or if the domain was stretched into a more slender cylinder. In such cases, the relaxation would have to be increased. More surprisingly, if the time step length was reduced, the convergence rate would be further worsened (CAUSIN; GERBEAU; NOBILE, 2005). These issues did not appear in aerodynamics simulations, because the density of air is much smaller than that of the solid.

We now describe two papers that have studied this effect. To make the so-called *added-mass operator* explicit, these articles pursue the same steps in different environments. In the already cited Causin, Gerbeau, and Nobile (2005), the steps are done in the framework of linear operators in function spaces. In Förster, Wall, and Ramm (2007), the equations have been discretised in space using Finite Elements so that we are dealing with finite-dimensional linear algebra. In either way, linearity is key because we employ the spectral analysis of a linear operator.

We start as in Förster, Wall, and Ramm (2007), carefully assuming conditions so that we reach a linear system for the fluid problem,

$$\begin{bmatrix} M_{II}^F & M_{I\Gamma}^F & G_I \\ M_{\Gamma I}^F & M_{\Gamma\Gamma}^F & G_\Gamma \\ G_I^T & G_\Gamma^T & \mathbf{0} \end{bmatrix} \begin{bmatrix} \dot{\mathbf{u}}_I \\ \dot{\mathbf{u}}_\Gamma \\ p \end{bmatrix} = \begin{bmatrix} \mathbf{0} \\ \mathbf{f}_\Gamma \\ 0 \end{bmatrix}, \tag{3.29}$$

where M and G are the matrices related to the fluid velocity $\dot{\mathbf{u}}$ and to the pressure p, respectively; I is the subindex of internal nodes and Γ the subindex of the interface nodes. We have also denoted by $\mathbf{f}_\Gamma$ the forces on the boundary that come from the coupling condition.

The idea is, then, assuming invertibility of matrices when needed, to solve the block linear system and write $\mathbf{f}_\Gamma$ in terms of $\dot{\mathbf{u}}_\Gamma$. It will be denoted as

$$\mathbf{f}_\Gamma = m^F \mathcal{M}_A \dot{\mathbf{u}}_\Gamma, \tag{3.30}$$

with $\mathcal{M}_A$ the operator that comes from the solving of the system and m^F a constant to normalise the operator. The *added-mass operator* is precisely this $\mathcal{M}_A$.

Then, for the structure, we also assume conditions enough to end up with a system, already replacing the coupling force by what we have previously found, of the form

$$\begin{bmatrix} M_{II}^S & M_{I\Gamma}^S \\ M_{\Gamma I}^S & M_{\Gamma\Gamma}^S \end{bmatrix} \begin{bmatrix} \dot{\mathbf{d}}_I \\ \dot{\mathbf{d}}_\Gamma \end{bmatrix} + \begin{bmatrix} K_{II}^S & K_{I\Gamma}^S \\ K_{\Gamma I}^S & K_{\Gamma\Gamma}^S \end{bmatrix} \begin{bmatrix} \mathbf{d}_I \\ \mathbf{d}_\Gamma \end{bmatrix} = \begin{bmatrix} \mathbf{0} \\ -m^F \mathcal{M}_A \dot{\mathbf{u}}_\Gamma \end{bmatrix}. \tag{3.31}$$

The name *added-mass* comes from the observation that the solid sees the fluid as an extra mass (i. e., a constant multiplying the acceleration). What we have done so far was to somehow "solve" the fluid part and substitute it in the structure. The stability analysis will be focused on this structure problem with the fluid part compacted as one operator.

The next step is the analysis of temporal discretisation. For example, Förster, Wall, and Ramm (2007) analyse, among other methods, a loosely-coupled algorithm which, at a time t^{n+1}, predicts the displacement of the structure, $\mathbf{d}_{\Gamma,P}^{n+1}$, and use it to calculate

$$\mathbf{u}_\Gamma^{n+1} = \frac{\mathbf{d}_{\Gamma,P}^{n+1} - \mathbf{d}_{\Gamma,P}^{n}}{\Delta t} \tag{3.32}$$

and solve the fluid subproblem. With a backward Euler method for the fluid and simple predictor $\mathbf{d}_{\Gamma,P}^{n+1} = \mathbf{d}_\Gamma^n$,

$$\dot{\mathbf{u}}_\Gamma^{n+1} = \frac{1}{\Delta t^2}(\mathbf{d}_\Gamma^n - 2\mathbf{d}_\Gamma^{n-1} + \mathbf{d}_\Gamma^{n-2}). \tag{3.33}$$

Replacing this $\dot{\mathbf{u}}_\Gamma^{n+1}$ on the structure equations above, and writing the equations in terms of eigenvectors of $\mathcal{M}_A$, one is able to analyse the resulting ODE's for stability, using eigenvalue estimations for the $\mathcal{M}_A$ found previously.

The above analysis has been done in Causin, Gerbeau, and Nobile (2005) on a simplified FSI model described. Since the domain is a simple cylinder, it was possible to find the eigenvalues of $\mathcal{M}_A$ analytically, which helped to prove the conditional stability found in experiments. In Förster, Wall, and Ramm (2007), the model was an incompressible fluid with a structure. Doing careful assumptions to apply the steps described above, they attempted to also analyse the effects of the SUPG stabilisation on the added-mass operator.

3.5.2 The Geometric Conservation Law

This concept is related to the ALE formulation of fluids and has been subject to considerable debate, summarised for instance in Étienne, Garon, and Pelletier (2009). It arises from the observation that, when a method for computational fluid dynamics meant for a fixed domain is used for a problem in the ALE format, its temporal accuracy may worsen.

The *Geometric Conservation Law* (GCL) was created to design methods that preserve the time accuracy, at least for simple solutions of fluid dynamics, like a uniform flow. Being more specific,

Definition 3.1. A numerical method for an ALE problem is said to satisfy the Geometric Conservation Law if it preserves constant solutions. That is, the constant solution is reproduced exactly by the method.

For each method, the GCL will be written in a different way, which is usually called its Discrete Geometric Conservation Law. For instance, for a Finite Element discretisation, it usually means

$$\int_{\Omega_t^{n+1}} \psi_i \psi_j d\Omega - \int_{\Omega_t^n} \psi_i \psi_j d\Omega = \mathcal{Q}\left[\int_{\Omega_t} \psi_i \psi_j \nabla_{\mathbf{x}} \cdot \mathbf{w} d\Omega\right], \tag{3.34}$$

for all basis functions $\{\psi_i\}$, using ALE, and $\mathcal{Q}(\cdot)$ the time integration of choice from t^n to t^{n+1}, or

$$\int_{\Omega_t^{n+1}} \psi_h d\Omega - \int_{\Omega_t^n} \psi_h d\Omega = \mathcal{Q}\left[\int_{\Omega_t} \psi_h \nabla_{\mathbf{x}} \cdot \mathbf{w} d\Omega\right], \tag{3.35}$$

for ψ_h in the discretised test space (FORMAGGIA; NOBILE, 1999). Hence, the GCL is in this case related to the accuracy of the time integrator used.

As stated in Étienne, Garon, and Pelletier (2009), this concept has gained attention because it has been proved that a specific class of Finite Volume methods is stable if, and only if, it satisfies the GCL. However, researchers have later constructed methods that do not satisfy the GCL and are stable, and also methods that satisfy the GCL but are not stable. Nowadays, the GCL condition is used because it is convenient in the analysis of the methods, since it offers an estimate independent from the ALE mesh velocity (FORMAGGIA; QUARTERONI; VENEZIANI, 2009). For example, it can be proved that the GCL property as stated above implies that

$$\mathcal{Q}\left[\int_{\Omega_t} |u_h^{n+1}(\mathbf{x})|^2 \nabla_{\mathbf{x}} \cdot \mathbf{w} d\Omega\right] = ||u_h^{n+1}||^2_{L^2(\Omega_{t^{n+1}})} - ||u_h^n||^2_{L^2(\Omega_{t^n})} \tag{3.36}$$

(FORMAGGIA; NOBILE, 1999).

We now summarise a few studies on the GCL. In Boffi and Gastaldi (2004), a 2D parabolic model with moving domains using ALE was used to study a few methods that satisfy and do not satisfy the GCL property. In the already mentioned Formaggia and Nobile (1999), a linear advection-difusion model was used for Finite Element Methods, and in Farhat, Geuzaine, and Grandmont (2001), a nonlinear system of hyperbolic conservation laws and Finite Volume methods. In the latter, it was proved that satisfying the GCL condition was sufficient to preserve a type of nonlinear stability for the method studied.

Finally, Étienne, Garon, and Pelletier (2009) have studied the GCL condition on incompressible fluids and Finite Element Methods. The goal was to keep the time integration method untouched and modify the calculation of divergence of the ALE velocity and the ALE velocity itself so that the method satisfies the GCL. That would ensure that less work is needed to change existing codes.

4 THE METHOD WITH A MONOLITHIC PREDICTOR

4.1 DESCRIPTION

Our method attempts to connect both types of methods, monolithic and partitioned. It is based on the idea that, if the values on the interface Γ were accurately predicted, then we would only need one use of structure and fluid solvers at each time-step. Since the functions might not be differentiable on the interface (cf. *Chapter 2*), we propose a more sophisticated predictor, by solving a smaller fluid-structure interaction problem, using the monolithic method, on a tube surrounding Γ.

To illustrate the method, we consider a hypothetical fluid-structure interaction problem with initial domains Ω_f and Ω_s, with an interface Γ. We then consider a tube $\widetilde{\Omega} = \widetilde{\Omega}_f \cup \widetilde{\Omega}_s$, around such interface.

FIGURE 2 - The predictor as a smaller problem surrounding the interface

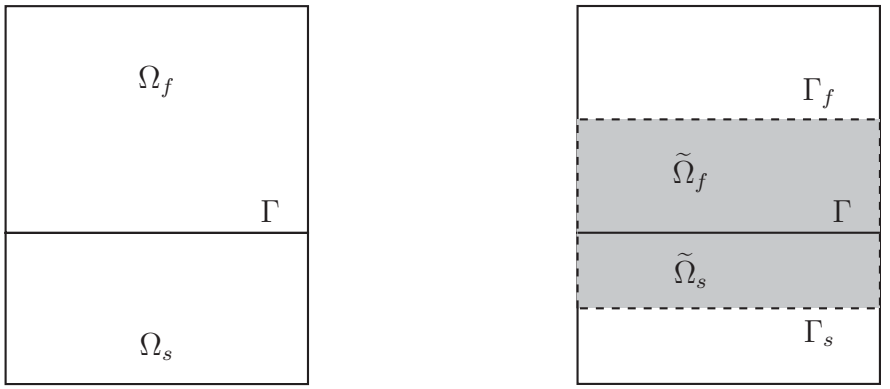

Original problem *Tube around* Γ*, in gray*

SOURCE: The author (2020).

In the notation of the *Figure 2*, $\widetilde{\Omega}_f$ is the portion of the tube inside the original domain Ω_f of the fluid, and $\widetilde{\Omega}_s$ is defined analogously. Also, $\Gamma_f \doteq \partial\widetilde{\Omega}_s \cap \text{int}(\Omega_s)$ and $\Gamma_s \doteq \partial\widetilde{\Omega}_s \cap \text{int}(\Omega_s)$, that is, they are the portions of the boundary of the tube that are in the interior of the original domains.

We consider a time discretization using a fixed step length Δt, and a generic time integrator procedure. The idea is to apply a monolithic time-step algorithm, using as previous iteration values, such as $\widehat{\mathbf{u}}_f^n$, the previous values of the whole (original) problem, and retain its original boundary conditions where the boundaries of the tube and original problem coincide.

We impose special boundary conditions on Γ_f and Γ_s. In this work, these will be extrapolations of the original problem, as Dirichlet conditions. The idea is that, even

though the functions on Γ are not differentiable, they are differentiable inside the domains. We could also consider different conditions, such as Neumann and Robin, but these will be left for future work.

For the extrapolation to be meaningful, the initial iterations must be done with another method. For example, when BDF time integrators are used, we may use another method to solve the n first steps it requires.

Our algorithm can be summarised as follows.

TABLE 3 - Algorithm with monolithic predictor

Step 1. Solve initial time-steps required for the time integrator of choice
For each time-step **until** reaching final time
Step 2. Extrapolate the boundary conditions for the monolithic predictor
Step 3. Solve the monolithic predictor
Step 4. Get the new fluid domain, using the prediction
Step 5. Use the prediction to solve the fluid and solid subproblems

SOURCE: The author (2020).

4.2 ANALYSIS USING PARABOLIC EQUATIONS

We shall use simple parabolic problems to detail the method and analyse some of its properties. In this case, the domain is artificially divided into two, to mimic the FSI situation. As future work, we could consider the coupling of two distinct parabolic problems.

We start by writing our main problem $(P1)$ on a fixed domain Ω, with Dirichlet conditions. We could also consider Neumann conditions, which cancel just as well during our calculations. Here, $t \in [0, T]$, and L is an elliptic operator. We require that its related bilinear form $a(u, v) \doteq (Lu) \cdot v$ satisfies the coercivity property with a constant α,

$$a(v, v) \geq \alpha ||v||_1^2, \, \forall v \in H^1(\Omega), \tag{4.1}$$

and continuity with constant M,

$$a(u, v) \leq M ||u||_1 ||v||_1, \, \forall u, v \in H^1(\Omega). \tag{4.2}$$

The problem is written as

$$(P1) \begin{cases} \dfrac{\partial u}{\partial t} + Lu = f, \text{ in } \Omega \\ u(0) = u_0, \text{ in } \Omega \\ u = g, \text{ on } \partial\Omega, \, \forall t \in [0, T] \end{cases} .$$

The function space in which we are looking for solutions and to which g belongs will be important later, by providing a simple existence and uniqueness theorem. We might consider, then, that $u \in V \doteq L^2(0, T; H^2(\Omega))$ (see *Section 2.1*).

Assuming that we know the solution $u(t)$, for $[0, t_1]$, we want to find $u(t_2)$ for some $t_2 < T$, with $t_2 > t_1$. Thus, we want to extend the solution u for $(t_1, t_2]$. The domain is divided in two, Ω_1 and Ω_2, with an interface Γ, and *Figure 3* is very similar to *Figure 2*.

FIGURE 3 - Tube description for the parabolic problem

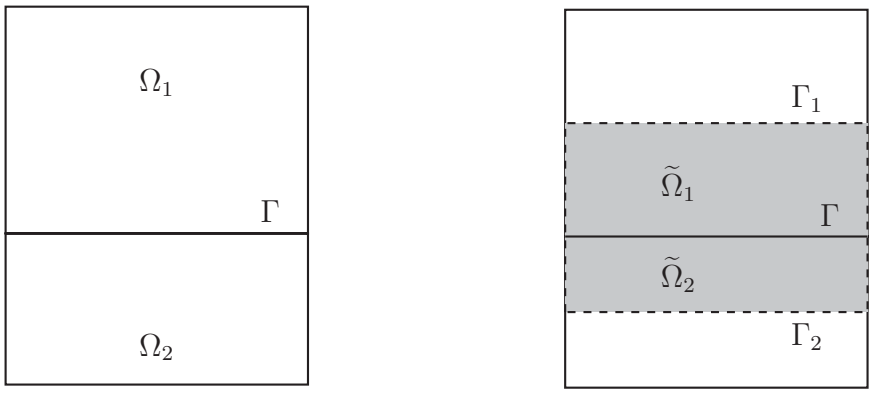

Original problem *Domain with the tube*

SOURCE: The author (2020).

The idea of the algorithm, written in its 'continuous form', consists of two steps:

First method: time-dependent Dirichlet conditions

Step 1. Prediction. Solve the problem inside the tube, using an extrapolation $u^*(t)$ of $u(t)$ based on its known values in $[0, t_1]$. We want to find $\widetilde{u}(t)$, for $t \in (t_1, t_2]$, such that

$$(P2)\begin{cases} \dfrac{\partial \widetilde{u}}{\partial t} + L\widetilde{u} = f, \text{ in } \widetilde{\Omega}_1 \cup \widetilde{\Omega}_2 \\ \widetilde{u}(t_1) = u(t_1), \text{ in } \widetilde{\Omega}_1 \cup \widetilde{\Omega}_2 \\ \widetilde{u}(t) = u^*(t), \text{on } \Gamma_1 \cup \Gamma_2, \forall t \in (t_1, t_2] \\ \widetilde{u} = g, \text{ on } (\partial\widetilde{\Omega}_1 \cap \partial\Omega) \cup (\partial\widetilde{\Omega}_2 \cap \partial\Omega) \end{cases}$$

Step 2. Solution in the subdomains. Use $\widetilde{u}$, assumed to be found within the interval $(t_1, t_2]$ to solve the two subproblems in Ω_1 and Ω_2,

Find u_1, for $t \in (t_1, t_2]$, such that

$$(P3.1)\begin{cases} \dfrac{\partial u_1}{\partial t} + Lu_1 = f, \text{ in } \Omega_1 \\ u_1(t_1) = u(t_1), \text{ in } \Omega_1 \\ u_1 = g, \text{ on } \partial\Omega_1 \cap \partial\Omega \\ u_1(t) = \widetilde{u}(t), \text{ on } \Gamma, \forall t \in (t_1, t_2] \end{cases}$$

Find u_2, for $t \in (t_1, t_2]$, such that

$$(P3.2)\begin{cases} \dfrac{\partial u_2}{\partial t} + Lu_2 = f, \text{ in } \Omega_2 \\ u_2(t_1) = u(t_1), \text{ in } \Omega_2 \\ u_2 = g, \text{ on } \partial\Omega_2 \cap \partial\Omega \\ u_2(t) = \widetilde{u}(t), \text{ on } \Gamma, \forall t \in (t_1, t_2] \end{cases}$$

We also consider a slightly simpler algorithm, in which the Dirichlet condition is taken as constant. This is because, if we want to reuse some black boxes, some do not have the implementation of a variable Dirichlet condition. The subproblems will be identified with the letter m.

Modified method: constant Dirichlet conditions

Step 1. Prediction. Solve the problem inside the tube, using an extrapolation $u^*(t_2)$ of $u(t_2)$ based on its known values in $[0, t_1]$. We want to find $\widetilde{u}(t)$, for $t \in (t_1, t_2]$, such that

$$(P2m)\begin{cases} \dfrac{\partial \widetilde{u}}{\partial t} + L\widetilde{u} = f, \text{ in } \widetilde{\Omega}_1 \cup \widetilde{\Omega}_2 \\ \widetilde{u}(t_1) = u(t_1), \text{ in } \widetilde{\Omega}_1 \cup \widetilde{\Omega}_2 \\ \widetilde{u}(t) = u^*(t_2), \text{on } \Gamma_1 \cup \Gamma_2, \forall t \in (t_1, t_2] \\ \widetilde{u} = g, \text{ on } (\partial\widetilde{\Omega}_1 \cap \partial\Omega) \cup (\partial\widetilde{\Omega}_2 \cap \partial\Omega) \end{cases}$$

Step 2. Solution in the subdomains. Use $\widetilde{u}$, assumed to be found within the interval $(t_1, t_2]$ to solve the two subproblems in Ω_1 and Ω_2,

Find u_1, for $t \in (t_1, t_2]$, such that

$$(P3.1m)\begin{cases} \dfrac{\partial u_1}{\partial t} + Lu_1 = f, \text{ in } \Omega_1 \\ u_1(t_1) = u(t_1), \text{ in } \Omega_1 \\ u_1 = g, \text{ on } \partial\Omega_1 \cap \partial\Omega \\ u_1(t) = \widetilde{u}(t_2), \text{ on } \Gamma, \forall t \in (t_1, t_2] \end{cases}$$

Find u_2, for $t \in (t_1, t_2]$, such that

$$(P3.2m)\begin{cases} \dfrac{\partial u_2}{\partial t} + Lu_2 = f, \text{ in } \Omega_2 \\ u_2(t_1) = u(t_1), \text{ in } \Omega_2 \\ u_2 = g, \text{ on } \partial\Omega_2 \cap \partial\Omega \\ u_2(t) = \widetilde{u}(t_2), \text{ on } \Gamma, \forall t \in (t_1, t_2] \end{cases}$$

4.2.1 Estimates for the continuous problem

We estimate how close $\widetilde{u}$ is from the solution of (P1), inside the tube $\widetilde{\Omega}$. We depend on an existence and uniqueness result, which itself depends on the function spaces being considered.

Theorem 4.1. Let u be the solution of

$$(\mathbf{i}) \begin{cases} \dfrac{\partial u}{\partial t} + Lu = f, \text{ in } \Omega \\ u(0) = u_0, \text{ in } \Omega \\ u = g, \text{ on } \partial\Omega, \end{cases}$$

for $t \in [0, T]$, and w the solution of

$$(\mathbf{ii}) \begin{cases} \dfrac{\partial w}{\partial t} + Lw = f, \text{ in } \widetilde{\Omega} \subset \Omega \\ w(0) = u_0, \text{ in } \widetilde{\Omega} \\ w = g, \text{ on } \partial\Omega \cap \partial\widetilde{\Omega} \\ w(t) = u(t), \forall t \in [0, T], \text{ on } \partial\widetilde{\Omega} - \partial\Omega \end{cases}$$

Under conditions that guarantee the uniqueness of the PDE above, then $w = u$ a. e. in $\widetilde{\Omega}$.

Proof. We observe that u satisfies the system (ii), and apply the existence and uniqueness result to that system. ///

We start with the analysis of the first algorithm, with time-dependent Dirichlet conditions. Our main theorem, below, estimates the difference between the solution of the original problem with the solution obtained inside the tube from problem $(P2)$.

We have simplified the theorem with the assumption that $\widetilde{\Omega}$ does not intersect $\partial\Omega$, that is, we do not have to worry about the original problem's boundary conditions. A more general proof, removing such assumption, would not be much more different, since the terms related to these boundary conditions would disappear when we subtract one weak formulation from the other.

To simplify our notation, we have denoted by $||\cdot||_0$ the $L^2(\widetilde{\Omega})$ norm; $(\cdot,\cdot)$ the inner product, also in $L^2(\widetilde{\Omega})$; and $V = H^1_{\Gamma_D}(\widetilde{\Omega})$. We also remind the reader that α and M are the coercivity and continuity constants, respectively, related to the operator L (*Equations* (4.1) and (4.2)).

Theorem 4.2. Let $\widetilde{w}$ be the solution of $(P2)$, on the tube, and w the solution of the original problem $(P1)$. Let us also denote by $u^* = u + s$ the extrapolation of choice, where u is the exact solution, s the approximation error, and U and S their corresponding liftings in the function space V. Then, we have that

$$\begin{aligned} &||(w - \widetilde{w})(t)||_0^2 + \alpha \int_{t_1}^{t} ||(w - \widetilde{w})(\tau)||_1^2 d\tau \\ &\quad \leq 2 \left\{ \frac{M\sqrt{t_2 - t_1}}{\sqrt{\alpha}} \max_{s\in(0,t_2]} ||S(\tau)||_1 + \int_{t_1}^{t} \left|\left| \frac{\partial S}{\partial t}(\tau) \right|\right|_0 d\tau \right\}^2 \\ &\qquad + 2||S(t)||_0^2 + 4 \int_{t_1}^{t} ||S(\tau)||_1^2 d\tau \end{aligned} \tag{4.3}$$

for $t \in (t_1, t_2]$. Moreover, if the approximation in u^* is of order p, and its lifting maintains such order, then

$$||(w - \widetilde{w})(t_2)||_0^2 + \alpha \int_0^{t_2} ||(w - \widetilde{w})(\tau)||_1^2 d\tau \leq C_2 t_2^p, \tag{4.4}$$

for $C_2 > 0$.

Proof. We shall consider two problems for $t \in (t_1, t_2]$: the one from the first theorem,

$$\textbf{(i)} \begin{cases} \dfrac{\partial \widetilde{w}}{\partial t} + L\widetilde{w} = f, \text{ in } \widetilde{\Omega} \\ \widetilde{w}|_{\partial\widetilde{\Omega}}(t) = u(t), \forall t \in (t_1, t_2] \\ \widetilde{w}(t_1) = u(t_1), \text{ in } \widetilde{\Omega}, \end{cases}$$

and its perturbed version

$$\textbf{(ii)} \begin{cases} \dfrac{\partial w}{\partial t} + Lw = f, \text{ in } \widetilde{\Omega} \\ w|_{\partial\widetilde{\Omega}}(t) = u^*(t) = u(t) + s(t), \forall t \in (t_1, t_2] \\ w(t_1) = u(t_1), \text{ in } \widetilde{\Omega}. \end{cases}$$

As stated in the theorem, we denote the lifting of u^* to $H^1(\widetilde{\Omega})$ as $U^* = U + S$, where U is the lifting of U, and S the lifting of s. The following are simple modifications of the standard calculation that can be found in Formaggia, Saleri, and Veneziani (2005).

We multiply problem (i) by $v \in V$ and integrate in $\widetilde{\Omega}$, to obtain its weak formulation. We want to find $\breve{w} = w - U \in V$ such that, for all $v \in V$ and almost all $t \in (t_1, t_2]$,

$$\left(\frac{\partial \breve{w}}{\partial t}, v\right) + a(\breve{w}, v) = F(v) - a(U, v) - \left(\frac{\partial U}{\partial t}, v\right). \tag{4.5}$$

Analogously, the weak formulation of the problem (ii) is to find $\overline{w} = \widetilde{w} - U - S \in V$ such that, for all $v \in V$ and almost all $t \in (t_1, t_2]$,

$$\left(\frac{\partial \overline{w}}{\partial t}, v\right) + a(\overline{w}, v) = F(v) - a(U + S, v) - \left(\frac{\partial (U + S)}{\partial t}, v\right) \tag{4.6}$$

Subtracting (4.6) from (4.5), we get

$$\left(\frac{\partial \breve{w} - \overline{w}}{\partial t}, v\right) + a(\breve{w} - \overline{w}, v) = -a(S, v) - \left(\frac{\partial (S)}{\partial t}, v\right) \tag{4.7}$$

Taking $v = \breve{w} - \overline{w}$,

$$\left(\frac{\partial (\breve{w} - \overline{w})}{\partial t}, \breve{w} - \overline{w}\right) + a(\breve{w} - \overline{w}, \breve{w} - \overline{w}) = -a(S, \breve{w} - \overline{w}) - \left(\frac{\partial S}{\partial t}, \breve{w} - \overline{w}\right). \tag{4.8}$$

We apply the continuity property for a and Young's inequality to get the relation

$$a(S, \breve{w} - \overline{w}) \leq M||S||_1||\breve{w} - \overline{w}||_1 \tag{4.9}$$

$$\leq \frac{M^2}{2\alpha}||S||_1^2 + \frac{\alpha}{2}||\breve{w} - \overline{w}||_1^2, \tag{4.10}$$

and substitute (4.10) in (4.8).

Using integration by parts in the first term of (4.8),

$$\frac{1}{2}\frac{\partial}{\partial t}||(\breve{w}-\overline{w})(t)||_0^2+\frac{\alpha}{2}||(\breve{w}-\overline{w})(t)||_1^2 \leq \frac{M^2}{2\alpha}||S(t)||_1^2+\left|\left|\frac{\partial S}{\partial t}(t)\right|\right|_0 ||(\breve{w}-\overline{w})(t)||_0. \quad (4.11)$$

Integrating in time, noting that $(\breve{w}-\overline{w})(t_1)=0$, and multiplying the inequality by 2,

$$\begin{aligned}&||(\breve{w}-\overline{w})(t)||_0^2+\alpha\int_{t_1}^{t}||(\breve{w}-\overline{w})(\tau)||_1^2 d\tau \\ &\quad\leq \frac{M^2}{\alpha}\int_{t_1}^{t}||S(\tau)||_1^2 d\tau+2\int_{t_1}^{t}\left|\left|\frac{\partial S}{\partial t}(\tau)\right|\right|_0 ||(\breve{w}-\overline{w})(\tau)||_0 d\tau \end{aligned} \quad (4.12)$$

We now bound the first term on the right,

$$\frac{M^2}{\alpha}\int_{t_1}^{t}||S(\tau)||_1^2 d\tau \leq \frac{M^2(t_2-t_1)}{\alpha}\text{max}_{\tau\in(t_1,t_2]}||S(\tau)||_1^2 \quad (4.13)$$

Replacing (4.13) in (4.12) and using the Gronwall Lemma,

$$\begin{aligned}&\left\{||(\breve{w}-\overline{w})(t)||_0^2+\alpha\int_{t_1}^{t}||(\breve{w}-\overline{w})(\tau)||_1^2 d\tau\right\}^{1/2} \\ &\quad\leq \frac{M\sqrt{t_2-t_1}}{\sqrt{\alpha}}\text{max}_{\tau\in(t_1,t_2]}||S(\tau)||_1+\int_{t_1}^{t}\left|\left|\frac{\partial S}{\partial t}\right|\right|_0 d\tau. \end{aligned} \quad (4.14)$$

Since $w=\breve{w}+U$ and $\widetilde{w}=\overline{w}+U+S$, using the convexity inequality from Rudin (1987, p. 64), which states that for positive functions f and g, and for p a positive integer,

$$|f+g|^p \leq 2^{p-1}(|f|^p+|g|^p), \quad (4.15)$$

we have

$$\begin{aligned}&||(w-\widetilde{w})(t)||_0^2+\alpha\int_{t_1}^{t}||(w-\widetilde{w})(\tau)||_1^2 d\tau \\ &\quad= ||(\breve{w}-\overline{w})(t)-S(t)||_0^2+\int_{t_1}^{t}||(\breve{w}-\overline{w})(\tau)-S(\tau)||_1^2 d\tau \quad (4.16)\\ &\quad\leq 2\left(||(\breve{w}-\overline{w})(t)||_0^2+\int_{t_1}^{t}||(\breve{w}-\overline{w})(\tau)||_1^2 d\tau+||S(t)||_0^2+\int_{t_1}^{t}||S(\tau)||_1^2 d\tau\right) \quad (4.17)\\ &\quad\leq 2\left\{\frac{M\sqrt{t_2-t_1}}{\sqrt{\alpha}}\text{max}_{\tau\in(t_1,t_2]}||S(\tau)||_1+\int_{t_1}^{t}\left|\left|\frac{\partial S}{\partial t}\right|\right|_0 d\tau\right\}^2 \\ &\qquad+2||S(t)||_0^2+4\int_{t_1}^{t}||S(\tau)||_1^2 d\tau. \quad (4.18)\end{aligned}$$

Now, our hypothesis indicates that there exists $C_1>0$ such that $|s(t)|\leq C_1 t^p$. If we suppose that this bound is maintained for its lifting, that is, $||S(t)||_1 \leq \overline{C}_1 t^p$, then we have that

$$||(w-\widetilde{w})(t_2)||_0^2+\alpha\int_{t_1}^{t_2}||(w-\widetilde{w})(\tau)||_1^2 d\tau \leq C_2 t_2^p, \quad (4.19)$$

for a constant $C_2 > 0$. ////

The result form *Theorem 4.2* indicates that our method is promising, at least in its continuous form, as our predictor maintains the approximation order used on its Dirichlet conditions.

We now attempt to proceed in the same way for the modified algorithm with constant Dirichlet conditions, and will use the extrapolation of u at t_2 for them. To simplify the notation, we consider $t_1 = 0$.

Theorem 4.3. (Modified algorithm with constant Dirichlet conditions) Let $\widetilde{w}$ be the solution of $(P2m)$, on the tube, and w the solution of $(P1)$, restricted to the tube. Let us also denote by $u^* = u(t_2) + s$ the extrapolation for time t_2, where $u(t_2)$ is the exact solution at time t_2, and s is the approximation error. As in the previous theorem, U and S denote the liftings of the functions u and s, respectively, in $H_1(\widetilde{\Omega})$. We then have

$$\begin{aligned} &||(w-\widetilde{w})(t_2)||_0^2 + \alpha \int_0^{t_2} ||(w-\widetilde{w})(\tau)||_1^2 d\tau \\ &\leq \left\{ \frac{M\sqrt{t_2}}{\sqrt{\alpha}} ||S||_1 + \int_0^t \left|\left| \frac{\partial U}{\partial t}(\tau) \right|\right|_0 d\tau \right\}^2 + ||S||_0^2 + \alpha \int_0^{t_2} ||U(\tau) - U(t_2) - S||_1^2 d\tau, \end{aligned} \tag{4.20}$$

for $t \in (0, t_2]$.

Proof. The proof is similar to the one for *Theorem 4.2*. We consider the original problem,

$$(\mathbf{i}) \begin{cases} \dfrac{\partial w}{\partial t} + Lw = f, \text{ in } \widetilde{\Omega} \\ w|_{\partial\widetilde{\Omega}}(t) = u(t), \, \forall t \in (0, t_2] \\ w(0) = u(0), \text{ in } \widetilde{\Omega} \end{cases}$$

and its perturbed version

$$(\mathbf{ii}) \begin{cases} \dfrac{\partial \widetilde{w}}{\partial t} + L\widetilde{w} = f, \text{ in } \widetilde{\Omega} \\ \widetilde{w}|_{\partial\widetilde{\Omega}}(t) = u^*(t_2) \doteq u(t_2) + s(t_2), \, \forall t \in (0, t_2] \\ \widetilde{w}(0) = u(0), \text{ in } \widetilde{\Omega}. \end{cases}$$

Let us denote the lifting of u^* to $H^1(\widetilde{\Omega})$ as $U^* = U + S$.

We multiply problem (i) by $v \in V$ and integrate in $\widetilde{\Omega}$, to obtain its weak formulation. We want to find $\breve{w} = w - U$ such that, for all v,

$$\left(\frac{\partial \breve{w}}{\partial t}, v \right) + a(\breve{w}, v) = F(v) - a(U, v) - \left(\frac{\partial U}{\partial t}, v \right). \tag{4.21}$$

Using the weak formulation of the problem (ii), we want to find $\overline{w} = \widetilde{w} - U - S$,

$$\left(\frac{\partial \overline{w}}{\partial t}, v \right) + a(\overline{w}, v) = F(v) - a(U + S, v) \tag{4.22}$$

Subtracting (4.22) from (4.21), we get

$$\left(\frac{\partial \breve{w} - \overline{w}}{\partial t}, v\right) + a(\breve{w} - \overline{w}, v) = -a(S, v) + \left(\frac{\partial U}{\partial t}, v\right) \tag{4.23}$$

Taking $v = \breve{w} - \overline{w}$,

$$\left(\frac{\partial(\breve{w} - \overline{w})}{\partial t}, \breve{w} - \overline{w}\right) + a(\breve{w} - \overline{w}, \breve{w} - \overline{w}) = -a(S, \breve{w} - \overline{w}) + \left(\frac{\partial U}{\partial t}, \breve{w} - \overline{w}\right), \tag{4.24}$$

Using the same ideas from the last theorem,

$$\frac{1}{2}\frac{\partial}{\partial t}||(\breve{w} - \overline{w})(t)||_0^2 + \frac{\alpha}{2}||(\breve{w} - \overline{w})(t)||_1^2 \leq \frac{M^2}{2\alpha}||S||_1^2 + \left|\left|\frac{\partial U}{\partial t}(t)\right|\right|_0 ||(\breve{w} - \overline{w})(t)||_0. \tag{4.25}$$

Integrating in time from 0 to t, and noticing that $(\breve{w} - \overline{w})(0) = 0$,

$$||(\breve{w}-\overline{w})(t)||_0^2+\alpha \int_0^t ||\breve{w}-\overline{w}(\tau)||_1^2 d\tau \leq \frac{M^2 t_2}{\alpha}||S||_1^2+2\int_0^t \left|\left|\frac{\partial U}{\partial t}(\tau)\right|\right|_0 ||(\breve{w}-\overline{w})(\tau)||_0 d\tau. \tag{4.26}$$

Using Gronwall's Lemma,

$$\left\{||(\breve{w} - \overline{w})(t)||_0^2 + 2\alpha \int_0^t ||\breve{w} - \overline{w}(\tau)||_1^2 d\tau\right\}^{1/2} \leq \frac{M\sqrt{t_2}}{\sqrt{\alpha}}||S||_1 + \int_0^t \left|\left|\frac{\partial U}{\partial t}(\tau)\right|\right|_0 d\tau. \tag{4.27}$$

Substituting $w = \breve{w} + U$ and $\widetilde{w} = \overline{w} + U(t_2) + S$, and using the same convexity inequality as in the previous proof,

$$\begin{aligned}
&||(w - \widetilde{w})(t_2)||_0^2 + \alpha \int_0^{t_2} ||(w - \widetilde{w})(\tau)||_1^2 d\tau \\
&= ||(\breve{w} - \overline{w})(t_2) - S||_0^2 + \alpha \int_0^{t_2} ||(\breve{w} - \overline{w})(\tau) + U(\tau) - U(t_2) - S||_1^2 d\tau \qquad (4.28)\\
&\leq 2||(\breve{w} - \overline{w})(t_2)||_0^2 + 2\alpha \int_0^{t_2} ||(\breve{w} - \overline{w})(\tau)||_1^2 d\tau + 2||S||_0^2 \\
&\qquad + 2\alpha \int_0^{t_2} ||U(\tau) - U(t_2) - S||_1^2 d\tau \qquad (4.29)\\
&\leq 2\left\{\frac{\sqrt{Mt_2}}{\sqrt{\alpha}}||S||_1 + \int_0^t \left|\left|\frac{\partial U}{\partial t}(\tau)\right|\right|_0 d\tau\right\}^2 + 2||S||_0^2 + 2\alpha \int_0^{t_2} ||U(\tau) - U(t_2) - S||_1^2 d\tau.///
\end{aligned}$$

(4.30)

This means that we may not have the original prediction order. Unfortunately, as the next chapter with numerical tests will show, considering the Dirichlet conditions as constants does have a significant impact on the solution, and the algorithm might really be unstable.

4.2.2 Estimates for the discretized problem

We can use the same arguments as above to couple the difference between w_h and $\widetilde{w}_h$, for a regular triangulation of the domain, into standard estimate theorems for parabolic

problems. The subscript h is used to denote the interpolation of a function from $H^1(\widetilde{\Omega})$ into the discrete function space given by the triangulation $\mathcal{T}_h$ (for instance, V_h^k from *Section 3.1*).

We consider, for example, the theorem concerning the semidiscretized generic parabolic problem, in Quarteroni and Valli (1994), with operator

$$Lw \doteq \sum_{i,j=1}^{d} D_i(a_{ij}D_j w) + \sum_{i,j=1}^{d} [D_i(b_i w) + c_i D_i w] + a_0 w, \tag{4.31}$$

with coercivity constant α, with Dirichlet conditions being zero along the entire $\partial\Omega$:

Theorem 4.4. (QUARTERONI; VALLI, 1994, Proposition 11.2.1) Let $\mathcal{T}_h$ be a regular family of triangulations and assume that piecewise-linear or -bilinear finite elements are used. Assume moreover that the solution of the continuous problem satisfies

$$||u(t)||_2^2 \leq C(||Lu(t)||_0^2 + ||u(t)||_1^2), \quad \text{for almost all } t \text{ in } [0,T], \tag{4.32}$$

and that $f \in L^2(Q_T)$, $u_0 \in V$, $a_{ij}, b_i \in C^1(\overline{\Omega}), c_i, a_0 \in L^\infty(\Omega)$. Then the solutions u and u_h to the original and Galerkin approximations, respectively, satisfy

$$\begin{aligned} &||u(t) - u_h(t)||_0^2 + \alpha \int_0^t ||(u-u_h)(\tau)||_1^2 d\tau \\ &\qquad \leq ||u_0 - u_{h,0}||_0 + C_{\alpha,\gamma} h^2 \left(||u_{h,0}||_1^2 + ||u_0||_1^2 + \int_0^t ||f(\tau)||_0^2 d\tau \right) \end{aligned} \tag{4.33}$$

for almost all $t \in [0,T]$. Here, α is the coerciveness constant of the bilinear form, γ its continuity constant and $C_{\alpha,\gamma}$ is a suitable constant independent of h.

Corollary 4.5. Let S_h be the lifting of the error s of the approximation of choice for the Dirichlet condition of our monolithic predictor. Then, the error inside of the monolithic predictor with time-dependent Dirichlet conditions and $t_1 = 0$ can be estimated as

$$\begin{aligned} &||(w_h - \widetilde{w}_h)(t)||_0^2 + \alpha \int_0^t ||(w_h - \widetilde{w}_h)(\tau)||_1^2 d\tau \\ &\qquad \leq 2||w_0 - w_{h,0}||_0 + 2C_{\alpha,\gamma} h^2 \left(||w_{h,0}||_1^2 + ||w_0||_1^2 + \int_0^t ||f(\tau)||_0^2 d\tau \right) \\ &\qquad\quad + 4 \left\{ \frac{\sqrt{Mt_2}}{\sqrt{\alpha}} \max_{\tau\in(0,t_2]} ||S_h(\tau)||_1 + \int_0^t \left|\left| \frac{\partial S_h}{\partial t}(\tau) \right|\right|_0 d\tau \right\}^2 \\ &\qquad\quad + 4||S_h(t)||_0^2 + 8 \int_0^t ||S_h(\tau)||_1^2 d\tau, \end{aligned} \tag{4.34}$$

for $t \in (0, t_2]$.

Proof. Using the same argument from *Theorem 4.2*,

$$\begin{aligned} &||(w_h - \widetilde{w}_h)(t)||_0^2 + 2\alpha \int_0^t ||(w_h - \widetilde{w}_h)(\tau)||^2 d\tau \\ &\qquad \leq 2 \left\{ \frac{M\sqrt{t_2}}{\sqrt{\alpha}} \max_{\tau\in(0,t_2]} ||S_h(\tau)||_1 + \int_0^t \left|\left| \frac{\partial S_h}{\partial t}(\tau) \right|\right|_0 d\tau \right\}^2 \\ &\qquad\quad + 2||S_h(t)||_0^2 + 4 \int_0^t ||S_h(\tau)||_1^2 d\tau \end{aligned} \tag{4.35}$$

Now, using the convexity inequality from the proof of *Theorem 4.2*,

$$\begin{aligned}
&||(w-\widetilde{w}_h)(t)||_0^2 + \alpha \int_0^t ||(w-\widetilde{w}_h)(\tau)||_1^2 d\tau \\
&\quad \leq 2||(w-w_h)(t)||_0^2 + 2\alpha \int_0^t ||(w-w_h)(\tau)||_1^2 d\tau + 2||(w_h-\widetilde{w}_h)(t)||_0^2 \\
&\qquad + 2\alpha \int_0^t ||(w_h-\widetilde{w}_h)(\tau)||_1^2 d\tau \qquad (4.36) \\
&\quad \leq 2||w_0 - w_{h,0}||_0 + 2C_{\alpha,\gamma} h^2 \left(||w_{h,0}||_1^2 + ||w_0||_1^2 + \int_0^t ||f(\tau)||_0^2 d\tau \right) \\
&\qquad + 4 \left\{ \frac{\sqrt{Mt_2}}{\sqrt{\alpha}} \max_{\tau\in(0,t_2]} ||S_h(\tau)||_1 + \int_0^t \left\| \frac{\partial S_h}{\partial t}(\tau) \right\|_0 d\tau \right\}^2 \qquad (4.37) \\
&\qquad + 4||S_h(t)||_0^2 + 8 \int_0^t ||S_h(\tau)||_1^2 d\tau. ////
\end{aligned}$$

In the same way,

Corollary 4.6. One estimate for the solution inside of the monolithic predictor with constant Dirichlet conditions is

$$\begin{aligned}
&||(w_h-\widetilde{w}_h)(t_2)||_0^2 + \alpha \int_0^{t_2} ||(w_h-\widetilde{w}_h)(\tau)||_1^2 d\tau \\
&\leq 2||w_0 - w_{h,0}||_0 + 2C_{\alpha,\gamma} h^2 \left(||w_{h,0}||_1^2 + ||w_0||_1^2 + \int_0^{t_2} ||f(\tau)||_0^2 d\tau \right) \\
&\quad + 4 \left\{ \frac{\sqrt{Mt_2}}{\sqrt{\alpha}} ||S_h||_1 + \int_0^t \left\| \frac{\partial U_h}{\partial t}(\tau) \right\|_0 d\tau \right\}^2 + 4||S_h||_0^2 \qquad (4.38) \\
&\quad + 4\alpha \int_0^{t_2} ||U_h(\tau) - U_h(t_2) - S_h||_1^2 d\tau.
\end{aligned}$$

Proof. The proof is analogous to that of the previous corollary. ////

We now analyze the fully discretized problem. Assuming a uniform time discretization of time step size Δt, we study what happens to the difference between the solution of the discretization of the original problem and the solution given by our algorithm. Our analysis is limited to the $\theta-$method.

There are two ways to introduce these θ-methods, and we follow these descriptions from Quarteroni (2016). Firstly, we proceed as in the *Section 3.1*, discretizing the equation in space using finite elements, to reach an ODE system of the format

$$M\dot{\mathbf{u}}(t) + A\mathbf{u}(t) = \mathbf{f}, \qquad (4.39)$$

where M and A are matrices and $\mathbf{u}$(t) is the vector of degrees of freedom. The θ-method consists of discretizing this ODE in time as

$$M\frac{\mathbf{u}^{k+1}-\mathbf{u}^k}{\Delta t} + A[\theta\mathbf{u}^{k+1} + (1-\theta)\mathbf{u}^k] = \theta\mathbf{f}^{k+1} + (1-\theta)\mathbf{f}^k, \qquad (4.40)$$

$\theta \in [0,1]$.

However, when dealing with weak formulations, a practical way to analyze the θ-method is by using the approximations

$$\dot{\mathbf{u}} \approx \frac{\mathbf{u}^{k+1} - \mathbf{u}^k}{\Delta t}, \tag{4.41}$$

$$\mathbf{u} \approx \theta \mathbf{u}^{k+1} + (1-\theta)\mathbf{u}^k, \tag{4.42}$$

and

$$\mathbf{f} \approx \theta \mathbf{f}^{k+1} + (1-\theta)\mathbf{f}^k. \tag{4.43}$$

Theorem 4.7. For the monolithic predictor with time-dependent Dirichlet conditions, the θ-method gives the estimates

$$||\breve{u}_h^{n+1} - \overline{u}_h^{n+1}||_0 \leq ||S_h^{n+1}||_0, \quad \text{when } \theta = 0, \tag{4.44}$$

and

$$||\breve{u}_h^{n+1} - \overline{u}_h^{n+1}||_1 \leq \frac{M}{\alpha}||S_h^{n+1}||_1 + \frac{1}{\alpha\theta\Delta t}||S_h^{n+1}||_0, \quad \text{when } \theta \neq 0. \tag{4.45}$$

Proof. Let us consider the weak formulations as above and apply the $\theta-$method to them:

The original formulation becomes

$$\begin{aligned}\frac{1}{\Delta t}(\breve{u}_h^{n+1} - \breve{u}_h^n, v_h) + a(\theta\breve{u}_h^{n+1} + (1-\theta)\breve{u}_h^n, v_h) \\ = (\theta f(t_{n+1}) + (1-\theta)f(t_n), v_h) - a(\theta U_h^{n+1} + (1-\theta)U_h^n, v_h) \\ - \frac{1}{\Delta t}(U_h^{n+1} - U_h^n, v_h),\end{aligned} \tag{4.46}$$

and our method gives

$$\begin{aligned}\frac{1}{\Delta t}(\overline{u}_h^{n+1} - \overline{u}_h^n, v_h) + a(\theta\overline{u}_h^{n+1} + (1-\theta)\overline{u}_h^n, v_h) \\ = (\theta f(t_{n+1}) + (1-\theta)f(t_n), v_h) - a(\theta(U_h^{n+1} + S_h^{n+1}) \\ + (1-\theta)(U_h^n + S_h^n), v_h) - \frac{1}{\Delta t}(U_h^{n+1} + S_h^{n+1} - U_h^n - S_h^n, v_h)\end{aligned} \tag{4.47}$$

From the construction of the algorithm, we have that $\widetilde{u}_h^n = u_h^n$, $S_h^n = 0$, and therefore, $\breve{u}^n = \overline{u}^n$. Therefore, subtracting (4.47) from (4.46),

$$\frac{1}{\Delta t}(\breve{u}_h^{n+1} - \overline{u}_h^{n+1}, v_h) + a(\theta(\breve{u}_h^{n+1} - \overline{u}_h^{n+1}), v_h) = a(\theta S_h^{n+1}, v_h) + \frac{1}{\Delta}(S_h^{n+1}, v_h). \tag{4.48}$$

Substituting $v_h = \breve{u}_h^{n+1} - \overline{u}_h^{n+1}$ in (4.48), multiplying the result by Δt, and using the coercivity and continuity properties of a,

$$\begin{aligned}||\breve{u}_h^{n+1} - \overline{u}_h^{n+1}||_0^2 + \alpha\theta\Delta t||\breve{u}_h^{n+1} - \overline{u}_h^{n+1}||_1^2 \\ \leq M\Delta t||\theta S_h^{n+1}||_1 \, ||\breve{u}_h^{n+1} - \overline{u}_h^{n+1}||_1 + ||S_h^{n+1}||_0 \, ||\breve{u}_h^{n+1} - \overline{u}_h^{n+1}||_0.\end{aligned} \tag{4.49}$$

If $\theta = 0$, then (4.49) gives

$$||\breve{u}_h^{n+1} - \overline{u}_h^{n+1}||_0 \leq ||S_h^{n+1}||_0. \tag{4.50}$$

In the case when $\theta \neq 0$, we now ignore the first term on the left side of (4.49), and use the fact that $||v||_0 \leq ||v||_1, \quad \forall v \in H^1(\widetilde{\Omega})$,

$$\begin{aligned}&\alpha\theta\Delta t||\breve{u}_h^{n+1} - \overline{u}_h^{n+1}||_1^2 \\ &\quad \leq M\Delta t||\theta S_h^{n+1}||_1 \, ||\breve{u}_h^{n+1} - \overline{u}_h^{n+1}||_1 + ||S_h^{n+1}||_0 \, ||\breve{u}_h^{n+1} - \overline{u}_h^{n+1}||_1.\end{aligned} \tag{4.51}$$

Assuming that $||\breve{u}_h^{n+1} - \overline{u}_h^{n+1}||_1$ is not zero,

$$\alpha\theta\Delta t||\breve{u}_h^{n+1} - \overline{u}_h^{n+1}||_1 \leq M\Delta t||\theta S_h^{n+1}||_1 + ||S_h^{n+1}||_0. \tag{4.52}$$

Finally,

$$||\breve{u}_h^{n+1} - \overline{u}_h^{n+1}||_1 \leq \frac{M}{\alpha}||S_h^{n+1}||_1 + \frac{1}{\alpha\theta\Delta t}||S_h^{n+1}||_0. \qquad //// \tag{4.53}$$

The result above once again indicates that the order of approximation of the extrapolation on the boundary of the predictor can be conserved into the solution, when $\theta = 0$. However, we may lose one order of convergence when $\theta \neq 0$.

We now apply the same procedure for the method with continuous Dirichlet conditions. In this case, however, we could only estimate the case when $\theta \neq 0$.

Theorem 4.8. Using the θ method, on the monolithic predictor with constant Dirichlet conditions, if $\theta \neq 0$,

$$||u_h^{n+1} - \widetilde{u}_h^{n+1}||_0 \leq \left(\frac{1}{\alpha\theta\Delta t} + \frac{M}{\alpha}\right)||U_h^{n+1} - U_h^n||_1 + \left(1 + \frac{1}{\theta}\right)||S_h||_1. \tag{4.54}$$

Proof. We once again consider the weak formulations of the problems as above and apply the $\theta-$method in them:

The original method becomes

$$\begin{aligned}&\frac{1}{\Delta t}(\breve{u}_h^{n+1} - \breve{u}_h^n, v_h) + a(\theta\breve{u}_h^{n+1} + (1-\theta)\breve{u}_h^n, v_h) \\ &\quad = (\theta f(t_{n+1}) + (1-\theta)f(t_n), v_h) - a(\theta U_h^{n+1} + (1-\theta)U_h^n, v_h) \\ &\qquad - \frac{1}{\Delta t}(U_h^{n+1} - U_h^n, v_h),\end{aligned} \tag{4.55}$$

and our method reads

$$\begin{aligned}&\frac{1}{\Delta t}(\overline{u}_h^{n+1} - \overline{u}_n^n, v_h) + a(\theta\overline{u}_h^{n+1} + (1-\theta)\overline{u}_h^n, v_h) \\ &\quad = (\theta f(t_{n+1}) + (1-\theta)f(t_n), v_h) - a(U_h^{n+1} - S_h, v).\end{aligned} \tag{4.56}$$

From the construction of the algorithm, we have that $\overline{u}_h^n = \breve{u}_h^n$. Subtracting the equality (4.56) from (4.55),

$$\begin{aligned}\frac{1}{\Delta t}(\breve{u}_h^{n+1} - \overline{u}_h^{n+1}, v_h) + a(\theta(\breve{u}_h^{n+1} - \overline{u}_h^{n+1}), v_h) \\ = -a((\theta-1)U_h^{n+1} + (1-\theta)U_h^n - S_h, v_h) - \frac{1}{\Delta t}(U_h^{n+1} - U_h^n, v_h) \qquad (4.57)\end{aligned}$$

Substituting $v_h = u_h^{n+1} - \widetilde{u}_h^{n+1}$ in (4.57), multiplying the result by Δt, and using the coercivity and continuity properties of a,

$$\begin{aligned}&||\breve{u}_h^{n+1} - \overline{u}_h^{n+1}||_0^2 + \alpha\theta\Delta t||\breve{u}_h^{n+1} - \overline{u}_h^{n+1}||_1^2 \\ &\quad\le M\Delta t||(\theta-1)U_h^{n+1} + (1-\theta)U_h^n - S_h||_1\,||\breve{u}_h^{n+1} - \overline{u}_h^{n+1}||_1 \\ &\qquad + ||U_h^{n+1} - U_h^n||_0\,||\breve{u}_h^{n+1} - \overline{u}_h^{n+1}||_0 \qquad (4.58)\end{aligned}$$

As in the last theorem, if $\theta \neq 0$, we can ignore the first term on the left,

$$\begin{aligned}&\alpha\theta\Delta t||\breve{u}_h^{n+1} - \overline{u}_h^{n+1}||_1^2 \\ &\quad\le M\Delta t||(\theta-1)U_h^{n+1} + (1-\theta)U_h^n - S_h||_1\,||\breve{u}_h^{n+1} - \overline{u}_h^{n+1}||_1 \\ &\qquad + ||U_h^{n+1} - U_h^n||_0\,||\breve{u}_h^{n+1} - \overline{u}_h^{n+1}||_1. \qquad (4.59)\end{aligned}$$

Therefore,

$$\begin{aligned}&\alpha\theta\Delta t||\breve{u}_h^{n+1} - \overline{u}_h^{n+1}||_1 \\ &\quad\le M\Delta t||(\theta-1)(U_h^{n+1} - U_h^n) + S_h||_1 + ||U_h^{n+1} - U_h^n||_1 \qquad (4.60) \\ &\quad\le (1 + M\theta\Delta t)||U_h^{n+1} - U_h^n||_1 + \alpha\Delta t||S_h||_1, \qquad (4.61)\end{aligned}$$

and

$$\begin{aligned}&\alpha\theta\Delta t||u_h^{n+1} - \widetilde{u}_h^{n+1}||_0 \\ &\quad= \alpha\theta\Delta t||\breve{u}_h^{n+1} + U_h^{n+1} - (\overline{u}_h^{n+1} + U_h^{n+1} + S_h)||_0 \qquad (4.62) \\ &\quad\le ((1 + M\theta\Delta t)||U_h^{n+1} - U_h^n||_1 + \alpha\Delta t||S_h||_1) + \alpha\theta\Delta t||S_h||_1. \qquad (4.63)\end{aligned}$$

So, assuming $\theta \neq 0$,

$$||u_h^{n+1} - \widetilde{u}_h^{n+1}||_0 \le \left(\frac{1}{\alpha\theta\Delta t} + \frac{M}{\alpha}\right)||U_h^{n+1} - U_h^n||_1 + \left(1 + \frac{1}{\theta}\right)||S_h||_1. //// \qquad (4.64)$$

Once again, this raises the possibility that the predictor with constant Dirichlet condition is not practical.

5 NUMERICAL TESTS

We now present results from an implementation of our method in a simple Fluid-structure Interaction problem. In the first section, we describe the software, code and hardware used in our simulations. The second section is meant to present the problem we are solving, which is an elastic tube with fluid inside. Finally, we show results and comparisons between our method, with two sizes of tube, against a simple extrapolation predictor.

5.1 COMPUTATIONAL ENVIRONMENT AND TOOLS

The test was run on a Dell G7 Laptop, with 8GB of RAM, and an octa-core 8th generation Intel Core i5. Although the software we used can be run in parallel, we have only tested its single-thread version. The maximum of RAM used was 3.3GB, when testing using a refined mesh and a thin predictor, to be described below.

As a base code, we have used LifeV, from EPFL, Politecnico di Milano and Emory University, which is distributed under the LGPL 3 license. It is written in C++, and contains finite element facilities, and some codes for Navier Stokes equations and Fluid-Structure Interaction. The code also uses the Trilinos Packages, from Sandia Corporation under BSD and LGPL licenses, which is also written in C++ and contains code that allows for parallel methods in numerical linear algebra and other utilities. The LifeV code has been retrieved from its BitBucket repository, in the 12th of June, 2019.

More specifically, our method's implementation is based on the FaCSI method (DE-PARIS; FORTI, et al., 2016; FORTI; DEDÈ, 2015). It is a block-preconditioned monolithic method, coded in LifeV by Davide Forti. The Navier-Stokes equations are discretized using the *Geometric Convective Explicit* approach, described in *Chapter 3*, and it uses the SUPG stabilization technique. The tube test problem was adapted from the one written by Paolo Crosetto (CROSETTO, 2011), also in LifeV.

We have used open-source auxiliary software such as ParaView, version 5.4, from Kitware Inc. and Los Alamos National Laboratory, to create figures and animations, and FreeFEM (HECHT, 2012), version 4.2, to build all the meshes.

5.2 THE TEST PROBLEM

The test problem, as in Crosetto (2011), consists of an elastic tube with an incompressible, Newtonian fluid inside. The fluid is modeled through the Navier-Stokes equations, and the structure is a linear elastic solid. We have retained the constants from the original problem, and its initial time-step size. Indeed, we have not checked whether any convergence condition, such as *CFL* is satisfied. The fully monolithic method, used as a benchmark in our tests, is also assumed to be convergent.

TABLE 4 - Properties for the fluid

Density	$\rho_f = 1g/cm^3$
Dynamic viscosity	$\nu_f = 0.03g/(cm\,s)$

SOURCE: The author (2020).

TABLE 5 - Properties for the structure

Young's modulus	$E_s = 3 \times 10^6 dyne/cm^2$
Poisson's ratio	$\nu_s = 0.3$
Density	$\rho_s = 1.2g/cm^3$

SOURCE: The author (2020).

The cylinder domain is depicted in the *Figure 4* below, with a top view on the left, and an axial cut on the right. The structure part is shown in grey, and the white interior is the fluid domain. The cylinder has a length of $5cm$; the fluid part has radius of $0.5cm$, and the solid external boundary has a radius of $0.6cm$.

FIGURE 4 - Cuts of the domain

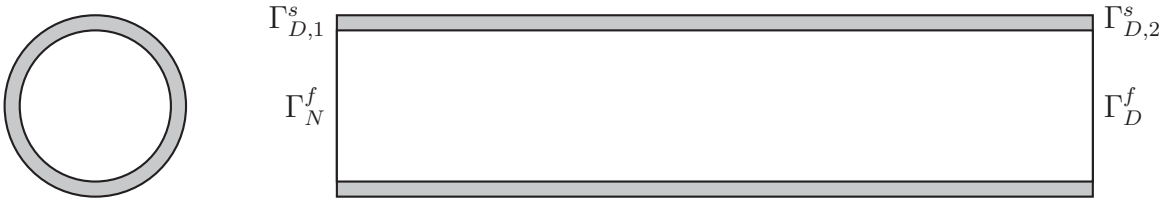

SOURCE: The author (2020).

The Dirichlet conditions $\Gamma^s_{D,1}$, $\Gamma^s_{D,2}$ and Γ^f_D are all zero, and the Neumann condition Γ^1_N is a constant normal stress of $\boldsymbol{\sigma} \cdot \mathbf{n} = 6650 dyne/cm^2$.

The meshes, with approximately $h = 0.25cm$, are shown in the *Figure 5* below.

FIGURE 5 - Mesh for the structure, with 1260 points, and for the fluid, with 2646 points

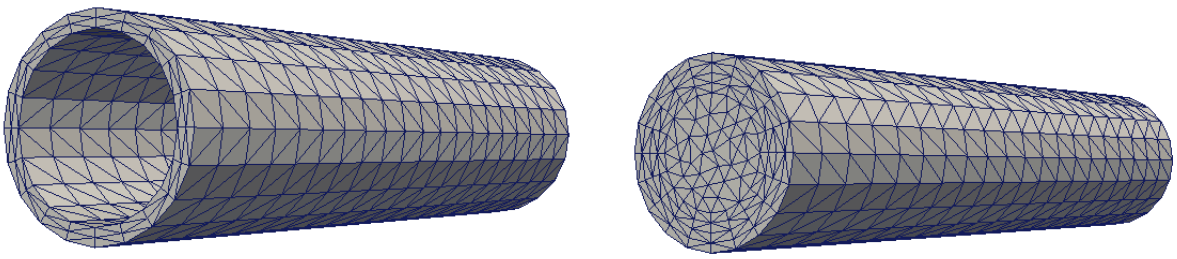

SOURCE: The author (2020).

We tested two different tubes for the monolithic predictor.

The first, that we refer to as *thin*, is made of all the structure domain, plus a tube of thickness 0.1 around the interface, for the fluid. In the *Figure 6*, accurately scaled, this would be the dashed, lighter gray portion of the fluid domain.

FIGURE 6 - Cuts of the thinner tube

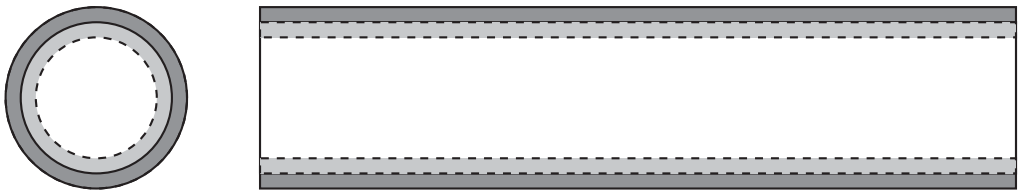

SOURCE: The author (2020).

The second tube for the predictor, referred to as *thick*, uses all of the structure's domain, plus a tube of thickness $0.2cm$, for the fluid. Once again, this corresponds to the dashed, lighter gray portion on the *Figure 7*.

FIGURE 7 - Cuts of the thicker tube

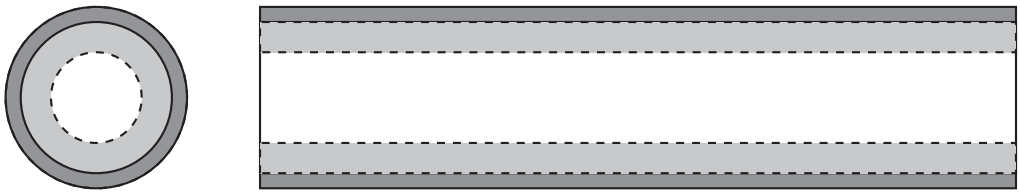

SOURCE: The author (2020).

Their corresponding meshes for the fluid part are as in *Figure 8*. The thin fluid tube has roughly 48% of the amount of points than the original problem, and the thick one, 79%.

FIGURE 8 - Fluid mesh part for the thin tube, with 1260 points, and for the thick one, with 2100 points

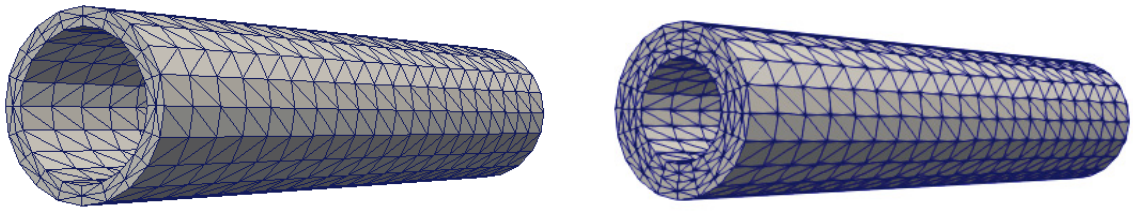

SOURCE: The author (2020).

Time is discretized through a second-order BDF method, and the polynomial order for the Finite Element Method is one. Once again, this choices correspond to what was already implemented.

5.3 RESULTS AND DISCUSSION

5.3.1 Stability

We first observe whether our method is stable. The following plots, *Figures 9*, *10* and *11*, show the l^2 error, that is, the l^2 difference between the solution using our method, with the thick tube, and the solution using the benchmark monolithic method. Along each solution function, we also plot its l^2 relative error, that is, the l^2 error divided by the l^2 norm of the benchmark solution. The markers *square*, *triangle* and *star* mark such an error, at the simulation time of the bottom axis.

We tested our method with three different time steps. Since our method begins in the third time step, because it requires two initial solutions to prepare for the BDF time integration, we omitted these initial results from the plots. The legends are the same for all plots, and Δt in these legends should be multiplied by 10^{-3}.

FIGURE 9 - Errors for the fluid velocity using the thick predictor

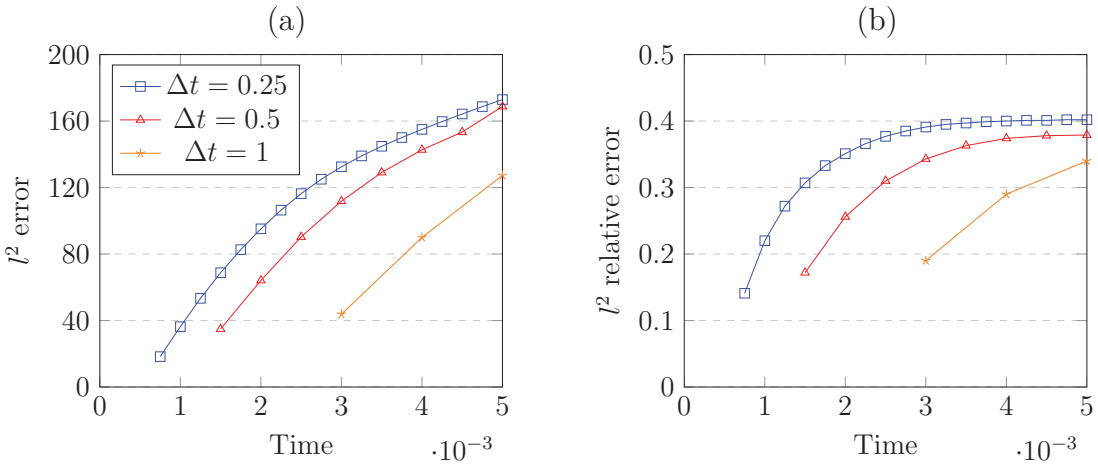

SOURCE: Data from this research (2020).

We notice that the error we got from our method is significant, especially in *Figures 9 (a)* and *10 (a)*, and although the relative error seems to stabilize, as in *Figure 9 (b)*, we cannot claim that our method converges for the fluid's velocity and fluid's pressure. This was our suspicion in the last chapter, by which we have seen that treating the Dirichlet conditions as constant might spoil the method.

FIGURE 10 - Errors for the fluid pressure using the thick predictor

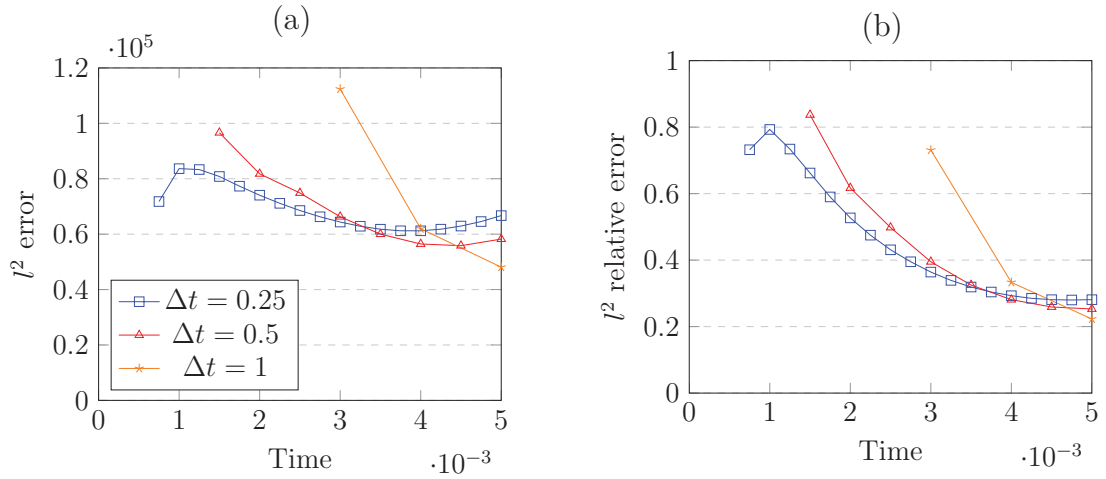

SOURCE: Data from this research (2020).

FIGURE 11 - Errors for the structure displacement using the thick predictor

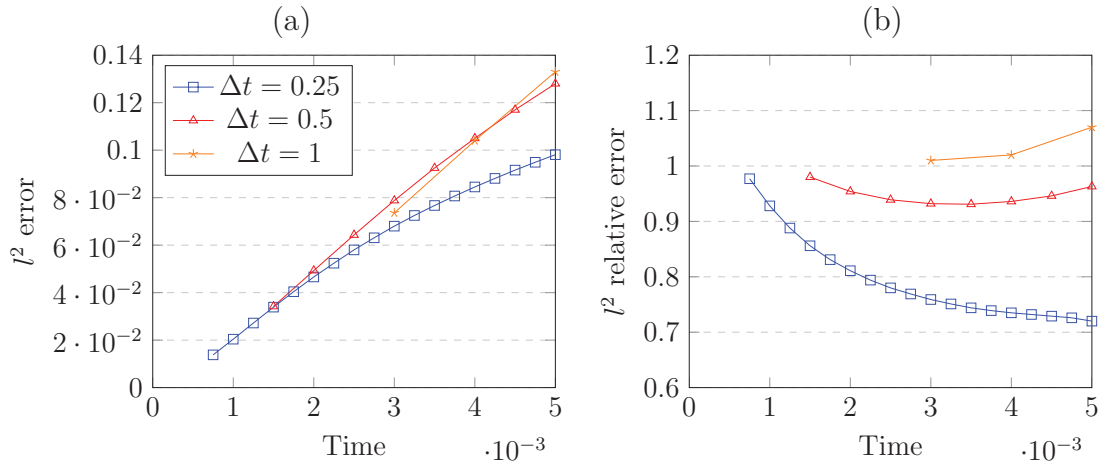

SOURCE: Data from this research (2020).

5.3.2 Quality of the prediction

We now compare the solutions from our method with the one from a simple predictor method, by which we extrapolate the interface functions, using the simple

$$u_f^* = 2u^n - u^{n-1} \text{ and } d_s^* = 2d^n - d^{n-1},$$

and feed these functions into the fluid and structure subproblems. We shall refer to the latter as the *simple* method.

For each variable, divided into the *Figures 12*, *13* and *14*, we compare the predictors within the same time-step size. These errors are, once again, calculated taking the solution using the fully monolithic method, as the benchmark.

FIGURE 12 - Comparison of the fluid's velocity using different predictors

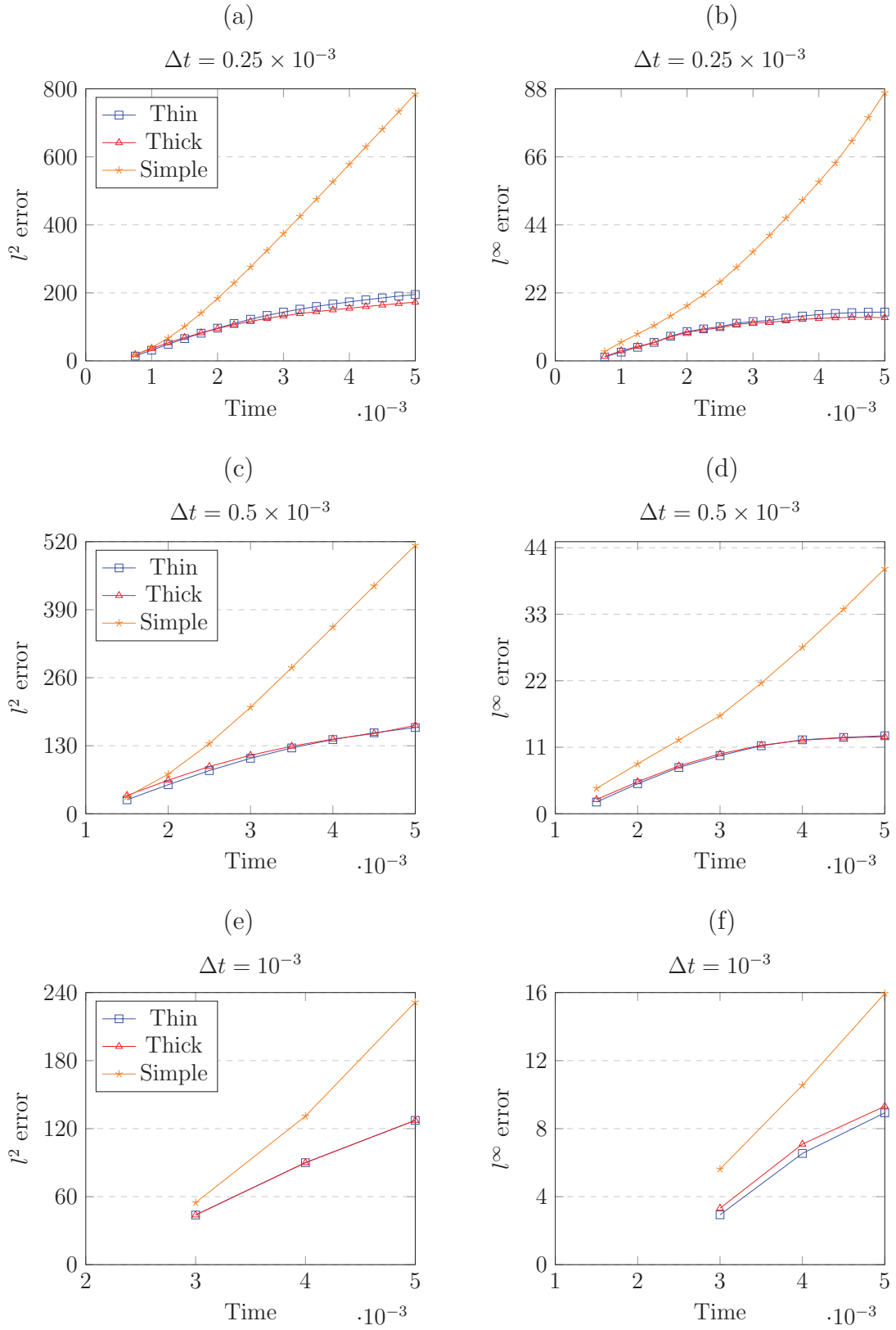

SOURCE: Data from this research (2020).

FIGURE 13 - Comparison of the fluid's pressure using different predictors

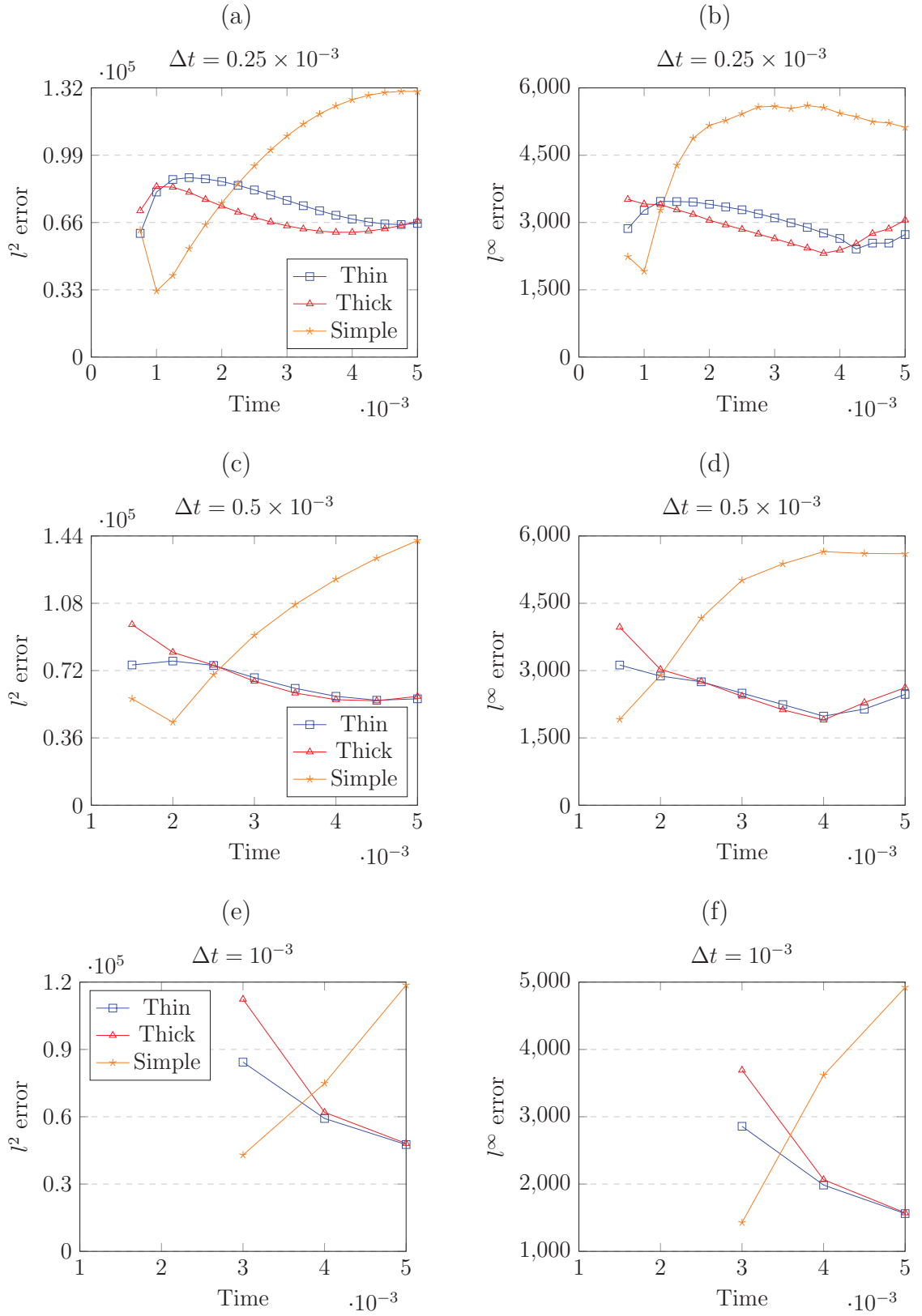

SOURCE: Data from this research (2020).

FIGURE 14 - Comparison of the structure's displacement using different predictors

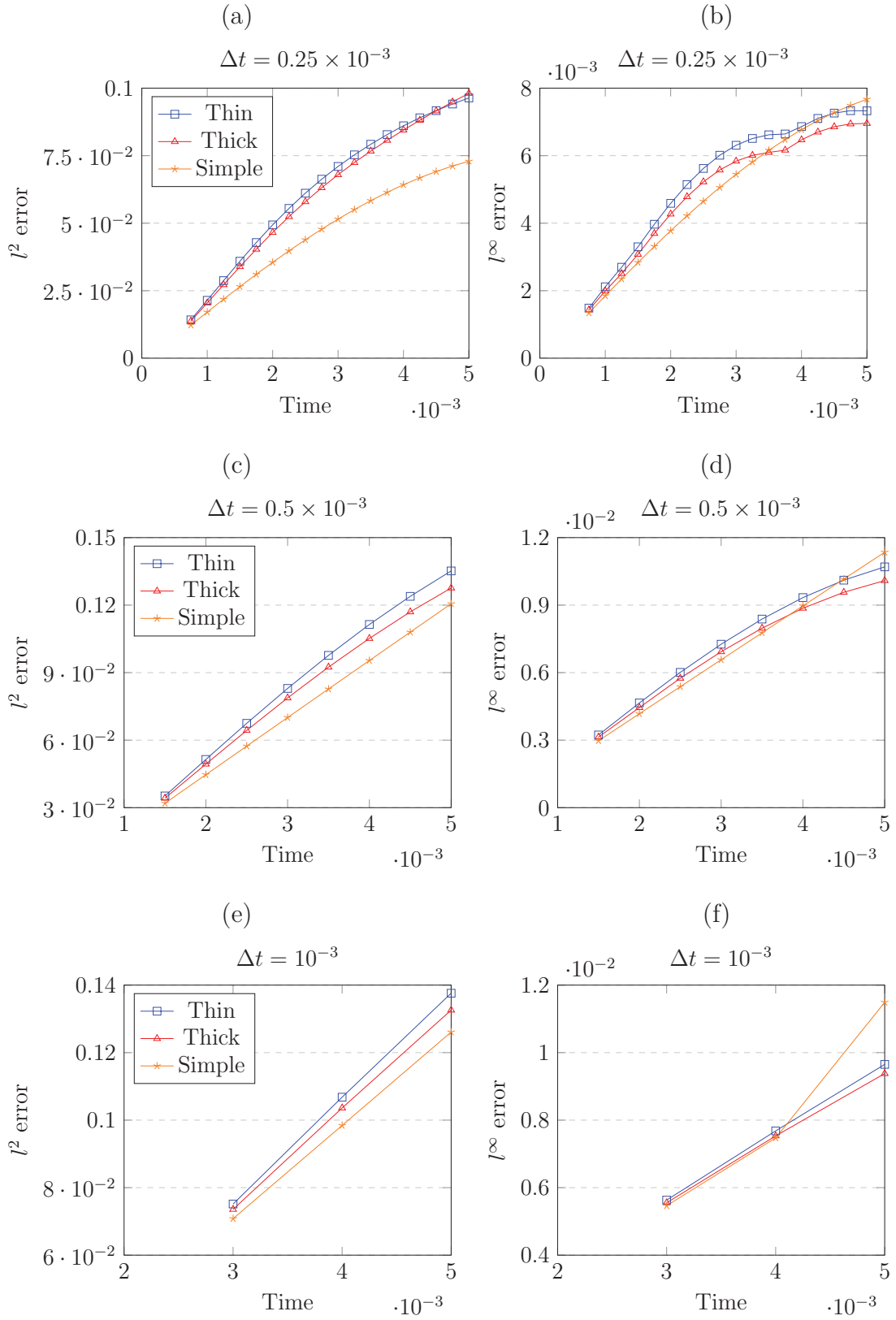

SOURCE: Data from this research (2020).

Figure 12 shows that our method has better stability properties than a simple predictor, for the fluid's velocity. The same happens for the fluid's pressure, in *Figure 13*, but

the simple predictor is more accurate in the first steps. For the structure's displacement, in *Figure 14*, the simple predictor is better in the l^2 norm, but becomes less accurate than our method after a few steps in the l^∞ norm.

Having done the quantitative comparison between the predictors, we now turn to a more qualitative analysis. We plot the functions found using the different predictors, to compare how close they fit in the benchmark solution, called **Full** in the legends. Since we have radial symmetry, we have selected a line, along the interface, from the point $(-0.5, 0, 0)$ to $(-0.5, 0, 5)$, along the cylinder's length, and plot each of the coordinates of the solutions. The results are shown for each of the time step sizes, but we plot only the third and last time steps, that is, the first prediction and the outcome of the algorithm until the end of the time period.

We report here the plots for a time step size of 0.25×10^{-3}. Those for $\Delta t = 0.5 \times 10^{-3}$ and $\Delta t = 10^{-3}$ are shown in the **Appendix**. In the following plots, *fluid's displacement* is equal to the displacement of the fluid's domain, $\widetilde{\boldsymbol{\eta}}$.

FIGURE 15 - Plots of the fluid's pressure on the line, with $\Delta t = 0.25 \times 10^{-3}$

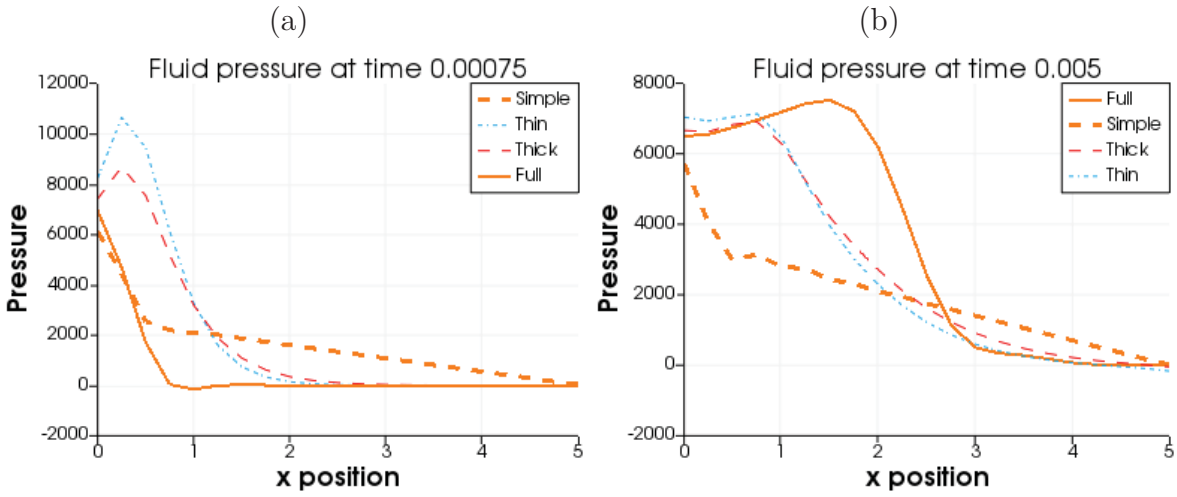

SOURCE: Data from this research (2020).

FIGURE 16 - Plots of the fluid's displacement on the line, with $\Delta t = 0.25 \times 10^{-3}$

(a)

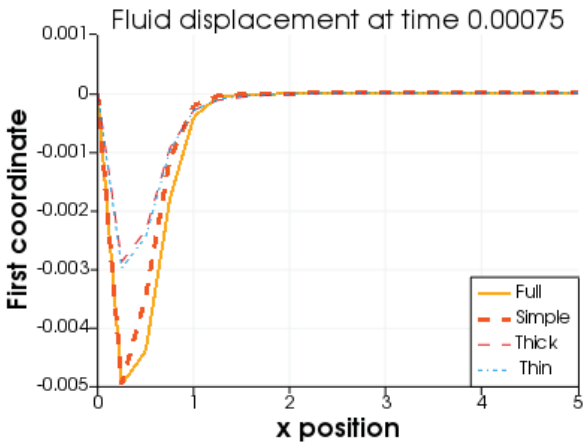

(b)

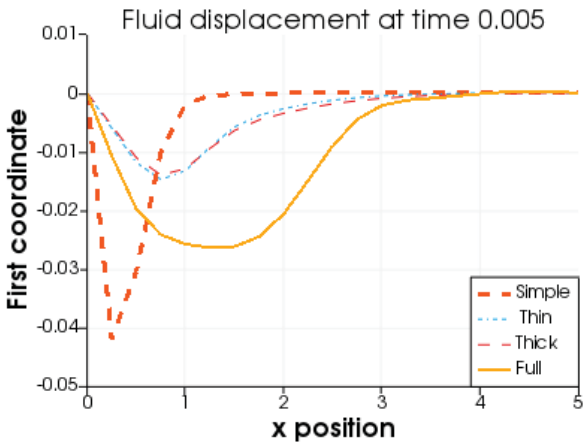

(c)

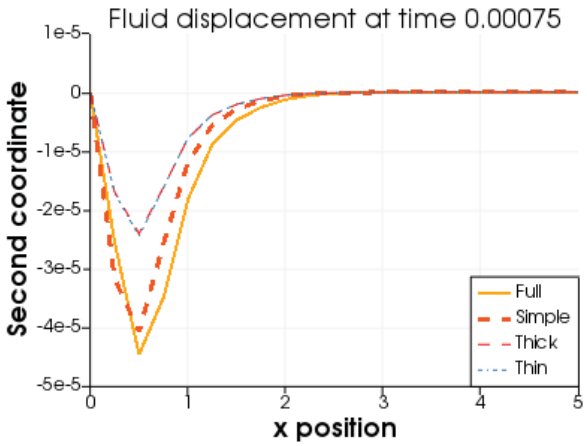

(d)

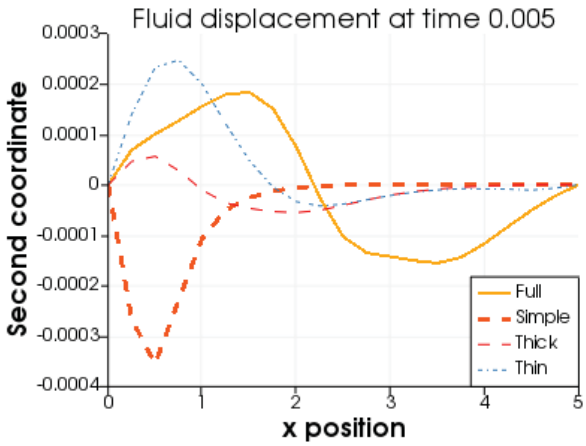

(e)

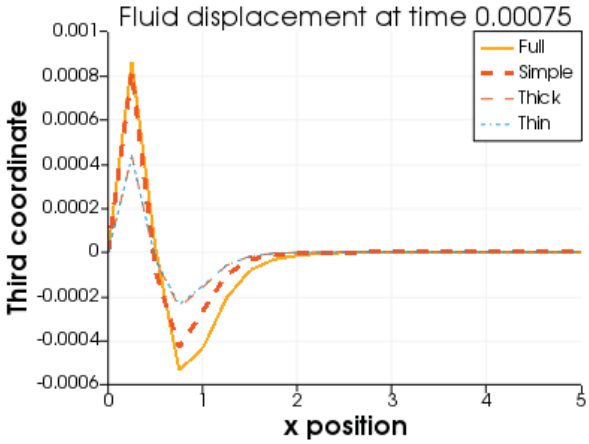

(f)

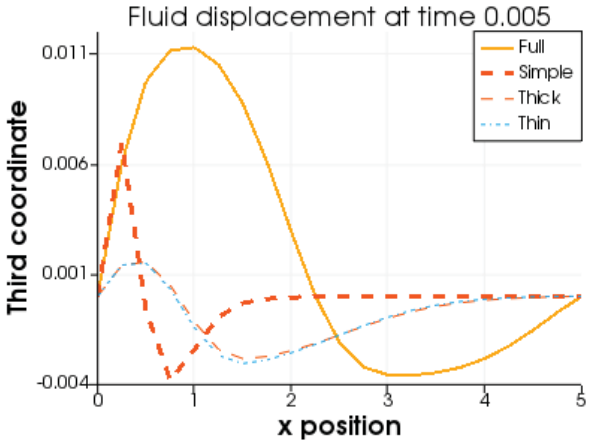

SOURCE: Data from this research (2020).

FIGURE 17 - Plots of the fluid's velocity on the line, with $\Delta t = 0.25 \times 10^{-3}$

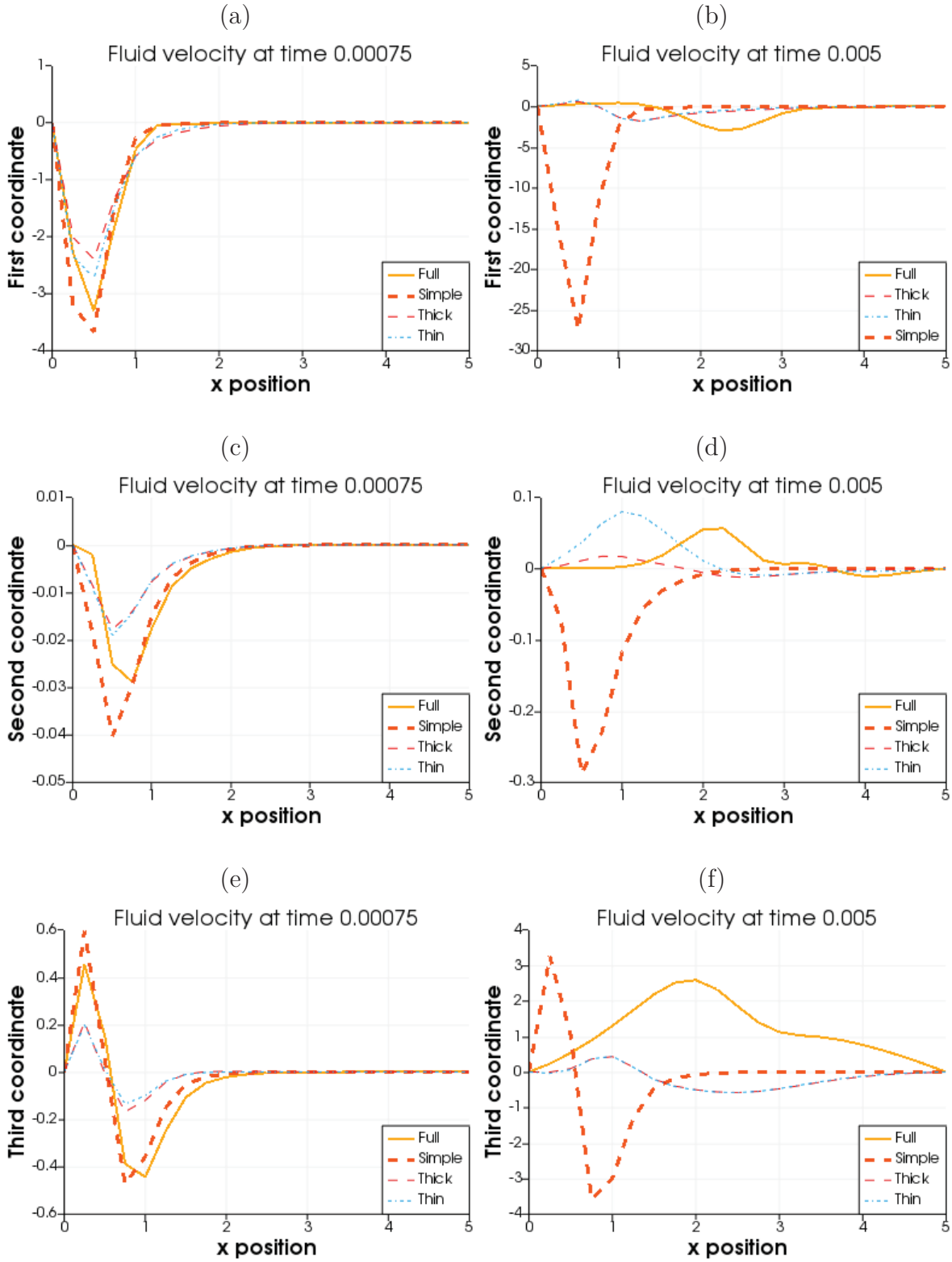

SOURCE: Data from this research (2020).

From these many plots, we highlight a few interesting features. Overall, our method correctly predicts the format of the benchmark solution. However, it seems to be "stuck" in the beginning of the cylinder, while the solution through the monolithic method propa-

gates through it. Also, apart from the first coordinate of the fluid's displacement, there is a significant error in the magnitude of our predictions. Such error was already highlighted in the quantitative comparison.

As for the comparison of our method with a simple prediction, there are two main observations. The first is that the simple predictor behaves much better at the first prediction. The second is that our method seems to be more stable, as in *Figure 17*, and it better predicts the format of the benchmark solution, also as in *Figure 17*.

5.3.3 Sensitivity to the boundary condition and mesh refinement

Our investigation continues into checking what happens when we double the Neumann condition on the boundary, by applying a normal stress of $13300 dyne/cm^2$. We show the plots for the thick predictor, in the *Figures 18*, *19* and *20*, but the behavior of the method is similar for the thin one: the error roughly doubles, and the relative error stays very similar to that of the problem with half the pressure.

Once again, the Δt from the legends in the plots are meant to be multiplied by 10^{-3}.

FIGURE 18 - Error for the fluid's velocity with the thick predictor

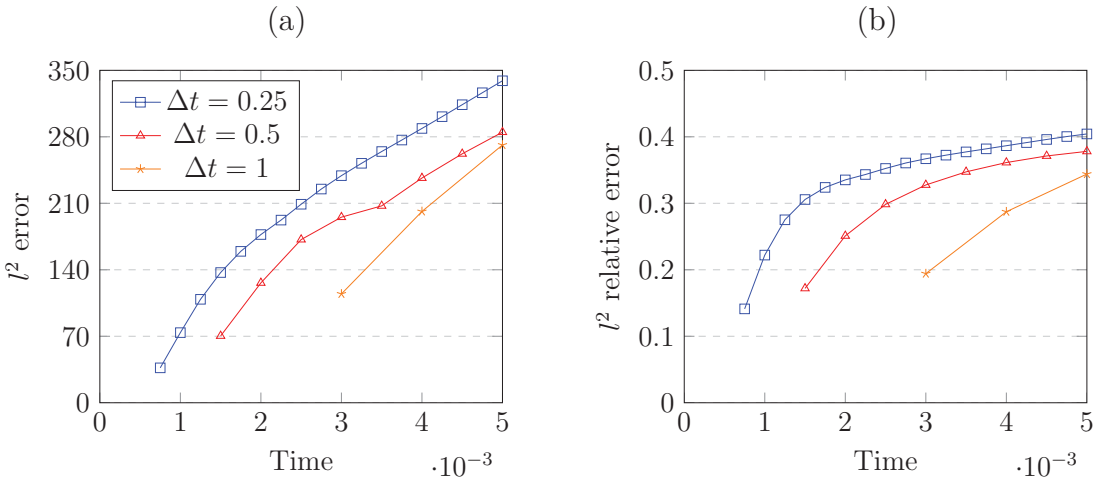

SOURCE: Data from this research (2020).

Our last test checks the behavior of our algorithm when we refine the mesh. We have attempted to use half the length of the tetrahedra. The fluid's full domain mesh contains 12997 points; the thin predictor for the fluid and structure meshes both contain 4920 points. Since the results are still very similar to the original, we only report that the l^2 errors have roughly doubled, while the l^∞ and relative l^2 errors stayed roughly the same.

FIGURE 19 - Error for the fluid's pressure with the thick predictor

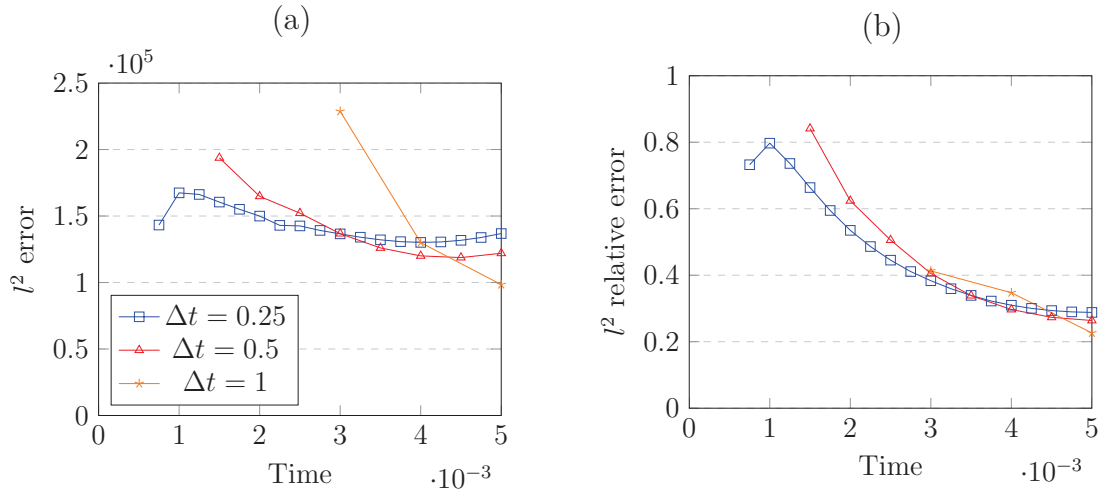

SOURCE: Data from this research (2020).

FIGURE 20 - Error for the structure's displacement with the thick predictor

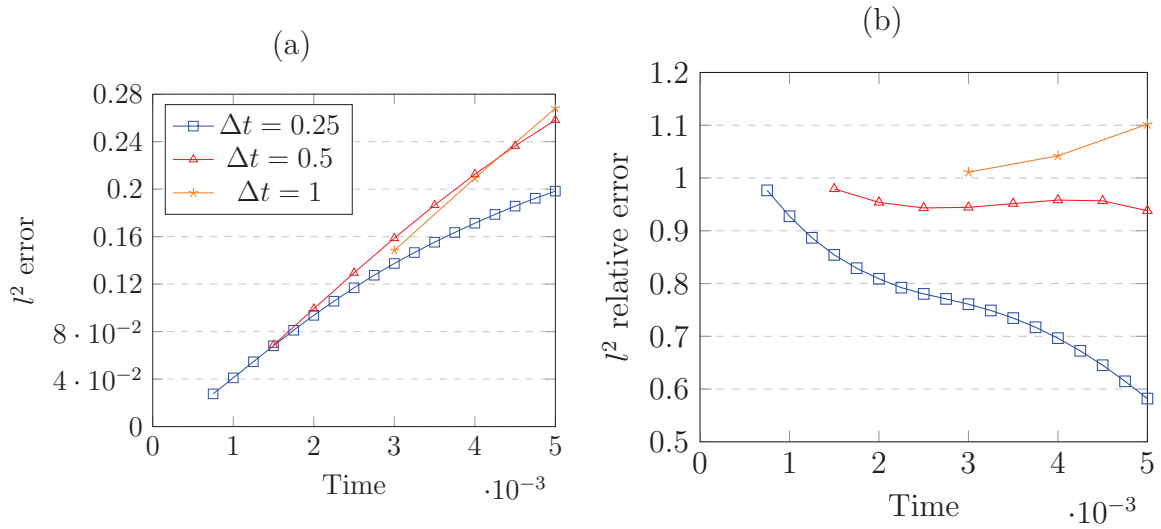

SOURCE: Data from this research (2020).

FIGURE 21 - Refinement of the full fluid mesh and the fluid part of the thin predictor

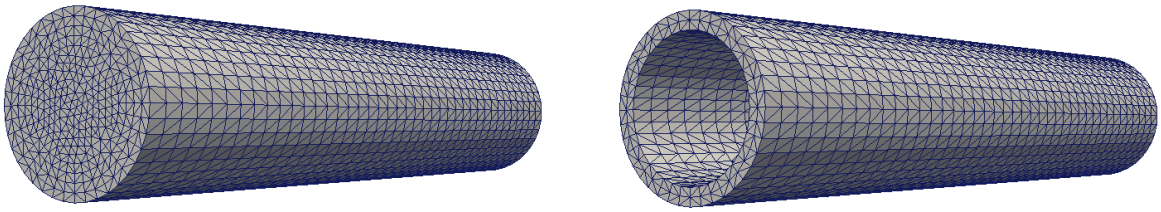

SOURCE: The author (2020).

6 CONCLUSION

As a starting point and motivation for our proposed method, we have given some background in how Fluid-Structure interaction problems are modelled, choosing the ALE option for the coupling. We then described the idea behind the two classes of methods available, namely monolithic and partitioned ones. While the main advantage of the first is the stability of the method, it is criticized for the fact that it does not allow for a straightforward use of specialized methods for fluid and structure. It is also a disadvantage that it generates a large nonlinear system of equations, when discretized. However, partitioned methods are sometimes not stable, through the *added mass effect*, and even when they are, they require many iterations at each time step of both fluid and structure problems, which can also be expensive.

With this context in mind, we have then shown our method. In one way, it can be presented as some sort of hybrid of monolithic and partitioned methods. But perhaps more simply, the idea of the method is to overcome the possible non-differentiability of the functions on the interface, which might not allow for the use of simple extrapolations as predictors. The point of our proposal is to use extrapolations inside of the fluid and structure domains, where the functions are assumed to be differentiable, and feed them into the monolithic method as Dirichlet conditions.

The more straightforward way is to consider these Dirichlet conditions as time-dependent, which is however addressed in a slightly more sophisticated way by the discretizations. By the use of a parabolic problem, we have shown that such method would translate the extrapolation order used on the boundaries into the prediction of the values on the interface.

The second idea, which we have used in our simulations, is to use constant Dirichlet conditions, which are simpler to implement and already present in most solvers of fluid and structure. However, by using the same analytical tools from the first method, we could not prove the stability of this method. While it could be that maybe another analytical technique could prove its stability and prediction order as in the first method, our simulations have provided with more evidence for this method's unpracticality.

Still, the simulation's results have hinted that, even if the method does not converge, it is more well-behaved after over a dozen of time steps, when compared to a simple extrapolation on the interface. Moreover, it maintains the interface solution's qualitative aspect. Quite surprisingly, the thickness of the tube used for the prediction had only a small influence on our results. These small achievements prompt us to continue the study of our method.

Indeed, the idea of a monolithic predictor offers quite a few opportunities for further research. The most pressing is the simulation of the predictor that uses time-dependent

Dirichlet conditions. Another important pursuit is the continuation of study in the stability properties of our methods with more sophisticated PDEs and even FSI models. What is more, we could test different boundary conditions, for instance Neumann or Robin, for the predictor. Finally, we could analyse our methods further to understand the role of the predictor's thickness in the accuracy of the solutions.

REFERENCES

ADAMS, R.; FOURNIER, J. J. F. **Sobolev Spaces**. Oxford: Academic Press, 2003.

BADIA, S.; NOBILE, F.; VERGARA, C. Fluid-structure partitioned procedures based on Robin transmission conditions. **Journal of Computational Physics**, v. 227, p. 7027–7051, 2008.

BARKER, A. T.; CAI, X-.C. Scalable parallel methods for monolithic coupling in fluid-structure interaction with application to blood flow modeling. **Journal of Computational Physics**, v. 229, p. 642–659, 2010.

BATCHELOR, G. K. **An introduction to fluid dynamics**. New York: Cambridge University Press, 2000. (Cambridge Mathematical Library).

BAZILEVS, Y.; TAKIZAWA, K.; TEZDUYAR, T. E. **Computational Fluid-Structure Interaction: methods and applications**. West Sussex: John Wiley & Sons Ltd, 2013.

BOFFI, D.; GASTALDI, L. Stability and geometric conservation laws for ALE formulations. **Computer methods in applied mechanics and engineering**, v. 193, p. 4717–4739, 2004.

BUKAC, M.; MUHA, B. Stability and convergence analysis of the extensions of the kinematically coupled scheme for the fluid-structure interaction. **SIAM Journal of Numerical Analysis**, v. 54, n. 5, p. 3032–3061, 2016.

CAI, X-.C.; KEYES, D. Nonlinearly preconditioned inexact Newton algorithms. **Siam Journal of Scientific Computing**, v. 24, n. 1, p. 183–200, 2002.

CAUSIN, P.; GERBEAU, J. F.; NOBILE, F. Added-mass effect in the design of partitioned algorithms for fluid-structure problems. **Computer methods in applied mechanics and engineering**, v. 194, p. 4506–4527, 2005.

CIARLET, P. G. **The Finite Element Method for Elliptic Problems**. Philadelphia: Society for Industrial and Applied Mathematics, 2002. (Classics in Applied Mathematics).

CROSETTO, P. **Fluid-structure interaction problems in hemodynamics: parallel solvers, preconditioners and applications**. 2011. PhD thesis – EPFL.

CROSETTO, P. et al. Parallel algorithms for fluid-structure interaction problems in haemodynamics. **Siam Journal of Scientific Computing**, 2011.

DEGROOTE, J. et al. Stability of a coupling technique for partitioned solvers in FSI applications. **Computers and Structures**, v. 86, p. 2224–2234, 2008.

DEPARIS, S.; DISCACCIATI, M.; QUARTERONI, A. Computational Fluid Dynamics 2004. In: ed. by C. Groth and D. Zingg. Springer Verlag, 2006. A domain decomposition framework for fluid-structure interaction problems, p. 41–58.

DEPARIS, S.; FORTI, D., et al. FaCSI: a block parallel preconditioner for fluid structure interaction in hemodynamics. **Journal of Computational Physics**, v. 327, p. 700–718, 2016.

DETTMER, W. G.; PERIĆ, D. A computational framework for fluid structure interaction: Finite element formulation and applications. **Computer methods in applied mechanics and engineering**, v. 195, p. 5754–5779, 2005.

_____. A new staggered scheme for fluid-structure interaction. **International Journal for Numerical Methods in Engineering**, v. 93, p. 1–22, 2013.

ÉTIENNE, S.; GARON, A.; PELLETIER, D. Perspective on the geometric conservation law and finite element methods for ALE simulations of incompressible flow. **Journal of Computational Physics**, v. 228, p. 2313–2333, 2009.

FARHAT, C.; GEUZAINE, P.; GRANDMONT, C. The discrete geometric conservation law and the nonlinear stability of ALE schemes for the solution of flow problems. **Journal of Computational Physics**, v. 174, p. 669–694, 2001.

FERNÁNDEZ, M. A.; MOUBACHIR, M. A Newton method using exact jacobians for solving fluid-structure coupling. **Computers and Structures**, v. 83, p. 127–142, 2005.

FERNÁNDEZ, M. A.; MULLAERT, J. Convergence and error analysis for a class of splitting schemes in incompressible fluid-structure interaction. **IMA Journal of Numerical Analysis**, v. 36, p. 1748–1782, 2015.

FORMAGGIA, L.; NOBILE, F. A stability analysis for the arbitrary Lagrangian Eulerian formulation with finite elements. **East-West Journal of numerical mathematics**, v. 7, n. 2, p. 105–131, 1999.

FORMAGGIA, L.; QUARTERONI, A.; VENEZIANI, A. (Eds.). **Cardiovascular Mathematics**. Milan: Springer Verlag, 2009.

FORMAGGIA, L.; SALERI, F.; VENEZIANI, A. **Applicazioni ed esercizi di modellistica numerica per problemi differenziali**. Milan: Springer Verlag, 2005.

FÖRSTER, C.; WALL, W. A.; RAMM, E. Artificial added mass instabilities in sequential staggered coupling of nonlinear structures and incompressible viscous flows. **Computer methods in applied mechanics and engineering**, v. 196, p. 1278–1293, 2007.

FORTI, D.; DEDÈ, L. Semi-implicit BDF time discretization of the Navier-Stokes equations with VMS-LES modeling in a High Performance Computing framework. **Comput. Fluids.**, v. 117, n. 1, p. 168–182, 2015.

GURTIN, M. E. **An introduction to continuum mechanics**. New York: Academic Press, 1981.

HAY, A. et al. Time-integration for ALE simulations of Fluid-Structure Interaction problems: Stepsize and order selection based on the BDF. **Computer methods in applied mechanics and engineering**, v. 295, p. 172–195, 2015.

HECHT, F. New development in FreeFem++. **Journal of numerical mathematics**, v. 20, n. 3-4, p. 251–265, 2012.

HIRT, C.W; AMSDEN, A.A.; COOK, J.L. An arbitrary Lagrangian-Eulerian computing method for all flow speeds. **Journal of Computational Physics**, v. 14, n. 3, p. 227–253, Mar. 1974.

HOU, G.; WANG, J.; LAYTON, A. Numerical methods for fluid-structure interaction — a review. **Commun. Comput. Phys**, v. 12, n. 2, p. 337–377, 2012.

KADAPA, C.; DETTMER, W. G.; PERIĆ, D. A stabilised immersed framework on hierarchical b-spline grids for fluid-flexible structure interaction with solid-solid contact. **Computer methods in applied mechanics and engineering**, v. 335, p. 472–489, 2018.

KIM, W.; LEE, I.; CHOI, H. A weak-coupling immersed boundary method for fluid-structure interaction with low density ratio of solid to fluid. **Journal of Computational Physics**, v. 359, p. 296–311, 2018.

KÜTTLER, U.; WALL, W. A. Fixed-point fluid-structure interaction solvers with dynamic relaxation. **Computational Mechanics**, v. 43, p. 61–72, 2008.

LANDAU, L. D.; LIFSHITZ, E. M. **Theory of elasticity**. Oxford: Pergamon Press, 1970. v. 7. (Course of Theoretical Physics).

MAYR, M. et al. A temporal consistent monolithic approach to fluid-structure interaction enabling single field predictors. **Siam Journal of Scientific Computing**, v. 37, n. 1, b30–b59, 2015.

NOBILE, F.; POZZOLI, M.; VERGARA, C. Inexact accurate partitioned algorithms for fluid-structure interaction problems with finite elasticity in haemodynamics. **Journal of Computational Physics**, v. 273, p. 598–617, 2014.

PESKIN, C. S. Flow patterns around heart valves: a numerical method. **Journal of Computational Physics**, v. 10, p. 252–271, 1972.

QUARTERONI, A. **Modellistica Numerica per Problemi Differenziali**. 6th. Milan: Springer Verlag, 2016.

QUARTERONI, A.; VALLI, A. **Numerical approximation of partial differential equations**. Berlin, Heidelberg: Springer Verlag, 1994.

RICHTER, Thomas. **Fluid-structure Interactions: Models, Analysis and Finite Elements**. Cham: Springer Verlag, 2017.

RUDIN, Walter. **Real and Complex Analysis**. 3. ed. New York: McGraw-Hill, 1987.

TALLEC, P. L.; MOURO, J. Fluid structure interaction with large structural displacements. **Computer methods in applied mechanics and engineering**, 2001.

APPENDIX

The plots below are a continuation of those in *Section 5.3.2*.

FIGURE 22 - Plots of the fluid's pressure on the line, with $\Delta t = 0.5 \times 10^{-3}$

(a) (b)

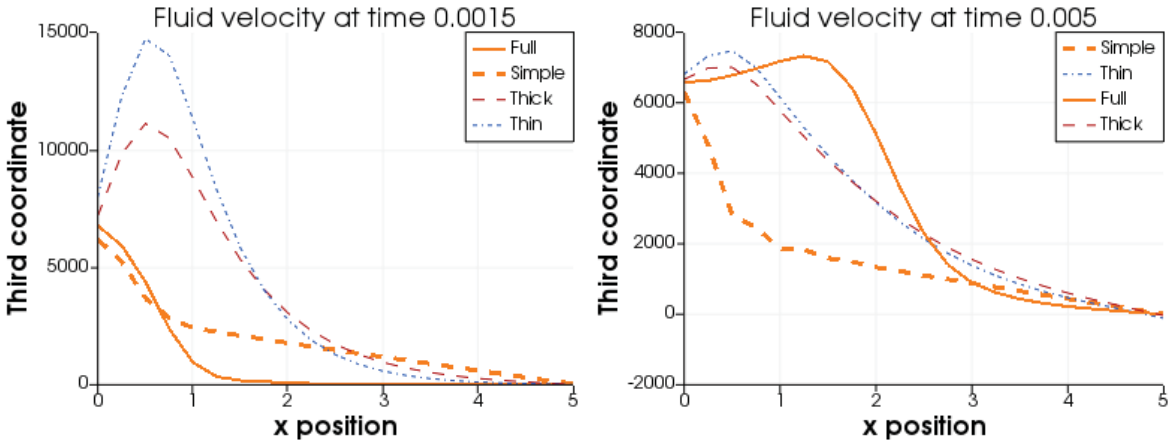

SOURCE: Data from this research (2020).

FIGURE 23 - Plots for the fluid's displacement on the line, with $\Delta t = 0.5 \times 10^{-3}$

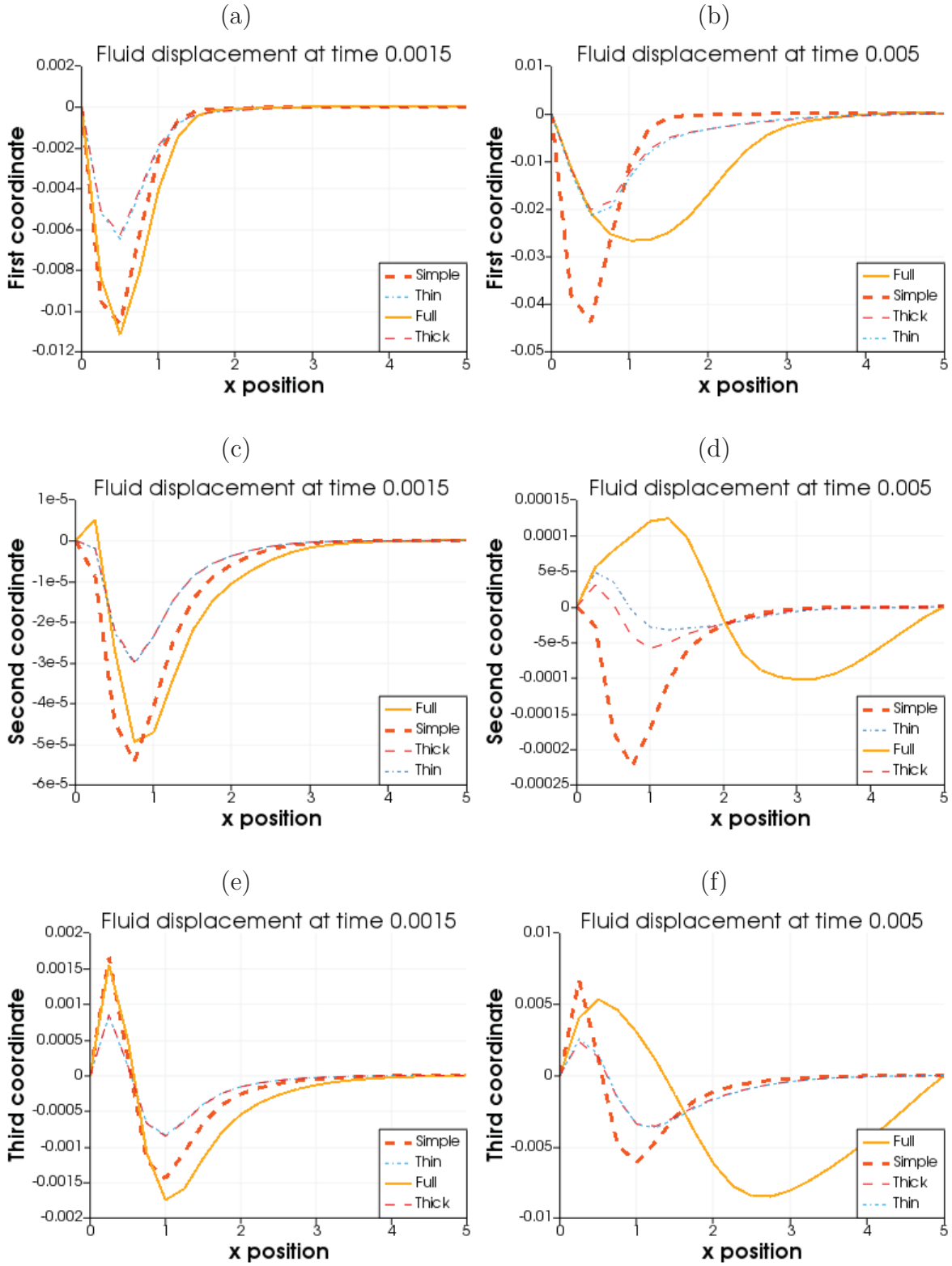

SOURCE: Data from this research (2020).

FIGURE 24 - Plots of the fluid's velocity on the line, with $\Delta t = 0.5 \times 10^{-3}$

(a)

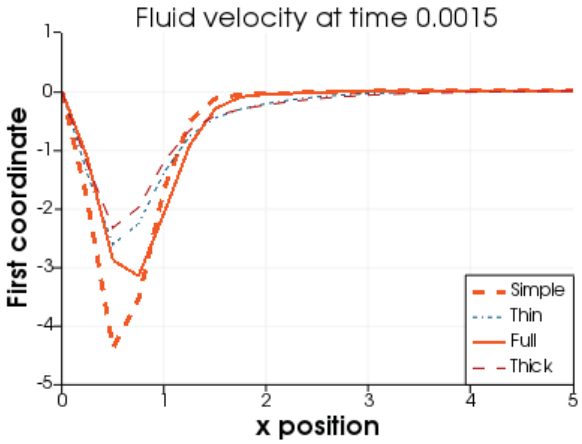

(b)

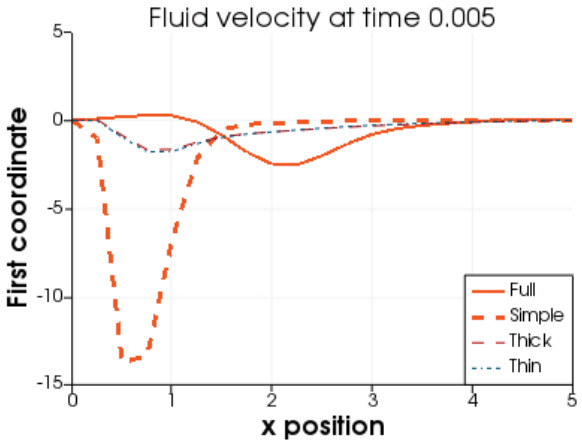

(c)

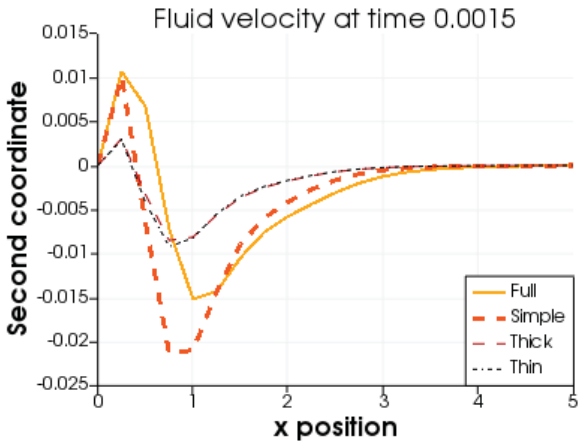

(d)

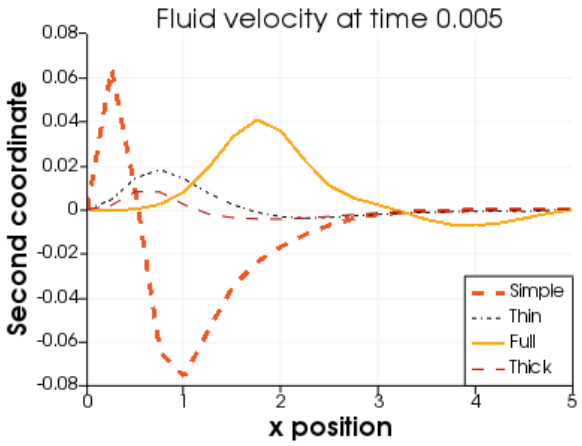

(e)

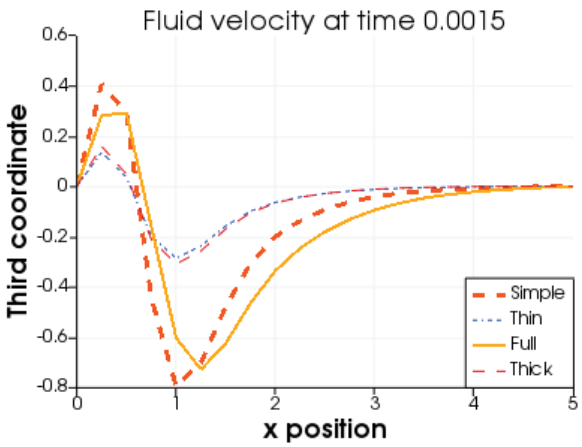

(f)

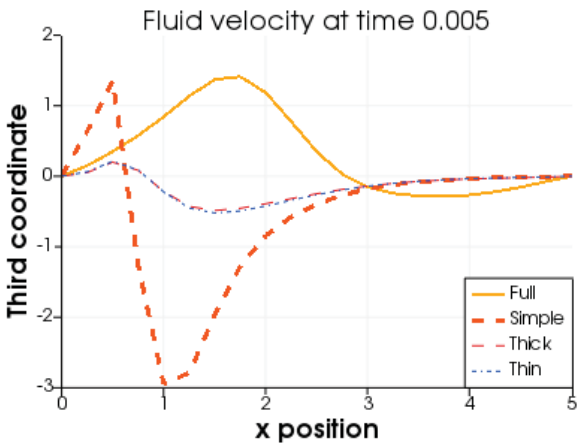

FIGURE 25 - Plots of the fluid's domain on the line, with $\Delta t = 10^{-3}$

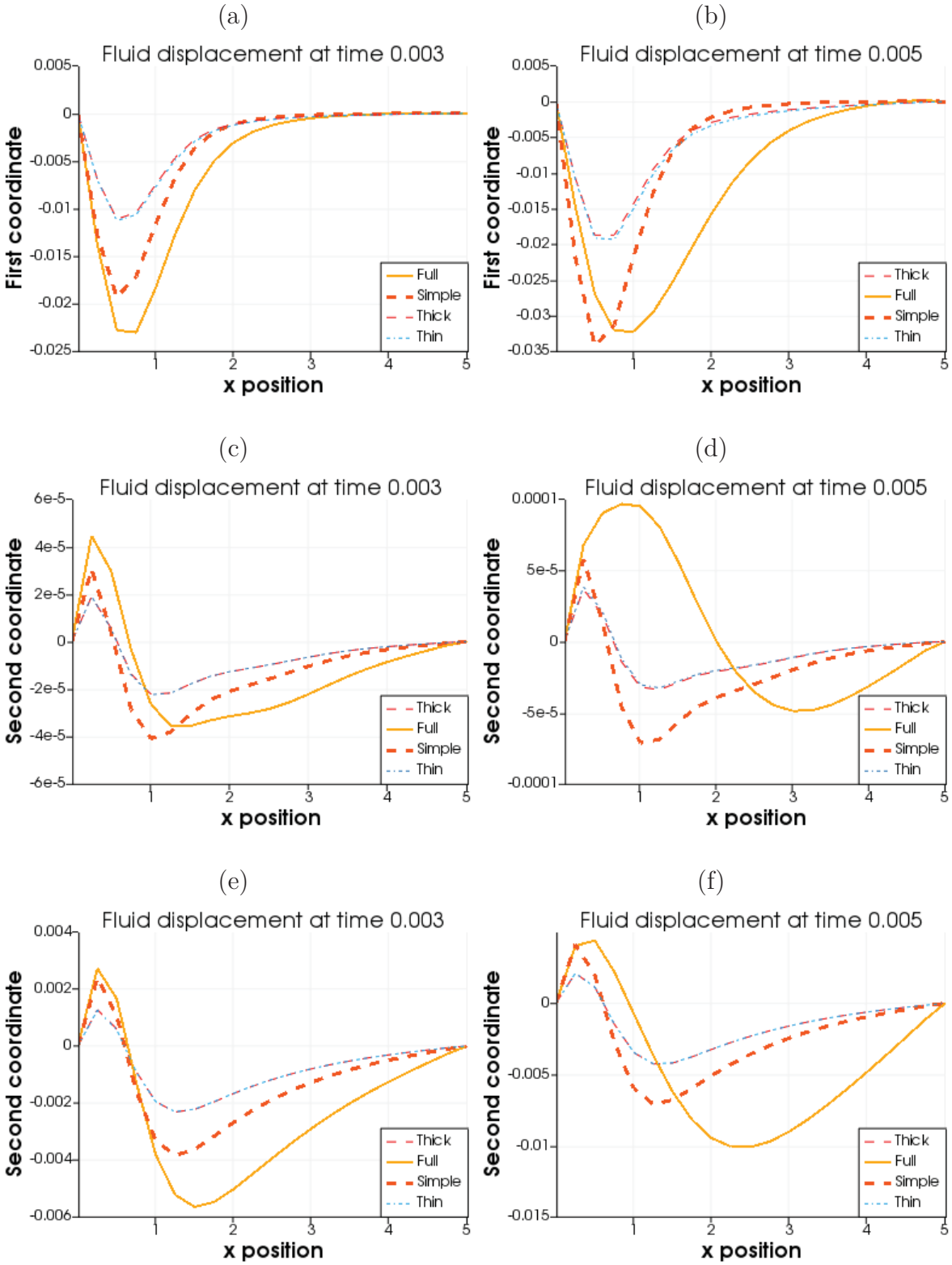

SOURCE: Data from this research (2020).

FIGURE 26 - Plots of the fluid's velocity on the line, with $\Delta t = 10^{-3}$

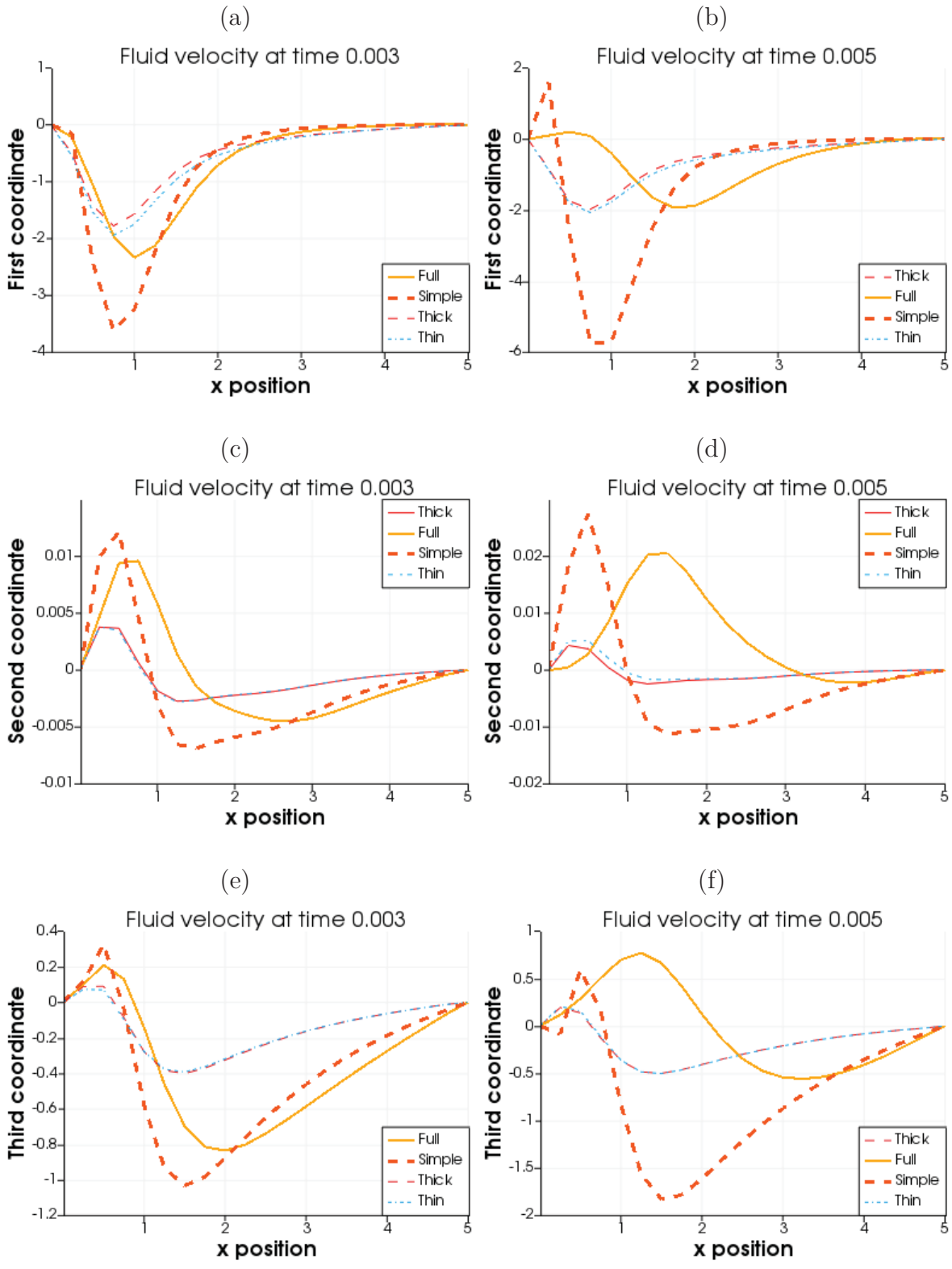

FIGURE 27 - Plots of the fluid's pressure on the line, with $\Delta t = 10^{-3}$

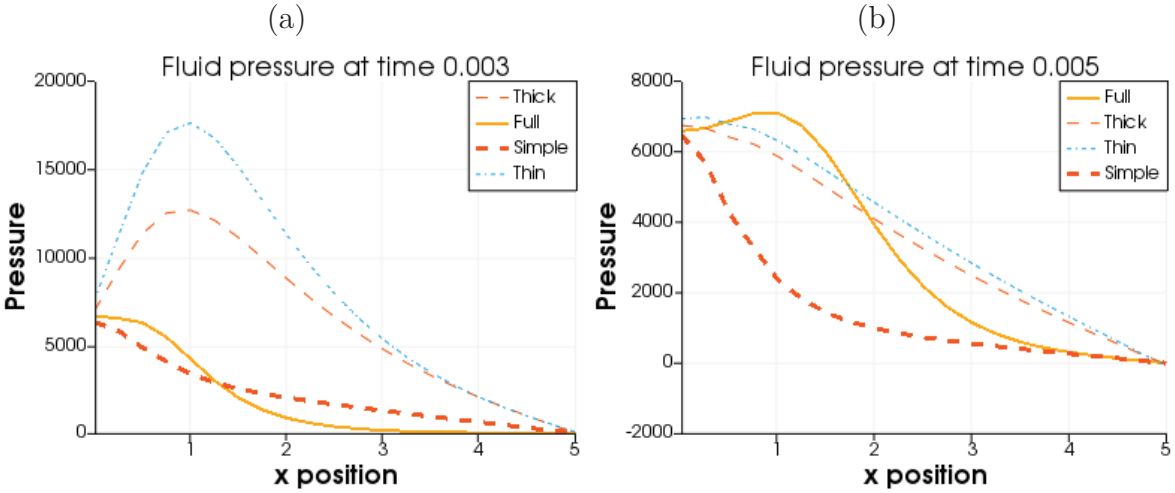

SOURCE: Data from this research (2020).